Modelling of Three-Phase Power Converters

A fundamental port-Hamiltonian approach

LTZ 3 (TD) S. Krul

Master of Science Thesis

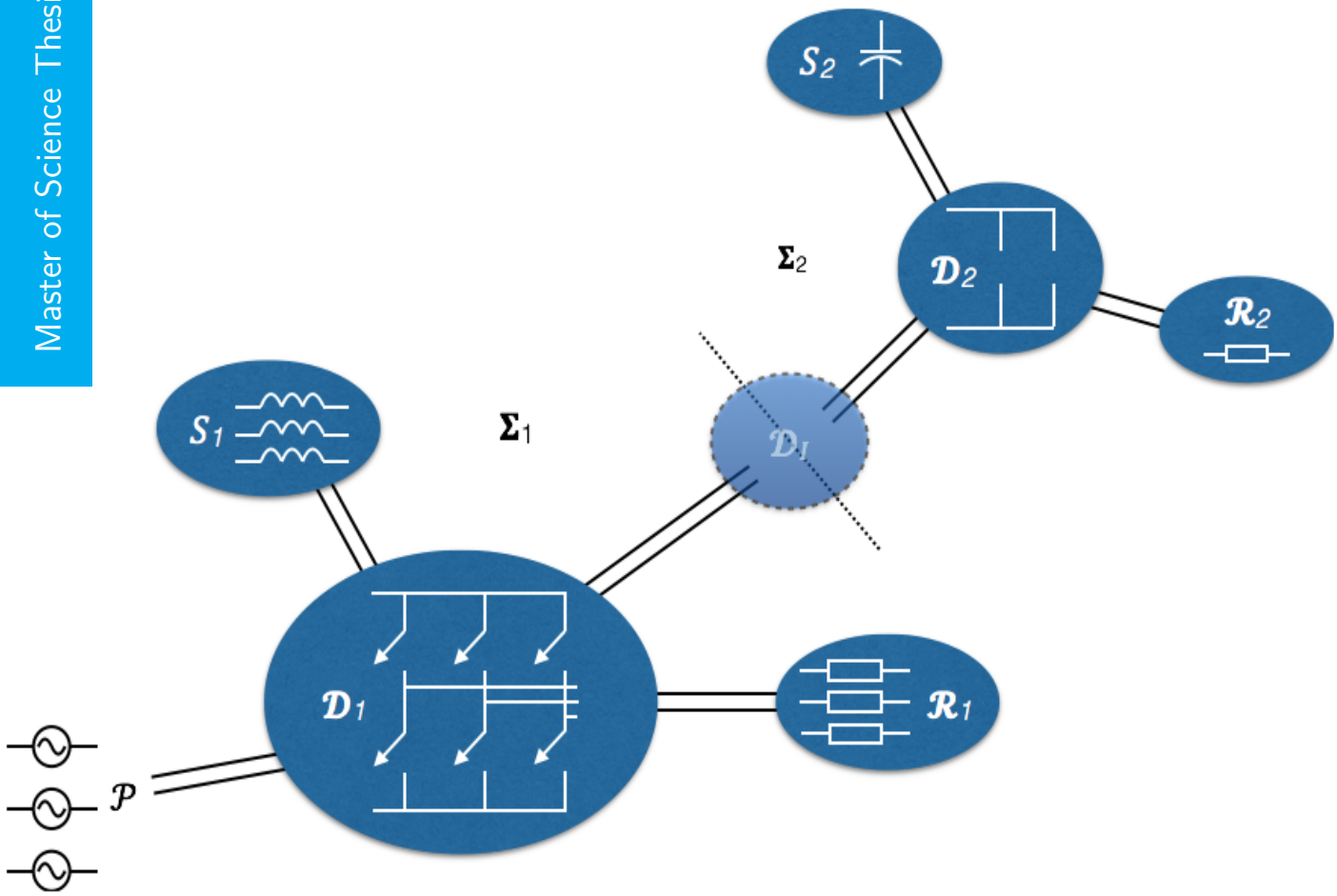

TU Delft Delft University of Technology

Delft Center for Systems and Control

Modelling of Three-Phase Power Converters

A fundamental port-Hamiltonian approach

Master of Science Thesis

For the degree of Master of Science in Systems and Control at Delft University of Technology

S. Krul
Luitenant-Ter-Zee der Derde Klasse van de Technische Dienst

June 4, 2015

Faculty of Mechanical, Maritime and Materials Engineering (3mE) · Delft University of Technology

Delft University of Technology
Department of
Delft Center for Systems and Control (dcsc)

The undersigned hereby certify that they have read and recommend to the Faculty of Mechanical, Maritime and Materials Engineering (3mE) for acceptance a thesis entitled

Modelling of Three-Phase Power Converters

by

S. Krul

in partial fulfillment of the requirements for the degree of

Master of Science Systems and Control

Dated: June 4, 2015

Supervisor(s):

prof.dr. R. Babuška

dr.ing. D. Jeltsema, M.Sc

Reader(s):

dr. G.A.D. Lopes

dr.ir. S. Baldi

Abstract

The port-Hamiltonian modelling and control of power converters has been the topic of a number of studies for the past couple years. However, the modelling of three-phase converters from fundamental port-Hamiltonian principles has been an unexplored direction. This study focusses on deducing a modelling procedure to model a three-phase rectifier and a three-phase inverter from a fundamental port-Hamiltonian perspective. Such a perspective involves the derivation of a model from a mathematical expression of the Dirac structure. Two procedures are formulated, where either the switches are viewed as virtual elements or as nonlinear elements. The study concludes that both techniques are equally suitable for the modelling of the rectifier and the inverter. Furthermore, incorporating non-ideal switches is easier when regarding them as nonlinear elements, but obtaining a parametrised form (parametrised by the switch state) is more straightforward when regarding them as virtual elements. Both methods require us to identify the currents and voltages in the network as efforts and flows based on the network topology. However, this turns out to be ambiguous for the conjugate variables of the interconnection ports and switches. To cope with this, two conventions are proposed.

Table of Contents

List of Figures

Preface

In August 2009, I embarked on my educational trajectory at the Royal Dutch Naval Academy, from which I graduated in 2013 for the academic part. Before I finalise the rest of this trajectory with an internship on board one of the Navy's vessels, the Navy has allowed me to attend the master program Systems & Control at the Technical University Delft, where I conducted this research. It was here that I had my first encounter with fundamental systems theory and the port-Hamiltonian framework, whose elegant and fundamental viewpoint towards physical phenomena, together with the mathematical theory enthralled me to study it further. It is safe to say that, I will finish this thesis with a new found love for fundamental mathematics and physics. A conviction enticed after reading works like, Breedveld (1984), Schuh (1968) and Willems (2007).

My sincere gratitude goes to dr. ing. Dimitri Jeltsema, my direct supervisor, whose guidance, enthusiasm and pragmatic viewpoint helped guide me through this project. Perhaps most of all, that he allowed my research to be directed from control, to the port-Hamiltonian modelling of power converters. Also, I would like to express my gratitude to dr. ir. Arthur Vermeulen, who helped me a lot with writing my thesis and I would like to thank prof. Robert Babuška for his effort in the project management. Last but not least, I like to thank my friends and family for all their support and patience, especially Margareth, who stood by me during this period. A special thanks goes to my friend Oliver, with whom I shared many evenings working through fundamental math, testing my knowledge and sharing concepts. Not to mention learning a thing or two, and talking, about fundamental physics and having a good laugh.

Although it is perhaps only reserved for PhD theses to append their work with a list of (some times ironic) epiphanies, I would like to use this preface to share, and end with, one.

> *Any form of mathematics, a problem, a theory or simply a notation, should always be approached with the utmost curiosity. Failing to do so, will result in a fear towards math and will prevent anyone to utilise and recognise its full potential. Therefore, the tendency of teachers and lectures to step-over or cut-down on mathematical notation or theory, will only degrade the incentive to understand, emphasise the fear and rob students of the opportunity to grasp its potential.*

Stephan Krul
June 4, 2015

"Get the physics right. The rest is just mathematics."
— *Rudy Kalman*

Chapter 1

Introduction

1-1 Background

Today's society sees an ever growing use of electrical devices and appliances that are increasingly interfaced or interconnected with one another. The power forms at the interfaces of these devices rarely commute, which requires devices that regulate and process the power flow between them. For example, laptops work on a direct current (DC) from a battery which is charged by connecting it to the power grid, but the power supplied from the net is an alternating current (AC). To accommodate energy exchange between these devices systems known as *power converters* are connected between the interfaces, which transform the power form of the power supplier to the form demanded by the power receiver[1]. In general, the broadest explanation of the task of power converters is (Mohan [1, Ch.1.1]): to process and control the flow of electric energy from one form to another in the most suitable manner through control of the currents and/or voltages. Figure 1-1 gives a schematic representation of this general power process (power form transformation) and the position of the power converter within this process.

The power forms vary from a constant or adjustable magnitude DC-voltage/current to an single or multiple-phase AC-voltage/current with adjustable or constant frequency and/or magnitude. The transformation of one power form to another is achieved by chopping the input signal with semiconductor switches in such a way that the resulting output signal is of (approximates) the desired form. The controller determines the opening and closing of the switches, which is usually done by a method known as *pulse-width-modulation*. Thus, the switches perform the central role in the operation of a power converter, but this also makes these devices nonlinear in their behaviour.

The hybrid nature of these devices makes modelling and controlling them an interesting topic [2]. Specifically, control of these devices with nonlinear techniques is still an ongoing field of research. Together with the development of nonlinear control techniques for power

[1] In some devices the power sometimes flows in the secondary direction, i.e., from the receiver to the supplier. For example, in electric drives during regenerative breaking.

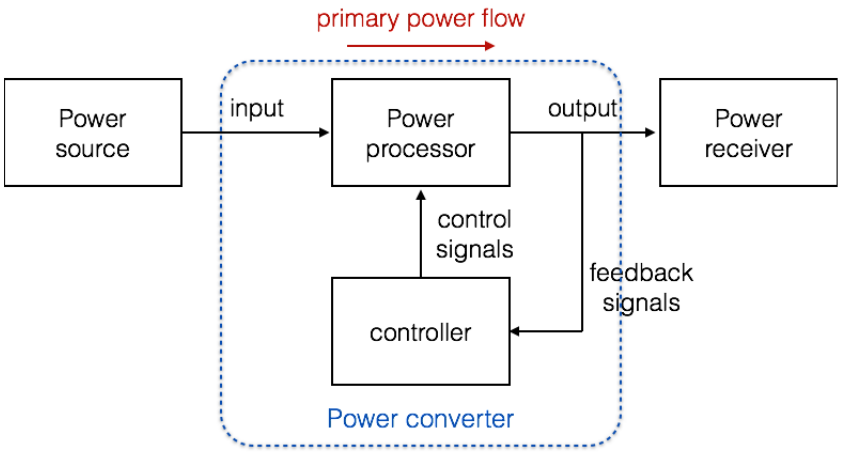

Figure 1-1: Schematic representation of a power process.

converters, there is also a growing interest in the modelling of power converters with energy-based methods, such as with the Euler-Lagrange or the Port-Hamiltonian (PH) formalism. Especially, the PH framework holds some advantages, for it provides a natural foundation for the application of *passivity-based* control techniques and allows for an easy interconnection of multiple (multi-domain) systems.

In general, the PH framework views physical systems as ideal elements, interconnected by *ports*, through which they exchange energy. The elements can be categorised into three types: *energy storage elements*, *energy dissipating elements* and *energy routing elements*. The energy flow through a port is described by a pair of dual variables, *efforts* (e) and *flows* (f), whose inner product yields the energy flow or power. As a result of this categorisation, energy sources in systems are not modelled as elements, but as additional (external) ports to the system. Figure 1-2 gives a graphical representation of this concept, where $\mathcal{S}$ denotes the structure of all storage elements, $\mathcal{R}$ the structure of all resistive elements and subscript $\mathcal{P}$ the external ports. The *Dirac structure*, $\mathcal{D}$, represents the interconnection of the elements and is consequently power preserving, i.e., the total power entering (or leaving) the Dirac structure is zero [3, Ch.2.1.2]. Appendix A lists the interpretation of the efforts and flows for different physical domains.

Although, much work has been done on control of power converters with port-Hamiltonian or passivity-based techniques, there is little literature on the modelling of power converters with port-Hamiltonian methods [2]. The research that has been done has been focussed on the modelling of DC/DC-converters, see for instance [4, 5, 6, 7]. However, three-phase power converters, which have a power form on either the input or output side (or both) that consists of three phases, are not yet considered. Therefore, this focus of this thesis is on the modelling of three-phase power converters from port-Hamiltonian modelling principles. Concretely, this thesis considers two types of three-phase power converters, the three-phase AC/DC converter (known as a three-phase *rectifier*) and the three-phase DC/AC converter (known as a three-phase *inverter*). These two power converters are at the core of most three-phase power processes and are common components in many electrical machines and power

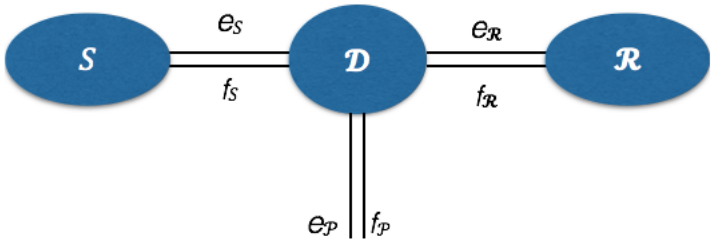

Figure 1-2: A port-Hamiltonian system.

generating configurations[2], see for instance Wildi [8, Ch.23.1]. For example, these devices can be found in wind turbines at the interconnection of the electrical generators to the power grid or between the battery and the power grid in solar panels. Furthermore, these devices perform a crucial role in regulating the angular velocity of induction motors by regulating the frequency of the input voltage [8, Ch.23].

1-2 Research objective

Currently, the development of PH models of the three-phase power converters, with the objective of passivity-based control in mind, is achieved by [2]:

1. expressing the system as a set of explicit differential equations with the Kirchhoff laws;
2. averaging the dynamics to obtain a continuous-time system and subsequently performing the *dq0-transformation* to project the phase variables unto an orthogonal frame;
3. rewriting the states in terms of PH variables by introducing the Hamiltonian.

This procedure has two implications: first, step (ii) implies that the systems are always assumed to be balanced, which is not necessarily always the case and second, step (iii) implies that the PH model is achieved by transformation, rather than modelling from PH principles, which is starting from the Dirac structure and Hamiltonian. The objective of this thesis is:

Model the three-phase rectifier and inverter from a fundamental PH viewpoint, which is to express the Dirac structure and the Hamiltonian and derive the model from thereon, and evaluate the modelling procedure for effectiveness, efficiency and practicality.

The obtained models of the power converters are compared to the models in the original papers [9, 10, 11][3].

[2]The three-phase AC to three-phase AC conversion used for electrical drives is, for example, commonly achieved by first rectifying and subsequently inverting the electrical signal [2, 8].

[3]It is the argument of the author that validation by comparison of the obtained models suffices, because the mathematical models of three-phase inverter and rectifiers are well established in textbooks and papers

1-3 Structure of the thesis

The structure of this thesis is as follows: Chapter 2 features some required port-Hamiltonian system theory and modelling theory for (switching) electrical networks. This chapter concludes with the modelling procedure for three-phase power converters used in this thesis. Subsequently, Chapter 3 deals with the modelling of the three-phase inverter from [10, 11] with this method. This leads to a differential-algebraic model of the inverter for an unbalanced system and an input-state-output model of the inverter for a balanced system. After that, in Chapter 4, we apply the same modelling procedure to the three-phase rectifier from [9]. This too, yields a differential-algebraic model and an input-state-output model for, respectively, the unbalanced and balanced case. Finally, Chapter 5 summarises the conclusions and lists the recommendations for further studies.

1-4 A word on the notation

In this thesis, we adhere to the following convention regarding the mathematical symbols:

- The lower case symbols, e.g., f, e, v, i, representing physical quantities are all assumed to be time-varying and therefore the arguments of time are omitted.
- To prevent excessive use of conventional vector symbols, all the variables are column vectors, e.g., $w = (w_1 \quad w_2 \quad \dots \quad w_n)^T$. Moreover, to reduce the use of the transpose operator, all the partial derivatives are defined to yield a column vector. This means that, $\nabla_w = \frac{\partial}{\partial w} = (\frac{\partial}{\partial w_1} \quad \frac{\partial}{\partial w_2} \quad \dots \quad \frac{\partial}{\partial w_n})^T$.
- The subscripts a, b, c refer to the phases a, b and c of an AC-variable. For instance, v_a, v_b, v_c are phase voltages and v_{ab} the line-to-line voltage between phases a and b.
- The variables j, k, ℓ are reserved for counters and indexes.
- The calligraphic symbols are reserved for spaces, e.g., $\mathcal{X}, \mathcal{D}, \mathcal{F}$.
- The symbol $\mathbb{O}$ denotes a zeromatrix, i.e., a matrix with all elements equal to zero and the symbol $\mathbb{I}$ denotes the identity matrix.

and verified in practise.

Chapter 2

Modelling theory

This chapter presents the theory and modelling techniques for the modelling of power converters from a fundamental port-Hamiltonian viewpoint. It concludes with two modelling methods that differ in the way they model the switches. One views these as virtual elements and the other as nonlinear elements. First, Section 2-1 provides some theoretical details on the interconnection and representation of PH systems. Second, Section 2-2 deals with the required network theory, including topics such as the network graph and the incidence matrix. Finally, in Section 2-3, we deduce two methods from literature for the modelling of power converters from a PH perspective and show that both of the methods – surprisingly – cannot be applied to the modelling of three-phase power converters in their current form. The methods are adapted and a new method is proposed to model the three-phase power converters.

2-1 Port-Hamiltonian system theory

For the modelling of power converter as port-Hamiltonian systems two additional topics need to be studied in more detail. The first is the interconnection of multiple PH systems, which is equivalent to interconnecting their Dirac structures. An important feature of PH systems is the *interconnectivity* or *compositionality* of the systems, which means that larger systems can be described by interconnecting simpler parts. This is an essential advantage in the modelling of complex and multi-domain systems. The second are the mathematical representations of PH systems and their Dirac structures. In this section we shall highlight two representations that are going to be used in this thesis. First, Section 2-1-1 deals with these two representations. Subsequently, Section 2-1-2 treats the theory regarding the interconnection of Dirac structures. The theory on the representations is taken from Duindam et al. [3], Van Der Schaft et al. [12] and the theory on the interconnection of PH systems is taken from Cervera et al. [13].

2-1-1 Port-Hamiltonian system representations

In this section we present two mathematical representations of PH systems: the *matrix kernel representation* of the Dirac structure and the *input-state-output* (ISO) PH form. The first is the most general, but the latter more convenient for control, because it forms a set of explicit differential equations, whose structure closely resembles the more common state-space notation. We start with the mathematical definition of a finite Dirac structure. Then, we give the implicit representation, the matrix kernel representation, and subsequently treat the ISO form, which follows naturally from the matrix kernel representation under certain conditions. In other words, the ISO representation is a special case of the matrix kernel representation.

The definition of a finite Dirac structure

A finite Dirac structure on $\mathcal{F} \times \mathcal{E}$, with $\mathcal{E}$ the dual space of $\mathcal{F}$ ($\mathcal{E} = \mathcal{F}^*$), is a subspace $\mathcal{D} \subset \mathcal{F} \times \mathcal{E}$ such that

1. $\langle e|f\rangle = 0 \; \forall \; (f,e) \in \mathcal{D}$,
2. $\dim \mathcal{D} = \dim \mathcal{F}$.

The first property represents the power conversation principle, where $\langle e|f\rangle$ denotes the duality product. In the case that $\mathcal{F} = \mathbb{R}^n$ and $\mathcal{E} = (\mathbb{R}^n)^*$, the duality product reduces to the inner-product between two vectors

$$\langle e|f\rangle = e^T f.$$

The second property guarantees that the subspace has maximal dimension with respect to the first property. This means that it is not possible to extend the subspace to a larger subspace that still has this property.

The matrix kernel representation

Any Dirac structure $\mathcal{D} \subset \mathcal{F} \times \mathcal{E}$ can be represented in a matrix kernel representation[1] defined as

$$\mathcal{D} = \{(f,e) \in \mathcal{F} \times \mathcal{E} \mid Ff + Ee = 0\}. \tag{2-1}$$

Take a linear space $\mathcal{V}$ of the same dimension as $\mathcal{F}$ and take linear coordinates $v_1, \ldots, v_n$ for $\mathcal{V}$, $f_1, \ldots, f_n$ for $\mathcal{F}$ and $e_1, \ldots, e_n$ for $\mathcal{E}$. Then, the linear maps $F : \mathcal{F} \to \mathcal{V}$ and $E : \mathcal{E} \to \mathcal{V}$ satisfying

$$\begin{aligned} (i) \quad & EF^T + FE^T = 0, \\ (ii) \quad & \operatorname{rank}[F \; E] = \dim \mathcal{F}, \end{aligned}$$

are $n \times n$ matrices that capture the interconnection of the flows and efforts through the characteristic equation

$$Ff + Ee = 0. \tag{2-2}$$

[1] Simply termed kernel representation henceforth.

The linear maps $F^T : \mathcal{V}^* \to \mathcal{F}^* = \mathcal{E}$ and $E^T : \mathcal{V}^* \to (\mathcal{F}^*)^* \cong \mathcal{F}$ ("$\cong$" means isomorphic) are the adjoint maps of F and E. The dimension of the linear space $\mathcal{V}$ can be greater than the dimension of $\mathcal{F}$. In which case, the matrices F and E are of dimension $n' \times n$ with $n' > n$ and the representation is called a *relaxed kernel representation*. The relaxed kernel representation leads to an excess of equations in (2-2), which means that there are multiple rows in (2-2) denoting the same relation.

Consider the PH system depicted in Figure 1-2. Equation (2-1) defines an implicit PH system of the form[2]

$$\left(-\dot{x},\ \frac{\partial H}{\partial x}(x),\ f_{\mathcal{R}},\ e_{\mathcal{R}},\ f_{\mathcal{P}},\ e_{\mathcal{P}}\right) \in \mathcal{D}, \tag{2-3}$$

where $(f_{\mathcal{R}},\ e_{\mathcal{R}}) \in \mathcal{R}$,

$$\begin{aligned} -f_{\mathcal{S}} &= \dot{x}, \\ e_{\mathcal{S}} &= \frac{\partial H}{\partial x}(x), \end{aligned} \tag{2-4}$$

are substituted and H denotes the *Hamiltonian* (the energy in the system), see Appendix A. This can readily be seen by rewriting (2-2) such that (2-1) reads as

$$\begin{aligned} \mathcal{D} = \Bigg\{ &(-\dot{x}, \frac{\partial H}{\partial x}, f_{\mathcal{R}}, e_{\mathcal{R}}, f_{\mathcal{P}}, e_{\mathcal{P}}) \in \mathcal{F}_{\mathcal{S}} \times \mathcal{E}_{\mathcal{S}} \times \mathcal{F}_{\mathcal{R}} \times \mathcal{E}_{\mathcal{R}} \times \mathcal{F}_{\mathcal{P}} \times \mathcal{E}_{\mathcal{R}} \\ &| -F_{\mathcal{S}}\dot{x} + E_{\mathcal{S}}\frac{\partial H}{\partial x} + F_{\mathcal{R}}f_{\mathcal{R}} + E_{\mathcal{R}}e_{\mathcal{R}} + F_{\mathcal{P}}f_{\mathcal{P}} + E_{\mathcal{P}}e_{\mathcal{P}} = 0 \Bigg\}, \end{aligned}$$

with $E_{\mathcal{S}}F_{\mathcal{S}}^T + F_{\mathcal{S}}E_{\mathcal{S}}^T + E_{\mathcal{R}}F_{\mathcal{R}}^T + F_{\mathcal{R}}E_{\mathcal{R}}^T + E_{\mathcal{P}}F_{\mathcal{P}}^T + F_{\mathcal{P}}E_{\mathcal{P}}^T = 0$ and $\text{rank}[F_{\mathcal{S}}\ E_{\mathcal{S}}\ F_{\mathcal{R}}\ E_{\mathcal{R}}\ F_{\mathcal{P}}\ E_{\mathcal{P}}] = \dim(\mathcal{X} \times \mathcal{F}_{\mathcal{R}} \times \mathcal{F}_{\mathcal{P}})$. The symbol $\mathcal{X}$ denotes the *state-space* manifold. The characteristic equation defines a PH system as

$$F_{\mathcal{S}}\dot{x} = E_{\mathcal{S}}\frac{\partial H}{\partial x} + F_{\mathcal{R}}f_{\mathcal{R}} + E_{\mathcal{R}}e_{\mathcal{R}} + F_{\mathcal{P}}f_{\mathcal{P}} + E_{\mathcal{P}}e_{\mathcal{P}}, \tag{2-5}$$

which in general forms a set of *differential-algebraic equations* (DAEs) [13].

The input-state-output (ISO) form

In system theory and control it is common to work with systems of the form

$$\Sigma : \begin{cases} \dot{x} = f(x,u), \\ y = h(x,u), \end{cases} \tag{2-6}$$

where $x \in \mathcal{X}$ is the state of the system, $u \in \mathbb{R}^m$ the input and $y \in \mathbb{R}^p$ the output. An implicit port-Hamiltonian system of the form in (2-3) is therefore preferably transformed into an explicit expression of the form in (2-6). For a PH system such an expression can be achieved if the matrices $F_{(\cdot)}$ and $E_{(\cdot)}$ in (2-5) are such that they can be transformed to [13]

$$\begin{bmatrix} \mathbb{I} \\ \mathbb{O} \\ \mathbb{O} \end{bmatrix} \dot{x} = \begin{bmatrix} J(x) \\ g_{\mathcal{R}}^T(x) \\ g^T(x) \end{bmatrix} \frac{\partial H}{\partial x}(x) + \begin{bmatrix} g_{\mathcal{R}}(x) \\ \mathbb{O} \\ \mathbb{O} \end{bmatrix} f_{\mathcal{R}} + \begin{bmatrix} \mathbb{O} \\ -\mathbb{I} \\ \mathbb{O} \end{bmatrix} e_{\mathcal{R}} + \begin{bmatrix} g(x) \\ \mathbb{O} \\ \mathbb{O} \end{bmatrix} u + \begin{bmatrix} \mathbb{O} \\ \mathbb{O} \\ -\mathbb{I} \end{bmatrix} y,$$

[2] The minus sign is to have a consistent power flow convention: $\frac{\partial^T H}{\partial x}(x)\dot{x}$ is the power flowing into the storage elements and $e_{\mathcal{S}}^T f_{\mathcal{S}}$ is the power flowing into the Dirac structure. See also the discussion in [12, Ch.2.3-2.4].

where $\mathbb{I}$ denotes the identity matrix, $\mathbb{O}$ a zeromatrix of appropriate dimension and $J(x)$ is a $n \times n$ matrix that depends smoothly on x and satisfies $J(x) = -J^T(x)$. Hence, the PH system can be represented by set of explicit equations, where the connection to the resistive structure is modelled as a separate input-output couple. This ISO form is given by the formulae

$$\begin{aligned} \dot{x} &= J(x)\frac{\partial H}{\partial x}(x) + g_{\mathcal{R}}(x)f_{\mathcal{R}} + g(x)u, \\ e_{\mathcal{R}} &= g_{\mathcal{R}}^T(x)\frac{\partial H}{\partial x}(x), \\ y &= g^T(x)\frac{\partial H}{\partial x}(x), \end{aligned} \tag{2-7}$$

for some resistive relation $f_{\mathcal{R}} = -\tilde{D}e_{\mathcal{R}}$ with $\tilde{D} = \tilde{D}^T$, $\tilde{D} \geq 0$ [3, Ch.2.2.3].

The resistance structure is often not modelled as a separate input-output port, but included into the system dynamics. The resistive structure is included by substituting $g_{\mathcal{R}}(x)f_{\mathcal{R}} = -g_{\mathcal{R}}(x)\tilde{D}e_{\mathcal{R}} = -g_{\mathcal{R}}(x)\tilde{D}g_{\mathcal{R}}^T(x)\frac{\partial H}{\partial x}(x)$, which yields the more common ISO form [12, Ch.10]

$$\begin{aligned} \dot{x} &= [J(x) - D(x)]\frac{\partial H}{\partial x}(x) + g(x)u, \\ y &= g^T(x)\frac{\partial H}{\partial x}(x), \end{aligned} \tag{2-8}$$

where the $n \times n$ matrix $D(x)$ depend smoothly on x and satisfies $D(x) = D^T(x)$, $D(x) \geq 0$.

Thus, the ISO form follows from the kernel representation (2-1) by first defining and substituting $f_{\mathcal{P}}$, $e_{\mathcal{P}}$ with u, y and $f_{\mathcal{S}}$, $e_{\mathcal{S}}$ with $-\dot{x}$, $\frac{\partial H}{\partial x}(x)$, respectively. Subsequently solving (2-2) for $\dot{x}$ and y leads to the ISO representation of the system conform the structure in (2-8). Likewise, solving (2-2) for $\dot{x}$, y and $e_{\mathcal{R}}$ yields an ISO system conform (2-7). Although both (2-7) and (2-8) are equally suitable, we chose to adhere to the ISO representation of (2-7) for the rest of this thesis.

2-1-2 Composition and interconnection of Dirac structures

Consider a PH system separated into two subsystems A and B, such that

$$\begin{aligned} \mathcal{D}_A &= \{(f_1, e_1, f_2, e_2) \in \mathcal{F}_1 \times \mathcal{E}_1 \times \mathcal{F}_2 \times \mathcal{E}_2 \mid \langle e_1 | f_1 \rangle + \langle e_2 | f_2 \rangle = 0\}, \\ \mathcal{D}_B &= \{(f_2', e_2', f_3, e_3) \in \mathcal{F}_2 \times \mathcal{E}_2 \times \mathcal{F}_3 \times \mathcal{E}_3 \mid \langle e_2' | f_2' \rangle + \langle e_3 | f_3 \rangle = 0\}. \end{aligned}$$

Figure 2-1 shows a graphical representation of the division and the two subsystems. The separation resulted into an additional port (f_2, e_2) in subsystem A and (f_2', e_2') in subsystem B. Logically, both Dirac structures share the same interconnection variables. However, due to the fact that $\langle e_2 | f_2 \rangle$ denotes the incoming power in $\mathcal{D}_A$ and $\langle f_2' | e_2' \rangle$ denotes the incoming power in $\mathcal{D}_B$, we cannot interconnect the two systems by simply equating the power variables [13]. Instead, they are related with, for instance, the *canonical interconnection*

$$\begin{aligned} f_2 &= -f_2', \\ e_2 &= e_2'. \end{aligned} \tag{2-9}$$

Subsequently, the *composition* of the two Dirac structures reads as[3] [13]

$$\mathcal{D}_A \circ \mathcal{D}_B := \{(f_1, e_1, f_3 e_3) \in \mathcal{F}_1 \times \mathcal{E}_1 \times \mathcal{F}_3 \times \mathcal{E}_3 \mid \exists (f_2, e_2) \in \mathcal{F}_2 \times \mathcal{E}_2 \\ \text{s.t. } (f_1, e_1, f_2, e_2) \in \mathcal{D}_A \text{ and } (-f_2, e_2, f_3, e_3) \in \mathcal{D}_B\}\,.$$

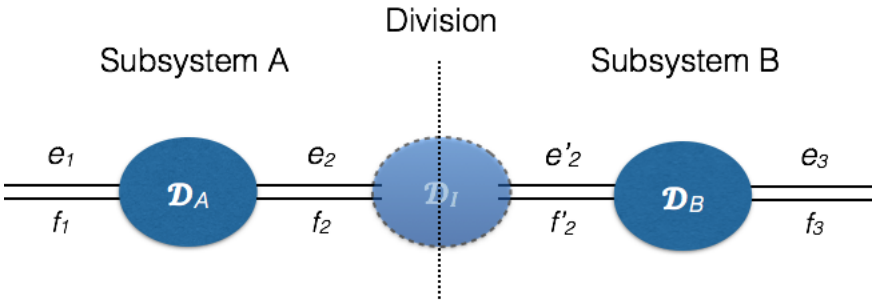

Figure 2-1: Graphical representation of a separated Dirac structure.

Note that the canonical interconnection structure, (2-9), in itself defines a Dirac structure $\mathcal{D}_I$ on the space of the interconnection variables $\mathcal{F}_2 \times \mathcal{E}_2$ given as

$$\mathcal{D}_I := \{(f_2, e_2, f_2' e_2') \in \mathcal{F}_2 \times \mathcal{E}_2 \mid f_2 = -f_2', e_2 = e_2' \\ \text{s.t. } (f_2, e_2) \in \mathcal{D}_A \text{ and } (f_2', e_2') \in \mathcal{D}_B\}\,.$$

Likewise, the *gyrative interconnection* [12, Ch.2.2.1],

$$\begin{aligned} f_{AI} &= \beta e_{IB}, \\ \beta e_{AI} &= -f_{IB}, \end{aligned} \tag{2-10}$$

is another interconnection, that also defines a Dirac structure on the space of the interconnection variables. Immediately it follows that, the interconnection of ℓ Dirac structures $\mathcal{D}_k \subset \mathcal{F}_k \times \mathcal{E}_k \times \mathcal{F}_{Ik} \times \mathcal{E}_{Ik}$, $k = 1, \ldots, \ell$, with $\ell - 1$ individual interconnections, can be described by the interconnection Dirac structure $\mathcal{D}_I \subset \mathcal{F}_{I1} \times \mathcal{E}_{I1} \times \ldots \times \mathcal{F}_{I\ell} \times \mathcal{E}_{I\ell}$ [13]. Moreover, the composition of Dirac structures is *associative*, i.e., $(\mathcal{D}_A \circ \mathcal{D}_B) \circ \mathcal{D}_C = \mathcal{D}_A \circ (\mathcal{D}_B \circ \mathcal{D}_C)$, which means that the order of composition does not matter and that the brackets can be omitted.

The theory for the composition of Dirac structures admits a number of ways to obtain and represent a composed system. We treat the one, where the Dirac structures are represented in a kernel representation.

Consider two Dirac structures $\mathcal{D}_A$ and $\mathcal{D}_B$ defined as

$$\mathcal{D}_A = \{(f_A, e_A) \in \mathcal{F}_A \times \mathcal{E}_A \mid F_A f_A + E_A e_A = 0\}\,,$$
$$\mathcal{D}_B = \{(f_B, e_B) \in \mathcal{F}_B \times \mathcal{E}_B \mid F_B f_B + E_B e_B = 0\}\,,$$

[3] The composition of Dirac structures is more commonly denoted in literature as $\mathcal{D}_1 || \mathcal{D}_2$, see [3, 13]. However, to prevent confusion with the "components in parallel" (e.g. $L_1 || L_2$) notation in electrical engineering, we opt to use the notation from [12] to denote a composition.

which are connected to each other by a set of ports, described by the pairs $(f_{AI}, e_{AI}) \in \mathcal{F}_A \times \mathcal{E}_A$, $(f_{BI}, e_{BI}) \in \mathcal{F}_B \times \mathcal{E}_B$. Denote the composed flow and effort vector as $f = [f_A^T \ f_B^T]^T$, $e = [e_A^T \ e_B^T]^T$, respectively, and the interconnection relations as $I(f_{AI}, f_{BI}, e_{AI}, e_{BI})$. Then, the interconnection Dirac structure in a kernel representation can be expressed as

$$\begin{aligned}\mathcal{D}_I = \{&(f_A, e_A, f_B, e_B) \in \mathcal{F}_A \times \mathcal{E}_A \times \mathcal{F}_B \times \mathcal{E}_B \mid F_I f + E_I e = 0 \\ &\text{s.t. } I(f_{AI}, f_{BI}, e_{AI}, e_{BI}),\ f_{AI} \in \mathcal{F}_A,\ e_{AI} \in \mathcal{E}_A,\ f_{BI} \in \mathcal{F}_B,\ e_{BI} \in \mathcal{E}_B\}.\end{aligned}$$

And the kernel representation of the composed Dirac structure is

$$\mathcal{D}_A \circ \mathcal{D}_B = \{(f_A, e_A, f_B, e_B) \in \mathcal{F}_A \times \mathcal{E}_A \times \mathcal{F}_B \times \mathcal{E}_B \mid Ff + Ee = 0\}, \tag{2-11}$$

where

$$F = \begin{bmatrix} F_A & \mathbb{O} \\ \mathbb{O} & F_B \\ & F_I \end{bmatrix}, \ E = \begin{bmatrix} E_A & \mathbb{O} \\ \mathbb{O} & E_B \\ & E_I \end{bmatrix}.$$

The representation in (2-11) provides a structured and straightforward way of mathematically constructing large systems from subsystems. However, the dimensions of the characteristic equation increase rapidly with every subsystem, because every separation generates interconnection variables. These interconnection variables disappear when computing the total model, which can be shown and done with the following theorem from [13].

Theorem 1. *Consider two Dirac structures $\mathcal{D}_A$ and $\mathcal{D}_B$ defined as*

$$\begin{aligned}\mathcal{D}_A &= \{(f_1, e_1, f_2, e_2) \in \mathcal{F}_1 \times \mathcal{E}_1 \times \mathcal{F}_2 \times \mathcal{E}_2 \mid F_1 f_1 + E_1 e_1 + F_{2A} f_2 + E_{2A} e_2 = 0\}, \\ \mathcal{D}_B &= \{(f_2', e_2', f_3, e_3) \in \mathcal{F}_2 \times \mathcal{E}_2 \times \mathcal{F}_3 \times \mathcal{E}_3 \mid F_{2B} f_2' + E_{2B} e_2' + F_3 f_3 + E_3 e_3 = 0\},\end{aligned}$$

where the flows and efforts corresponding to an interconnection port are separated from the rest of the flows and efforts, and the two Dirac structures are connected with the canonical connection (2-9)*. Then, there exists a matrix $L = [L_A \ L_B]$ with $\ker L = \text{im } M$ and $\text{im } L^T = \ker M^T$, where*

$$M = \begin{bmatrix} F_{2A} & E_{2A} \\ -F_{2B} & E_{2B} \end{bmatrix},$$

such that the composed Dirac structure reads as

$$\mathcal{D}_A \circ \mathcal{D}_B = \{(f_1, e_1, f_3, e_3) \in \mathcal{F}_1 \times \mathcal{E}_1 \times \mathcal{F}_3 \times \mathcal{E}_3 \mid Ff + Ee = 0\}, \tag{2-12}$$

where $f = [f_1^T \ f_3^T]^T$, $e = [e_1^T \ e_3^T]^T$, $F = [L_A F_1 \ L_B F_3]$ and $E = [L_A E_1 \ L_B E_3]$.

This result can be readily understood by substituting the interconnection constraint of (2-9) into the characteristic equation of $\mathcal{D}_B$, which yields

$$-F_{2B} f_2 + E_{2B} e_2 + F_3 f_3 + E_3 e_3 = 0.$$

Then, premultiply the equations characterising $\mathcal{D}_A \circ \mathcal{D}_B$

$$\begin{bmatrix} F_1 & E_2 & F_{2A} & E_{2A} & \mathbb{O} & \mathbb{O} \\ \mathbb{O} & \mathbb{O} & -F_{2B} & E_{2B} & F_3 & E_3 \end{bmatrix} \begin{bmatrix} f_1 \\ e_1 \\ f_2 \\ e_2 \\ f_3 \\ e_3 \end{bmatrix} = 0,$$

with L. Since, $LM = 0$, this leads to

$$L_A F_1 f_1 + L_A E_1 e_1 + L_B F_3 f_3 + L_B E_3 e_3 = 0,$$

which is the equation characterising the composed Dirac structure in (2-12). See [13] for the proof and more details on this theory. This theorem shows that the interconnection variables characterising the interconnection port at the separation line are excessive variables in the sense that they do not manifest themselves to the outside world. They simply intermediate between the subsystems. Willems refers to these variables as *latent* variables, see Willems [14].

2-2 Modelling electrical networks

Electrical systems are often represented by a lumped circuit and subsequently described by the two fundamental postulates in electrical circuit theory: Kirchhoff's voltage law (KVL) and Kirchhoff's current law (KCL). As far as these laws are concerned, only the interconnection of the elements of the circuit is required. Therefore, the KVL and KCL can be derived from the *network graph* of the circuit. This network graph representation of electrical networks forms the basis to express the Dirac structure of switching electrical systems. As such, this section first briefly treats some required definitions from graph theory in Section 2-2-1. Subsequently, the concept of representing the Kirchhoff laws from the graphs in *incidence matrices* is presented in Section 2-2-2. Finally, Section 2-2-3 deals with the methods for representing the switching elements in graphs and in PH systems.

2-2-1 Graph theory

Graph theory is an effective tool for representing the interconnection of elements in networks, see for instance Chua et al. [15, Ch.5]. In fact, the graph and the Dirac structure (interconnection structure) are closely related. However, before we start with treating the theory to express (switching) electrical networks and their Dirac structures on the basis of graphs, it is convenient to discuss some basic definitions and concepts from graph theory. The definitions and theory in this section are taken from Diestel [16].

The graph

A graph, G, consists of a set of nodes, N, and a set of branches[4], B, and is defined as the pair $G = (N, B)$ of sets satisfying $B \subset N^2$ [16, Ch.1.1]. A branch, b, from the graph connects two nodes, n, from the graph, i.e., $b = \{n_k,\ n_\ell\},\ b \in B(G),\ n_k, n_\ell \in N(G)$. For the sake of simplicity, we write from here on instead of $b \in B(G)$ and $n \in N(G)$, respectively $b \in G$ and $n \in G$. Moreover, we simply write $b = n_k n_\ell$ instead of $b = \{n_k,\ n_\ell\}$.

The *degree of a node* is the number of branches that are connected to it [16, Ch.1.2]. In *directed graphs*[5], where each branch is given a direction and thus has a starting and end node,

[4] In graph theory the terms *vertices* (v) and *edges* (e) are used instead of nodes and branches, but these terms will not be used in this thesis to prevent ambiguity in the notation with the variables efforts and voltages.

[5] Also called oriented graphs or digraphs.

the degree of a node is further split into an *indegree* and an *outdegree*. The indegree of a node is the number of branches that enter the node, while the outdegree of a node is the number of branches that leave the node.

Path, cycles and connectivity

A *path* is a non-empty graph $G_P = (N, B)$ of the form [16, Ch.1.3]

$$N = \{n_0, n_1, \ldots, n_k\}, \quad B = \{n_0n_1, n_1n_2, \ldots, n_{k-1}n_k\},$$

where n_i are all distinct. Thus, a path in a graph is a subgraph of the graph, $G_P \subset G$. The number of branches in a path is the path length, denoted by $||G_P||$.

A *cycle* is a non-empty graph, $G_C = (N, B)$, that consists out of a path $G_P = n_0, \ldots, n_{k-1}$ with $k \geq 3$ and an additional branch $b = n_{k-1}n_0$ [16, Ch.1.3]. Thus, one can write

$$G_C = G_P + n_{k-1}n_0, \ k \geq 3. \tag{2-13}$$

Similarly to paths the number of branches in a cycle is the length of a cycle and denoted by $||G_C||$. Furthermore, a cycle in a graph is a subgraph of the graph, $G_C \subset G$. In directed graphs it is possible to have multiple branches between two nodes and *self-loops*. Thus, for directed graphs it is possible to have a cycle with $||G_C|| = 1$ and the restriction in (2-13), $k \geq 3$, reduces to $k \geq 1$.

A non-empty graph is called *connected* if any two of its nodes are linked by a path in G [16, Ch.1.4]. Similarly, a non-empty graph is *cyclically connected* if any two of its nodes are part of a cycle in G.

Dual graphs

Graphs are commonly drawn by denoting the nodes as dots and the branches as lines between these dots. If a graph can be drawn on a plane without any of its branches crossing each other, other than in a node, the graph is a *plane graph* [16, Ch.4.1]. Moreover, abstract graphs that can be drawn this way are known as *planar graphs*. Before we formally define these two concepts two additional terms must be introduced: an *arc* is a straight line segment in $\mathbb{R}^2$ and *the interior of an arc* is the point set between the starting and end point of the line segment.

Plane graph: a plane graph[6] G is a pair of (N, B) of finite sets with the following properties [16, Ch.4.2, Ch.4.4]

1. $N \subset \mathbb{R}^2$;
2. every branch is an arc between two nodes;
3. different, undirected branches have different sets of end points;
4. the interior of an branch contains no node and no point of any other branch.

[6]The same symbol (G) is used for both plane graphs, planar graphs and graphs.

Planar graph: a graph G is planar if it is isomorphic to a plane graph.

An important property of planar graphs is that every planar graph has a *dual graph*. In Section 2-2-2 we find that the dual graphs are very convenient in expressing the KVL. To describe how a dual graph is obtained from a plane graph we must first introduce the term *face* [16, Ch.4.2]. A face of G is a region in the set $\mathbb{R}^2 \backslash G$. Since G is always bounded (i.e., G can always be placed within a domain of finite size), there will always be exactly one face that is unbounded. This one is the *outer face* of G. The others are the *inner faces* of G.

The dual graph, G^*, of a planar graph, G, is obtained in the following way [16, Ch.4.6]:

1. place a new node, n^*, in every face of G.
2. link these "dual" nodes by a branch, b^*, for every b that separates two faces and let b^* cross the corresponding b.

If a branch, b, is adjacent with only one face, then the corresponding dual branch, b^*, creates a (self-) loop to n^* of that face, again crossing b. Applying this procedure to the dual graph yields the original graph. Figure 2-2 gives an example of a graph and its dual graph.

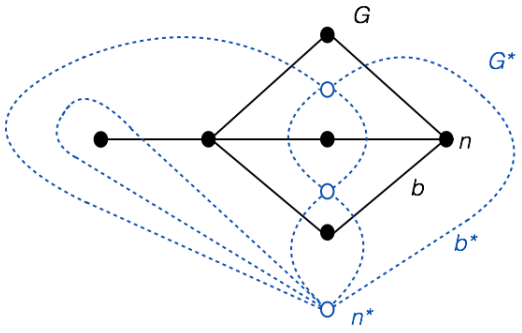

Figure 2-2: Example of a graph (solid lines, closed dotes) and its dual graph (dashed lines, open dotes).

2-2-2 Representing electrical networks

Modelling electrical networks starts off with applying the two fundamental laws in network theory, the Kirchhoff laws, to the network. The Kirchhoff laws are formulated in a number of equivalent ways and can be mathematically represented by the incidence matrix. As mentioned earlier, a constructive approach to express the Kirchhoff laws of the network in any form is to transform the circuit into a network graph. To that end, this section first presents the transformation from the electrical circuit to the network graph. Subsequently, we deal with the representations of the Kirchhoff laws and introduce the incidence matrix. Finally, a procedure to get from the Kirchhoff laws to the kernel representation is given.

Network graphs

The network graph[7] of an electrical circuit suppresses the information on the type of component and considers only the voltage (cross variable) and the current (through variable). The voltage (v) is a cross variable, because it is defined as the difference between the potentials on the two sides of an element. Similarly, the current (i) is a through variable, because it goes through the element. The fact that these variables change as a function of time in a linear or nonlinear way does not affect the geometric interconnection of these variables with one another. For instance, two components in series share the same current regardless how this changes as function of time. Hence, a circuit is replaced by a graph where the currents are the branches and the potentials (λ) are the nodes. In the dual graph, the voltages are the dual branches (b^*) and the loop currents[8] (i_L), the dual nodes (n^*). Figure 2-3 gives an example of an electrical circuit and its network graph and dual network graph. In the graph the potentials at each interconnection of the elements in the network have become the nodes and the currents became the branches [15, Ch.1.5]. Likewise, in the dual graph the loop currents (not depicted in the network) have become the nodes and the voltages became the branches.

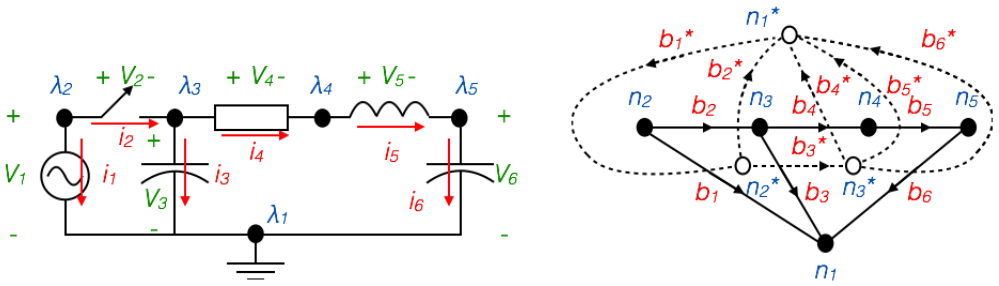

(a) The circuit. **(b)** The network graph.

Figure 2-3: Example of an electrical circuit and its network graph.

The voltages and currents in an electrical network have a direction depending on the reference chosen. The directions of the voltages and currents is represented in the network graph by giving the branches an orientation, indicated by the arrow in the branch (the network graph is a directed or orientated graph). Henceforth, we mean by graph, a network graph, since in the following all graphs are network graphs. By definition, the current flows from the higher potential (+ sign) to the lower potential (- sign) of the element [15, Ch.5.1]. Consequently, by fixing the direction of the current, the reference direction of the voltage is fixed and *vice versa*.

The Kirchhoff laws

Several (equivalent) formulations exist for the Kirchhoff laws. For this thesis the following formulation is adopted [15, Ch4.1]:

[7] Also known as the circuit graph or digraph.
[8] The current in a cycle (loop).

> **Kirchhoff's voltage law (KVL)**: For all connected lumped circuits, for all closed node sequences and for all times t, the algebraic sum of all the node-to-node voltages around the chosen closed node sequence (loop) is zero.
> **Kirchhoff's current law (KCL)**: For all connected lumped circuits and for all times t, the algebraic sum of the currents leaving any node is equal to zero.

Sometimes a more general form is advocated for these laws from the perspective of the graph. Although these forms essentially define the same laws, we treat the generalised form and the more regular form (above) as two different concepts. The generalised form reads as [5]:

> **Kirchhoff's cycle law (CL)**: The sum of cycle variables (cross variables, node-to-node variables) along any cycle (i.e., chains of branches with a common start and end node) in the graph is equal to zero.
> **Kirchhoff cocycle law (CCL)**: The sum of cocycle variables (through variables, branch variables) along any cocycle (set of branches which splits the nodes of the graph into two disjoint sets) in the graph is equal to zero.

Clearly, the CL is equal to the KVL and the CCL to the KCL for the graph. However, for the dual graph the CCL yields the KVL and the CL the KCL. We advocate the following point of view in this thesis: the KVL and KCL are the two fundamental laws that the circuit must satisfy, while the CL and the CCL are viewed as two methods to obtain these laws from the graph and dual graph.

This difference in viewpoint becomes apparent in the mathematical formulation of the interconnection of the circuit. The interconnection of any connected network graph, which does not contains a self-loop[9] can be represented by a matrix, called the incidence matrix [15, Ch.6.2]. Both the CL and the CCL yield an incidence matrix, but commonly the matrix is derived by applying the CCL.

Incidence matrix [15, Ch.6.2]: Let N_b be the number of branches and N_n the number of nodes in a graph, G. Then, the incidence matrix, $A(G) \in \mathbb{R}^{N_n \times N_b}$, is defined as follows:

$$a_{k\ell} = \begin{cases} +1 & \text{if branch } \ell \text{ leaves node } k, \\ -1 & \text{if branch } \ell \text{ enters node } k, \\ 0 & \text{otherwise,} \end{cases} \tag{2-14}$$

for $k = 1, 2, \ldots, N_n$ and $\ell = 1, 2, \ldots, N_b$.

Consequently, the CCL reads as

$$A(G)C_{cocy} = 0, \tag{2-15}$$

where C_{cocy} is the vector containing all cocycle variables (branches, dual branches). Since, the CL the is dual of this equation [15, Ch.6.3], its incidence matrix is related to (2-15) by a transpose operation, such that

$$A^T(G)N = C_{cy},$$

where N is the vector containing all the nodes and C_{cy} the vector containing all the node-to-node variables.

[9] A self-loop generates a zero row in the incidence matrix and as a result the corresponding current is a free variable.

This leads to the following observation: the CL leads to an image representation of a graph, while the CCL leads to a kernel representation of a graph. Applying the CCL on the graph of a circuit yields the KCL in kernel formulation and applying the CCL on the dual graph of a circuit yields the KVL in kernel formulation. Equivalently, applying the CL on the graph and dual graph yields the KCL and KVL in an image representation. Let I denote the vector of currents, V the vector of voltages, Λ the vector of potentials and I_L the vector of loop currents. Then, the KVL in image and kernel representation is, respectively,

$$A^T(G)\Lambda = V, \tag{2-16}$$
$$A(G^*)V = 0. \tag{2-17}$$

And the KCL in image and kernel representation is, respectively,

$$A^T(G^*)I_L = I, \tag{2-18}$$
$$A(G)I = 0. \tag{2-19}$$

Thus, (2-17) and (2-19) are the mathematical representations corresponding to the formulation of the KVL and the KCL defined above.

The relationship between Kirchhoff's laws and Dirac structures

Equations (2-17) and (2-19) capture the interconnection of the electrical network in a kernel representation, which bears a close resemblance to the kernel representation of the Dirac structure in (2-1). In fact, (2-17) and (2-19) already form a Dirac structure in the following manner

$$\mathcal{D} = \{(I, V) \mid A(G)I = 0,\ A(G^*)V = 0\}. \tag{2-20}$$

The kernel representation of the Dirac structure, defined by (2-1), follows easily from (2-20). First, combine (2-17) and (2-19) to form an equation of the same form as (2-2) [6]. This leads to

$$\underbrace{\begin{bmatrix} A(G) \\ \mathbb{O} \end{bmatrix}}_{\hat{F}} I + \underbrace{\begin{bmatrix} \mathbb{O} \\ A(G^*) \end{bmatrix}}_{\hat{E}} V = 0. \tag{2-21}$$

Clearly, (2-21) is of the same form as (2-2). However, some elements in I and V are efforts and others are flows depending on the type of element and their location in the network. For instance, an inductor's flow is a voltage ($\dot{\phi}$) and a capacitor's flow a current ($\dot{q}$), see Table A-1. Subsequently, transform (2-21) to

$$\begin{bmatrix} \hat{F}_f & \hat{F}_e \end{bmatrix} \begin{bmatrix} I_f \\ I_e \end{bmatrix} + \begin{bmatrix} \hat{E}_e & \hat{E}_f \end{bmatrix} \begin{bmatrix} V_e \\ V_f \end{bmatrix} = 0, \tag{2-22}$$

where the elements of I and V corresponding to flows and efforts are stacked into the vectors I_f and V_f, and I_e and V_e, respectively. The columns of the matrices $\hat{F}$ and $\hat{E}$ are grouped accordingly. Then, swapping the columns $\hat{F}_e$ with the columns $\hat{E}_f$ and their corresponding vectors I_e and V_f yields

$$\underbrace{\begin{bmatrix} \hat{F}_f & \hat{E}_f \end{bmatrix}}_{F} \underbrace{\begin{bmatrix} I_f \\ V_f \end{bmatrix}}_{f} + \underbrace{\begin{bmatrix} \hat{E}_e & \hat{F}_e \end{bmatrix}}_{E} \underbrace{\begin{bmatrix} V_e \\ I_e \end{bmatrix}}_{e} = 0, \tag{2-23}$$

which is (2-2) again. Thus, a Dirac structure in the form of (2-20) can be systematically transformed into the kernel representation of a generalised port-Hamiltonian system given by (2-1). Do note that a kernel representation derived with the incidence matrices is non-minimal. Henceforth, we mean by kernel representation a relaxed kernel representation, because they are all non-minimal.

It should be noted that the Dirac structure of an electric network can also be expressed in an image representation or a combination of both the kernel and image representations by using any combination of (2-16)-(2-19). However, the image representation of either the KVL or KCL, does not yield the required interconnection of the voltages and currents, i.e., they do not naturally (directly) yield the sums of efforts and flows that form the dynamical equations of the system. On the contrary, any combination of the kernel and image representations does provide enough information to reconstruct the graph, but this is not the objective in this case. Concluding, only the kernel representation contains all the relations to form the set of equations describing the dynamical, electrical system.

2-2-3 Representing switching networks

Power converters have hybrid dynamics, because they contain switching elements. This section presents the modelling theory for systems with switching elements. There exist two fundamental viewpoints to include switching elements in the port-Hamiltonian framework. The first comes from Escobar et al. [4], where the switches are modelled as non-linear elements. This leads to an ISO system with additional input-output pairs for the switches. The other comes from Magos et al. [5] and Valentin et al. [6, 7], where the switches are viewed as virtual elements that change the Dirac structure. This viewpoint leads to a parametrised Dirac structure and the *parametrised incidence matrix*. First, the viewpoint from [4] is explained. Subsequently, we elucidate the method from [5, 6, 7] to parametrise the Dirac structure.

Switches as non-linear elements

Escobar and co-workers model switching systems by considering a fixed graph with the switches (and diodes) as nonlinear components. This means that the Dirac structure (the interconnection) does not change with switch state. As the switching elements neither belong to $\mathcal{S}$ or $\mathcal{R}$, they form their own structure $\mathcal{W}$, see Figure 2-4. The switching structure $\mathcal{W}$ is connected to the rest of the system by the Dirac structure through the port $(f_{\mathcal{W}}, e_{\mathcal{W}})$. This explains why the system has an additional input-output couple.

Let $(\cdot)_{\mathcal{W}}$ denotes a port variable belonging to a switching element. With this viewpoint the Dirac structure of a switching system in kernel representation is [12]

$$\begin{aligned}\mathcal{D} = \{&(f_{\mathcal{S}}, e_{\mathcal{S}}, f_{\mathcal{R}}, e_{\mathcal{R}}, f_{\mathcal{P}}, e_{\mathcal{P}}, f_{\mathcal{W}}, e_{\mathcal{W}}) \in \mathcal{F}_{\mathcal{S}} \times \mathcal{E}_{\mathcal{S}} \times \mathcal{F}_{\mathcal{R}} \times \mathcal{E}_{\mathcal{R}} \times \mathcal{F}_{\mathcal{P}} \times \mathcal{E}_{\mathcal{P}} \times \mathcal{F}_{\mathcal{W}} \times \mathcal{E}_{\mathcal{W}} \\ &\mid F_{\mathcal{S}} f_{\mathcal{S}} + E_{\mathcal{S}} e_{\mathcal{S}} + F_{\mathcal{R}} f_{\mathcal{R}} + E_{\mathcal{R}} e_{\mathcal{R}} + F_{\mathcal{P}} f_{\mathcal{P}} + E_{\mathcal{P}} e_{\mathcal{P}} + F_{\mathcal{W}} f_{\mathcal{W}} + E_{\mathcal{W}} e_{\mathcal{W}} = 0\}\,.\end{aligned} \tag{2-24}$$

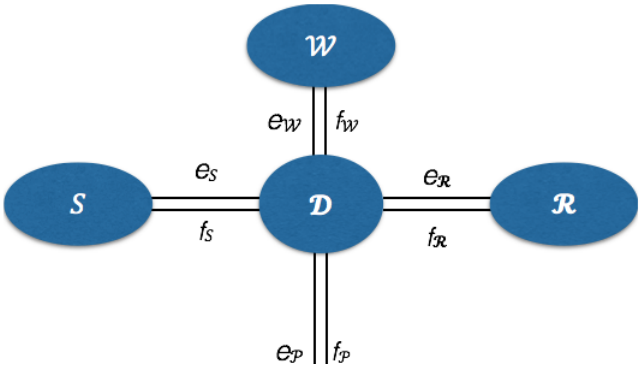

Figure 2-4: A port-Hamiltonian system with the switches as nonlinear elements.

The ISO model associated with (2-24) (assuming (2-24) admits this structure) is[10] [4]

$$\begin{aligned} \dot{x} &= J\frac{\partial H}{\partial x}(x) + gu + g_{\mathcal{R}} f_{\mathcal{R}} + g_s u_{\mathcal{W}}(s), \\ \begin{bmatrix} y \\ e_{\mathcal{R}} \\ y_{\mathcal{W}}(s) \end{bmatrix} &= \begin{bmatrix} g^T \\ g_{\mathcal{R}}^T \\ g_{\mathcal{W}}^T \end{bmatrix} \frac{\partial H}{\partial x}(x) + Z \begin{bmatrix} u \\ u_{\mathcal{R}} \\ u_{\mathcal{W}}(s) \end{bmatrix}, \end{aligned} \tag{2-25}$$

where Z is the direct feedthrough matrix and $s \in \{0, 1\}$ denotes the switch state. Figure 2-5 gives the constitutive relation of the ideal switch presented in [4]. Substituting the constitutive relation of the switching elements into the system and computing the dynamical equations for each switch configuration yields an ISO model, parametrised by the switch state s, of the form

$$\begin{aligned} \dot{x} &= J(s)\frac{\partial H}{\partial x}(x) + g(s)u + g_{\mathcal{R}}(s) f_{\mathcal{R}}, \\ y &= g^T(s)\frac{\partial H}{\partial x}(x), \\ e_{\mathcal{R}} &= g_{\mathcal{R}}^T(s)\frac{\partial H}{\partial x}(x). \end{aligned} \tag{2-26}$$

Switches as virtual elements

Valentin, Magos and Maschke [5, 6, 7] propose a different viewpoint in the modelling of switching elements. They view and model the switches in a switching network as virtual elements, because, in terms of the graph, these switches merge or disjoin the nodes connected by their branches. For example, the circuit from Figure 2-3 yields the graph in Figure 2-6a for $s = 1$ (closed) and yields the graph in Figure 2-6b for $s = 0$ (open). As such, the graph of a switching system Σ consists out of two subgraphs, a virtual graph ($G_v \subset G$) and a reference graph ($G_r \subset G$). The virtual graph contains all the nodes and branches corresponding to the switches and the reference graph contains all the nodes and branches corresponding to the

[10] The LCR networks considered in [4] contain only linear elements and therefore none of the matrices, J, g, $g_{\mathcal{R}}$, g_s depend on the state x.

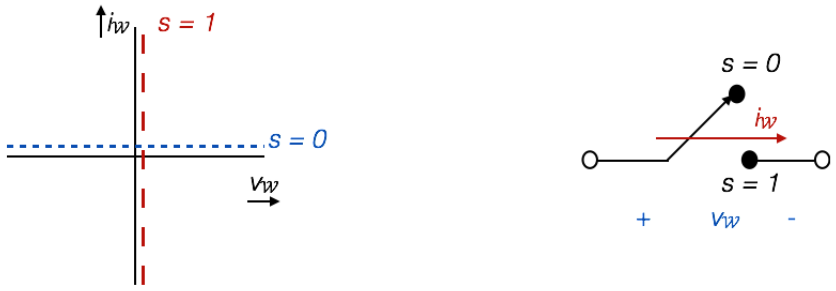

(a) The constitutive relation. **(b)** The ideal switch.

Figure 2-5: The constitutive relation of an ideal switch.

functional elements, which is the same as the graph with all switches open. For example, in the case of Figure 2-6, the reference graph is the graph in Figure 2-6b and the virtual graph (which is not shown) consists of the nodes n_1, n_2 and the branch b_2.

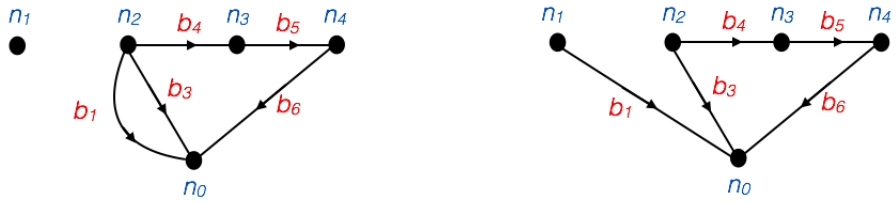

(a) Switch closed ($s = 1$). **(b)** Switch open ($s = 0$).

Figure 2-6: The graphs of the electrical network in Figure 2-3 for each switch configuration.

Since, the elements of the virtual graph can only merge or disjoin nodes from the reference graph, the graph for a specific switch configuration is a transformation of the reference graph. The incidence matrix corresponding to a switch configuration is obtained by linear transformation of the incidence matrix of the reference graph [5]. To clarify this, consider the incidence matrices corresponding to the graph in Figure 2-6a,

$$A_{s=1}(G) = \begin{bmatrix} -1 & -1 & 0 & 0 & -1 \\ 0 & 0 & 0 & 0 & 0 \\ 1 & 1 & 1 & 0 & 0 \\ 0 & 0 & -1 & 1 & 0 \\ 0 & 0 & 0 & -1 & 1 \end{bmatrix},$$

and Figure 2-6b,

$$A_{s=0}(G) = \begin{bmatrix} -1 & -1 & 0 & 0 & -1 \\ 1 & 0 & 0 & 0 & 0 \\ 0 & 1 & 1 & 0 & 0 \\ 0 & 0 & -1 & 1 & 0 \\ 0 & 0 & 0 & -1 & 1 \end{bmatrix}.$$

$A_{s=1}(G)$ follows from $A_{s=0}(G)$ by multiplying $A_{s=0}(G)$ from the left with the transformation matrix

$$A_T(G) = \begin{bmatrix} 1 & 0 & 0 & 0 & 0 \\ 0 & 0 & 0 & 0 & 0 \\ 0 & 1 & 1 & 0 & 0 \\ 0 & 0 & 0 & 1 & 0 \\ 0 & 0 & 0 & 0 & 1 \end{bmatrix}.$$

For this network it is easy to see that a transformation matrix can be formulated, parametrised by the switch state,

$$A_T(G)(S) = \begin{bmatrix} -1 & 0 & 0 & 0 & 0 \\ 0 & 1-s & 0 & 0 & 0 \\ 0 & s & 1 & 0 & 0 \\ 0 & 0 & 0 & 1 & 0 \\ 0 & 0 & 0 & 0 & 1 \end{bmatrix},$$

such that $A_{s=0}(G) = A_T(G)(S)A_{s=0}(G)$ for $s = 0$ and $A_{s=1}(G) = A_T(G)(S)A_{s=0}(G)$ for $s = 1$.

Parametrised incidence matrix (PIM) [5]: For a general switching electric network Σ with N_s number of switches it is possible to obtain a single incidence matrix, parametrised by $S = (s_1, \ldots, s_{N_s})^T \in \{0, 1\}^{N_s}$, that yields the incidence matrice of the graph for each switch configuration through

$$A(G)(S) = A_T(G)(S)A(G_r), \tag{2-27}$$

where $A(G)(S)$ is the parametrised incidence matrix (PIM), $A_T(G)(S)$ the transformation matrix, which is parametrised by the switch state, $A(G_r)$ the incidence matrix of the reference graph and S the vector containing all the switch states. Given that Σ satisfies the following assumptions [5, 6, 7]:

Assumption 1. The graph associated with Σ is planar.

Assumption 2. The graph associated with Σ is cyclically connected.

Assumption 3. The graph associated with Σ has no self-loop.

Assumption 4. The outdegree of each node in G_v is below or equal to one.

Assumption 5. All virtual nodes are indexed such that, in an oriented sequence of virtual branches, one branch has a index number lower than its predecessor.

Assumption 1 provides that a dual exists, which means that (2-17) can be used and the kernel representation be derived. Assumption 2 ensures that a closed-loop exists for each element in the electrical network. Assumption 3 follows from the definition of an incidence matrix. Assumption 4 grantees that the merging of more than one switch (a sequence of switches or switches in parallel) realised by a linear transformation, groups all the nodes connected to the switches. Finally, Assumption 5 ensures that the transformation matrix respects the merging of the nodes when a sequence of switches is closed.

Parametrised transformation matrix [6]: For each switch s_j, $j \in \{1, \ldots, N_s\}$ there exists a virtual branch, $b_v = (n_k, n_\ell)$, $(k, \ell) \in \{1, \ldots, N_n\}^2$, with a disconnection-reconnection

matrix $M_j(G)(s_j)$ of dimension $N_n \times N_n$. The elements within this disconnection-reconnection matrix are defined by

$$M_j(G)(s_j)_{m,n} = \begin{cases} s_j & \text{if } m = \ell,\ n = k \text{ and } k \neq \ell, \\ -s_j & \text{if } m = n = k,\ \text{and } k \neq \ell, \\ 0 & \text{otherwise,} \end{cases} \tag{2-28}$$

with $(m, n) \in \{1, \ldots, N_n\}^2$. The transformation matrix is given by

$$A_T(G)(S) = \prod_{j=1}^{N_s} (I^{N_n \times N_n} + M_j(s_j)). \tag{2-29}$$

Substituting (2-29) into (2-27) we find that

$$A(G)(S) = \prod_{j=1}^{N_s} (I^{N_n \times N_n} + M_j(s_j)) A(G_r). \tag{2-30}$$

The procedure is the same to find the matrices of the dual graph, denoted by $A(G^*)(S^*)$, $A_T(G^*)(S^*)$, $S^* = \{s_1^*, \ldots, s_{N_s}^*\}$ etc.

Admissible switch configurations: The method from [5, 6, 7] views each of the switches as an independent switch, i.e., a switch with a switch state that is independent of all the other switch states. This viewpoint leads to the result that not all switch configurations are feasible or admissible in the model. *Non-admissible configurations* are [5, 17, Ch.1.1.1]

1. A voltage source in short-circuit or several independent voltage sources connected in parallel.
2. A current source in open-circuit or several independent current sources connected in series.

In this thesis we include dependency between (some of) the switches, which in many cases removes the issue of non-admissible configurations. Nonetheless, for completeness, we always give the admissible configuration set in which the Dirac structure is valid. The set of *admissible configurations* is denoted by $\mathcal{A}(\Sigma)$. The non-admissible configurations are easily detected from the PIM of the graph for voltage sources and from the PIM of the dual graph for the current sources [5], because a voltage source in short-circuit or a current source in open-circuit makes the corresponding column in the PIM equal to zero. Moreover, independent voltage sources in parallel or current sources in series make the corresponding columns equal or opposite of each other. To conclude, the PIMs together with $\mathcal{A}(\Sigma)$ form a Dirac structure in the form of (2-20) which is transformed to the kernel representation by following (2-21)-(2-23). This leads to the Dirac structure of a switching system parametrised by the switch state given as

$$\mathcal{D}(S) = \{(f, e) \in \mathcal{F} \times \mathcal{E} \mid F(S)f + E(S)e = 0\},\ S \in \mathcal{A}(\Sigma). \tag{2-31}$$

2-3 Modelling power converters

The required theory for the modelling of power converters have been discussed in the previous two sections. Summarising and combining this theory allow us to postulate two methods to model power converters from a fundamental PH viewpoint. These two techniques differ in the way they view and approach the modelling of the switches. One uses the approach from [4], in which the switches are modelled as nonlinear elements and is referred to as the *nonlinear element method* (NEM). The other uses the theory from [5, 6, 7], in which the switches are modelled as virtual elements and is referred to as the *virtual element method* (VEM). First, Section 2-3-1 presents the VEM. Subsequently, Section 2-3-2 presents the NEM. Finally, Section 2-3-3 further adapts these methods to be suitable for the modelling of three-phase power converters.

2-3-1 The virtual element method

The modelling of power converters with the VEM consists of the following procedure:

1. Express the electrical network in a graph and dual graph. Consider the switches to be virtual elements that merge or separate nodes in the graph and the dual graph. Split both graphs into two subgraphs: a virtual graph with all the virtual branches and corresponding nodes, and a reference graph with the functional branches and corresponding nodes.

2. Apply the Kirchhoff cocycle law to the reference graph of the graph and the dual graph, in order to obtain the reference incidence matrix with (2-14) for both the graph and dual graph. Furthermore, define the transformation matrix parametrised by the switch state with (2-28) and (2-29) for G and G_v. Then, combine the reference matrix and the disconnection-reconnection matrix with (2-27) to find the parametrised incidence matrices of the network.

3. Use the PIMs of the graph and the dual graph to express the Dirac structure in a kernel representation (2-31) by using (2-20)-(2-23).

4. Convert the implicit PH system in (2-31) into a set of DAEs of the form (2-5) or when possible into ISO form (2-7) by solving (2-2) for the states and outputs.

The advantage of this method is that the parametrisation is achieved in an algorithmic and structured way. However, this algorithmic approach can lead to complex and incomprehensible parametrisations, which means that the change of the Dirac structure as a function of the switch state can be difficult to interpret and that the resulting parametrised model might not be one that is expected.

2-3-2 The nonlinear element method

The modelling of PH, switching systems with the NEM consists of the following procedure:

1. Transform the electrical network into its graph and dual graph. Consider the switches to be nonlinear elements with their own current and voltage.
2. Apply the Kirchhoff cocycle law to find the incidence matrix of both the graph and the dual graph.
3. Use the incidence matrices to express the Dirac structure of the system in a kernel representation conform (2-31) by using (2-20)-(2-23).
4. Convert the implicit PH system in (2-3) into a set of DAEs (2-5) and if possible to an ISO model (2-25) by solving (2-2) for the states and outputs (the switch ports are also an input-output pair). Do note that the switches will lead to a direct feedthrough matrix.
5. Compute the model for each switch state to find the parametrised (in terms of the switch state) representation.

Technically speaking, using the graphs and dual graphs is not obligatory to obtain the KVL and KCL, and thereby the E and F matrices. For simple networks, the correct KVL and KCL equations are easily deducted from the network directly, but working with the graphs provides a structured approach to find the incidence matrices that works for every general network, however complicated. The advantage should become obvious when modelling multi-phase power converters with large and complex loads (for instance, multi-level converters [17] or cyclo-converters with detailed load models [8, Ch.21, 23.4] and [18].).

The advantage of this method is that the graph only needs to satisfy Assumptions 1-3. On the other hand, the characteristic equation is not parametrised by the switch state. To get a model parametrised by the switch state the dynamical behaviour must be computed for each switch state and the parametrisation deduced from the results. Although it lacks the algorithmic parametrisation of the equations, this method can accommodate non-ideal switches without any adjustment, because the constitutive relation is not predefined. In the VEM the switches are automatically assumed to be ideal.

2-3-3 The augmentation for three-phase power converters

This section shows that the two modelling methods formulated in the previous two sections cannot be applied in their current form for the modelling of three-phase inverter and the three-phase rectifier. Hence, an augmentation to the methods is proposed.

The problem with three-phase power converters

The most important assumption for the two modelling methods is that the graph is planar. However, both the three-phase rectifier and inverter are not planar. Consider the general three-phase inverter in Figure 2-7a with an unspecified DC source and an unspecified load in Δ-(delta-)connection. A direct transformation of the network in Figure 3-1 to its graph yields the graph in Figure 2-7b[11]. The switches are modelled as virtual elements (denoted

[11] Obviously, the topology and graph of a general three-phase rectifier are essentially the same. Therefore, the conclusions also apply to the rectifier.

by blue branches), but the conclusions also apply if they are viewed as nonlinear elements. Clearly, the graph is not planar and therefore the dual graph does not exist. This has to

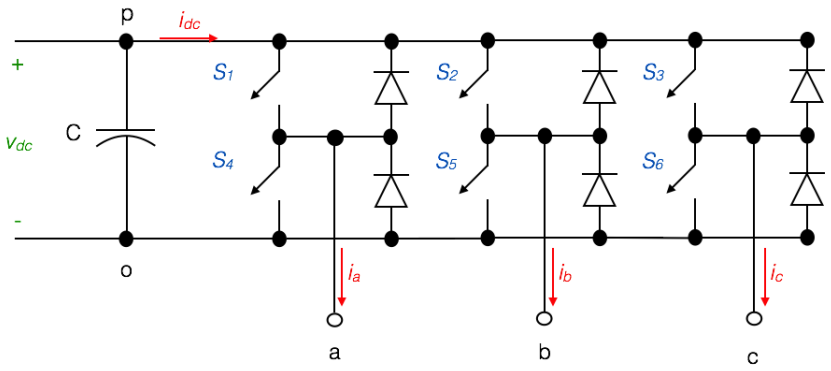

(a) Topology of a general three-phase inverter.

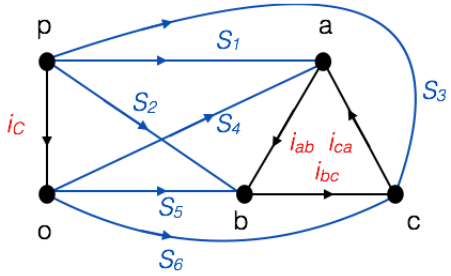

(b) The graph of a general three-phase inverter.

Figure 2-7: The topology and graph of a general three-phase inverter to show the non-planarity of the system.

do with the fact that the interconnection of the DC-source with a three-phase output, Δ- or Y-(star-)connected, cannot be achieved such that the connection is planar. Consequently, the KVL (2-17) cannot be obtained. Apart form violating Assumption 1, the virtual graph also violates Assumptions 4 and 5. The later observation is not important if the switches are modelled as nonlinear elements. In the original papers that consider the PH modelling of DC/DC converters this problem does not arise, because these power converters are always planar. This problem does not occur for DC/DC converter, because their graphs are always planar.

The adaptation for the modelling of three-phase power converters

A solution to the violation of Assumption 1 is to adapt the method such that it can cope with non-planar graphs. A intuitive first attempt is to draw the graphs in three dimensions and thereby avoid any crossing of the branches. Expressing the interconnection of a higher dimensional graph could potentially be done with *tensors*. Tensors are - in simple terms - the generalisation of vectors and matrices [19, Ch.10] and might be used to express three dimensional graphs. However, a different and more straightforward solution is already avail-

able within the PH framework. This solution involves exploiting the compositionality of PH systems. In specific, a non-planar system can divided into individual planar subsystems. The combined model can then be represented using the theory discussed in Section 2-1. We arrive at the following proposition.

Proposition 1. *Consider an electrical switching system Σ with a non-planar network graph, G, and N_s number of switches. Decompose the system into k subsystems, $\Sigma_1, \dots, \Sigma_k$, such that their corresponding graphs $G_{\Sigma_1}, \dots, G_{\Sigma_k}$ are planar and satisfy the additional assumptions (Assumption 2-5 for the VEM or Assumption 2-3 for the NEM). Each separation of the system results in a port in the two created subsystems, which is represented by a branch and a node-to-node variable in the associated graphs of which the interconnection is represented by an interconnection Dirac structure, $\mathcal{D}_I$. Then, the Dirac structure of the total system in kernel representation is described by*

$$\mathcal{D}(S) = \{(f,e) \in \mathcal{F} \times \mathcal{E} \mid F(S)f + E(S)e = 0\}, \ S \in \mathcal{A}(\Sigma), \tag{2-32}$$

where $F(S) = [\tilde{F}^T(S) \ F_I^T]^T$ and $E(S) = [\tilde{E}^T(S)^T \ E_I^T]^T$,

$$\tilde{F}(S) = \begin{bmatrix} F_{\Sigma_1}(S_1) & \mathbb{O} & \cdots & \mathbb{O} \\ \mathbb{O} & F_{\Sigma_2}(S_2) & \cdots & \mathbb{O} \\ \vdots & \vdots & \ddots & \vdots \\ \mathbb{O} & \mathbb{O} & \cdots & F_{\Sigma_k}(S_k) \end{bmatrix},$$

$$\tilde{E}(S) = \begin{bmatrix} E_{\Sigma_1}(S_1) & \mathbb{O} & \cdots & \mathbb{O} \\ \mathbb{O} & E_{\Sigma_2}(S_2) & \cdots & \mathbb{O} \\ \vdots & \vdots & \ddots & \vdots \\ \mathbb{O} & \mathbb{O} & \cdots & E_{\Sigma_k}(S_k) \end{bmatrix},$$

with $S = [S_1^T, \dots, S_k^T]^T \in \{0,1\}^{N_s}$ (which is empty in case of the NEM, because the switches have an effort and flow) and F_I, E_I are the matrices of the characteristic equation of $\mathcal{D}_I$ containing the interconnection the subsystems. The effort and flow vectors are composed of the effort and flow vectors of the subsystems. The matrices $F_{(\cdot)}(S)$ and $E_{(\cdot)}(S)$ are composed of the columns of the corresponding (parametrised) incidence matrices $A(G_{(\cdot)}(S)$ and $A(G^*_{(\cdot)}(S)$ associated with flows and efforts respectively, i.e.,

$$F_{(\cdot)}(S) = \begin{bmatrix} A_f(G_{(\cdot)})(S) \\ A_f(G^*_{(\cdot)})(S) \end{bmatrix}, \text{ and } E_{(\cdot)}(S) = \begin{bmatrix} A_e(G_{(\cdot)})(S) \\ A_e(G^*_{(\cdot)})(S) \end{bmatrix},$$

where the subscripts f and e denote that the matrix is composed of columns associated with flows and efforts, respectively.

Chapter 3

Modelling the three-phase inverter

This Chapter deals with deriving the model of a three-phase inverter. As presented in the previous Chapter, there are two methods to model the power converter, the VEM and the NEM. The primary difference being the viewpoint taken to model the switches. Both these methods are used to model the power converter in this chapter. In general, the methods summarise to the following: (i) determining the subsystems and their graphs, (ii) expressing the Dirac structure of the system in a kernel representation with the (parametrised) incidence matrices of the graphs, (iii) solving the characteristic equation of the kernel representation to obtain the system as a set of differential algebraic equations (DAEs), (iv) rewrite the set of DAE into a set of explicit differential equations; the input-state-output (ISO) representation. First, the reference model of the inverter is introduced in Section 3-1. Second, the modelling of the three-phase inverter with the VEM is presented in Section 3-2. Finally, Section 3-3 deals with the modelling of the three-phase inverter with the NEM.

3-1 The reference model for the three-phase inverter

This section presents the reference (PH) model of a three-phase inverter. Both the model of general three-phase inverter and a three-phase inverter with a load are included in this section. The mathematical model for the general three-phase inverter in Figure 2-7a is

$$\begin{aligned} i_{dc} &= s_a i_a + s_b i_b + s_c i_c, \\ v_{ab} &= (s_a - s_b) v_{dc}, \\ v_{bc} &= (s_b - s_c) v_{dc}, \\ v_{ca} &= (s_c - s_a) v_{dc}, \end{aligned} \tag{3-1}$$

where $s_a, s_b, s_c \in \{0, 1\}$, which are 0 when the lower switch is in the leg is closed and 1 when the upper switch in the leg is closed[1]. This general model of an inverter is taken from Holmes et al. [17]. For its derivation and further details see Appendix B-1.

[1] This definition for s_a, s_b, s_c shall be used for the rest of the thesis.

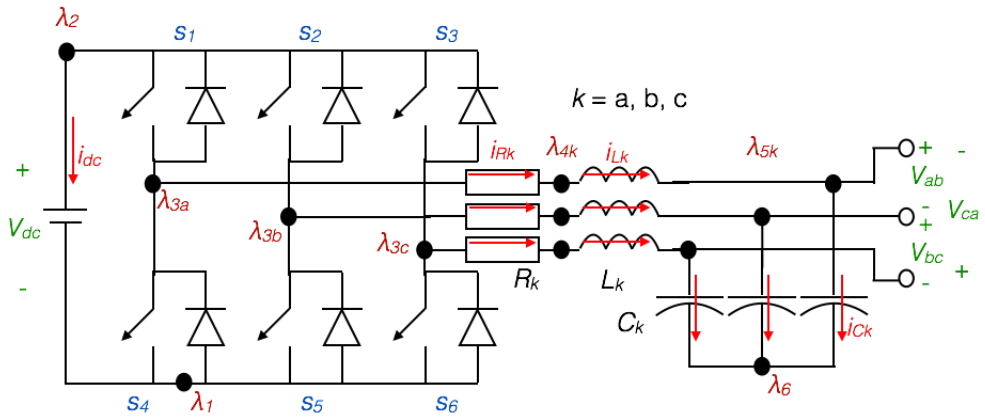

Figure 3-1: The three-phase inverter topology.

Figure 3-1 depicts the network of the three-phase inverter from Mu et al. [10, 11], see Appendix B-2 for further details. The subscript L denotes the load and the network is assumed to be balanced, i.e., $R_a = R_b = R_c = R$, $L_a = L_b = L_c = R$ and $C_a = C_b = C_c = C$. The corresponding Hamiltonian of the system is

$$H(q,\phi) = \sum_{j=a,b,c,} \left(\frac{1}{2}\frac{\phi_j^2}{L} + \frac{1}{2}\frac{q_j^2}{C} \right), \tag{3-2}$$

where $\phi = (\phi_a \ \phi_b \ \phi_c)^T$ denotes the flux-linkage across the inductors and $q = (q_a \ q_b \ q_c)^T$ the charge in the capacitors. The PH-ISO model reads as

$$\begin{aligned}
\begin{bmatrix} \dot{q} \\ \dot{\phi} \end{bmatrix} &= \begin{bmatrix} 0 & 0 & 0 & 1 & 0 & 0 \\ 0 & 0 & 0 & 0 & 1 & 0 \\ 0 & 0 & 0 & 0 & 0 & 1 \\ -1 & 0 & 0 & -R & 0 & 0 \\ 0 & -1 & 0 & 0 & -R & 0 \\ 0 & 0 & -1 & 0 & 0 & -R \end{bmatrix} \begin{bmatrix} \frac{\partial H}{\partial q}(q,\phi) \\ \frac{\partial H}{\partial \phi}(q,\phi) \end{bmatrix} + \begin{bmatrix} \mathbb{O}^{3\times 1} \\ \hat{s}_a \\ \hat{s}_b \\ \hat{s}_c \end{bmatrix} v_{dc} \\
&\quad + \begin{bmatrix} -\mathbb{I}^{3\times 3} \\ \mathbb{O}^{3\times 3} \end{bmatrix} \begin{bmatrix} i_{La} \\ i_{Lb} \\ i_{Lc} \end{bmatrix}, \\
i_{dc} &= \begin{bmatrix} \mathbb{O}^{1\times 3} & \hat{s}_a & \hat{s}_b & \hat{s}_c \end{bmatrix} \begin{bmatrix} \frac{\partial H}{\partial q}(q,\phi) \\ \frac{\partial H}{\partial \phi}(q,\phi) \end{bmatrix}, \\
\begin{bmatrix} v_{ao} \\ v_{bo} \\ v_{co} \end{bmatrix} &= \begin{bmatrix} -\mathbb{I}^{3\times 3} & \mathbb{O}^{3\times 3} \end{bmatrix} \begin{bmatrix} \frac{\partial H}{\partial q}(q,\phi) \\ \frac{\partial H}{\partial \phi}(q,\phi) \end{bmatrix},
\end{aligned} \tag{3-3}$$

where $\hat{s}_j = s_j - \frac{1}{3}\sum_{k=a,b,c} s_k$, $j \in \{a,b,c\}$. Although the reference model is given for a balanced system, we start with modelling this system for the unbalanced case to start with as least

assumptions as possible. From this general model we subsequently derive the model for a balanced system. For the sake of simplicity, the elements are assumed to be linear and the load connected in Δ-connection.

3-2 Modelling the inverter with the vitual element method

This section features the modelling of the three-phase inverter with the switches viewed as virtual elements. First, we discuss the separation of the system into planar subsystems and their representations in Section 3-2-1. Subsequently, the Dirac structure is formulated and analysed in Section 3-2-2. Next, Section 3-2-3 deals with solving the characteristic equation of the Dirac structure. This leads to a set of DAEs. Finally, this differential-algebraic model (DAM) is transformed into an ISO system by assuming a balanced load in Section 3-2-4.

3-2-1 Separating the system into planar subsystems

We divide the system into three planar subsystems, Σ_1, Σ_2 and Σ_3, see Figure 3-2. The separation of Σ_1 and Σ_2 removed the non-planar interconnection. As a result, the single voltage source is now modelled as three independent voltage sources from the perspective of Σ_2. Subsystem Σ_1 couples these three independent ports to a single DC source. The separation into $\Sigma_1, \Sigma_2, \Sigma_3$ underpins the modularity of this approach, because the DC (Σ_1) or AC (Σ_3) side can simply be replaced.

Subsystems Σ_1 and Σ_3 do not contain any switches and, therefore their graphs need to satisfy Assumptions 1-3. Figures 3-3 and 3-6 depict the resulting graph and dual graph for Σ_1 and Σ_3, respectively. For clarity, the branches corresponding to an interconnection port have the additional subscript p. From observation of Σ_2 follows that Σ_2 is symmetrical for every DC to line-to-line AC output jk with $jk \in \{ab, bc, ca\}$. Splitting Σ_2 provides three identical, smaller subsystems, which are easier to model. Figure 3-4 shows the identical networks in the network of Σ_2 and Figure 3-5 gives the graph and the dual graph of the identical networks. The (dual) branches for the virtual elements are denoted with the blue lines and the (dual) branches for the functional elements with black lines. Furthermore, the branches b_{s1} and b_{s2} resemble the upper switches S_1, S_2, S_3 and the branches b_{s3} and b_{s4} resemble the lower switches S_4, S_5, S_6.

Subsystem Σ_2 contains switching elements and therefore needs to satisfy Assumption 1-5, but on close inspection of the graph in Figure 3-5 we find that it violates Assumption 5. Recall that Assumption 5's purpose is to guarantee the validity of the transformation matrix in the case that a sequence of switches is closed. This violation can be circumvented by introducing the coupling between the switch states in each switch leg. Hence, the switch states $s_1, \ldots, s_6$ are replaced with a switch state per phase leg, s_a, s_b, s_c, such that

$$\begin{aligned} s_a &= s_1, \quad s_4 = 1 - s_a, \\ s_b &= s_2, \quad s_5 = 1 - s_b, \\ s_c &= s_3, \quad s_6 = 1 - s_c. \end{aligned} \tag{3-4}$$

Consequently, the branches, $b_{s1}, b_{s2}, b_{s3}, b_{s4}$, are a function of the switch states, which are respectively, $s_j, s_k, 1 - s_k, 1 - s_j$ for every leg $jk \in \{ab, bc, ca\}$. In other words, closing

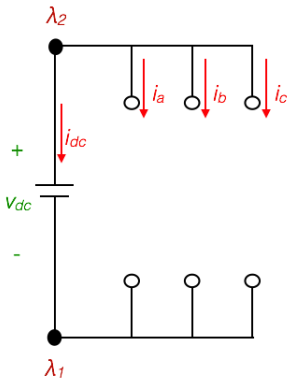

(a) Subsystem Σ_1.

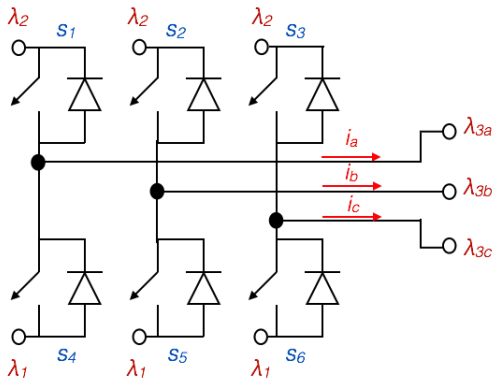

(b) Subsystem Σ_2.

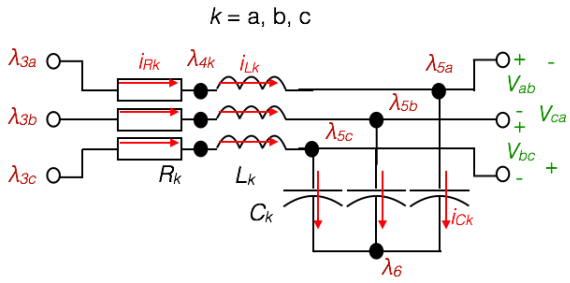

(c) Subsystem Σ_3.

Figure 3-2: The subsystems of the three-phase inverter.

the sequence b_{s4},b_{s1} never occurs and the PIM properly describes the graphs in each switch configuration. The orientation of the branches is chosen in accordance with Assumptions 4 and 5.

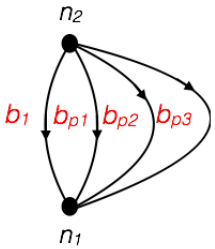

(a) Graph of Σ_1.

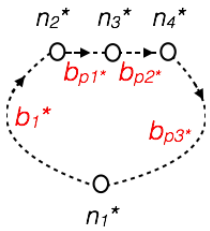

(b) Dual graph of Σ_1.

Figure 3-3: The graph and dual graph of Σ_1.

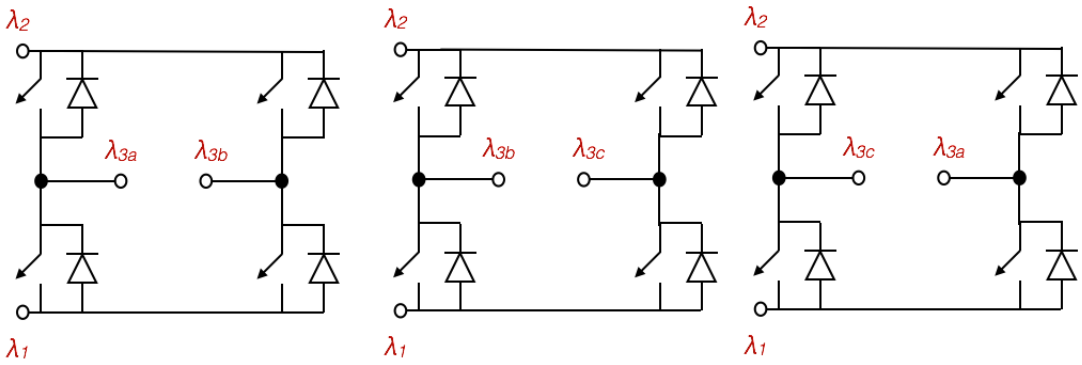

Figure 3-4: The identical subnetworks of Σ_2.

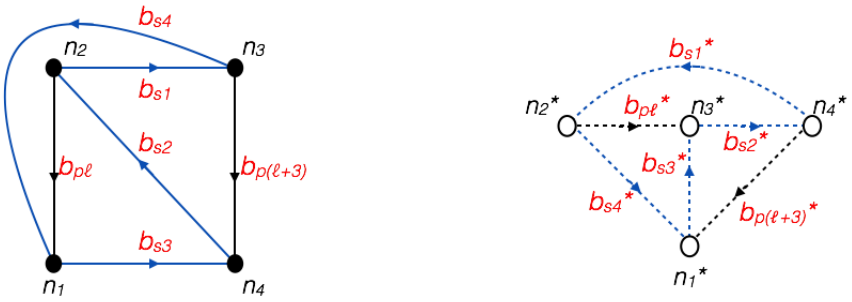

(a) Graph of Σ_2.

(b) Dual graph of Σ_2.

Figure 3-5: The simplified graph and dual graph of Σ_2 with the switches as virtual elements.

Having defined the subsystems and their graphs, we continue with formulating the subsystems in matrix formulation by using the CCL (2-15). Thereby, obtaining the KVL and KCL in kernel representation, see (2-17) and (2-19) for the matrix formulation of the Kirchhoff laws.

Subsystem Σ_1: applying (2-14) to the graph in Figure 3-3a leads to the incidence matrix

$$A(G_{\Sigma_1}) = \begin{bmatrix} -1 & -1 & -1 & -1 \\ 1 & 1 & 1 & 1 \end{bmatrix},$$

with $B_{\Sigma_1} = [b_1\ b_{p1}\ b_{p2}\ b_{p3}]^T$. Similarly, applying (2-14) to the dual graph in Figure 3-3b gives

$$A(G^*_{\Sigma_1}) = \begin{bmatrix} 1 & 0 & 0 & -1 \\ -1 & 1 & 0 & 0 \\ 0 & -1 & 1 & 0 \\ 0 & 0 & -1 & 1 \end{bmatrix},$$

with $B^*_{\Sigma_1} = [b^*_1\ b^*_{p1}\ b^*_{p2}\ b^*_{p3}]^T$.

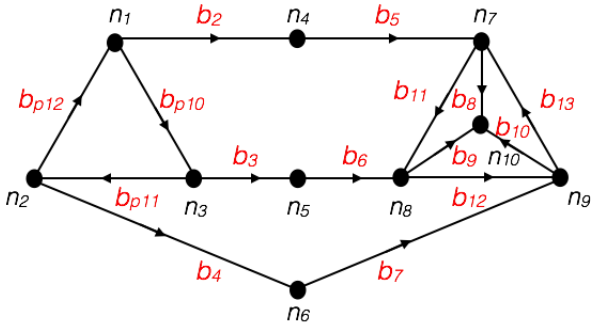

(a) Graph of Σ_3.

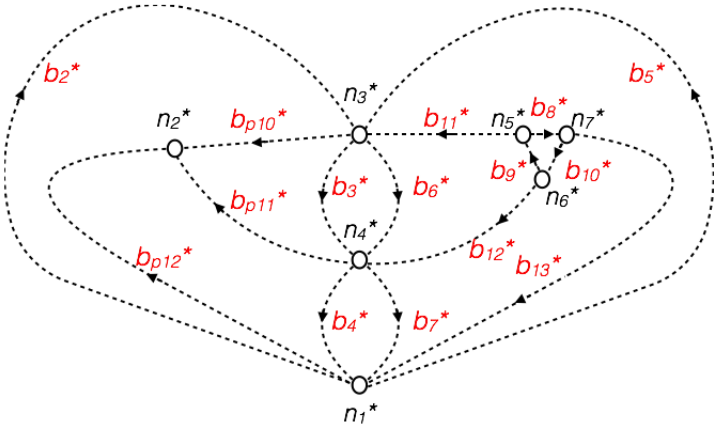

(b) Dual graph Σ_3.

Figure 3-6: The graph and dual graph of Σ_3.

Subsystem Σ_2: the subsystem contains switching elements and therefore has a reference graph and a virtual graph. First consider the graph in Figure 3-5a. The incidence matrix corresponding to the reference graph reads as

$$A(G_r)\begin{bmatrix} -1 & 0 \\ 1 & 0 \\ 0 & 1 \\ 0 & -1 \end{bmatrix}.$$

The virtual graph leads to four disconnection-reconnection matrices defined by (2-28). Also, substituting (3-4) into the disconnection-reconnection matrices gives

$$M_1(G_{\Sigma_2})(s_j) = \begin{bmatrix} 0 & 0 & 0 & 0 \\ 0 & -s_j & 0 & 0 \\ 0 & s_j & 0 & 0 \\ 0 & 0 & 0 & 0 \end{bmatrix}, \qquad M_2(G_{\Sigma_2})(s_k) = \begin{bmatrix} 0 & 0 & 0 & 0 \\ 0 & 0 & 0 & s_k \\ 0 & 0 & 0 & 0 \\ 0 & 0 & 0 & -s_k \end{bmatrix},$$

$$M_3(G_{\Sigma_2})(s_k) = \begin{bmatrix} -(1-s_k) & 0 & 0 & 0 \\ 0 & 0 & 0 & 0 \\ 0 & 0 & 0 & 0 \\ (1-s_k) & 0 & 0 & 0 \end{bmatrix}, \quad M_4(G_{\Sigma_2})(s_j) = \begin{bmatrix} 0 & 0 & (1-s_j) & 0 \\ 0 & 0 & 0 & 0 \\ 0 & 0 & -(1-s_j) & 0 \\ 0 & 0 & 0 & 0 \end{bmatrix},$$

with $jk \in \{ab, bc, ca\}$ and $s_j, s_k \in \{0, 1\}$. Applying (2-30) and simplifying the result yields the PIM of the simplified graph[2]

$$A_{jk}(G_{\Sigma_2})(S_{jk}) = \begin{bmatrix} -s_k & -s_k(s_j - 1) \\ 1 - s_j & s_k(s_j - 1) \\ s_j & s_j(1 - s_k) \\ s_k - 1 & s_j(s_k - 1) \end{bmatrix}, \tag{3-5}$$

with $S_{jk} = [s_j \ s_k]^T \in \{0, 1\}^2$. The PIM denoting the KCL for Σ_2 is thus

$$A(G_{\Sigma_2})(S) = \begin{bmatrix} A_{ab}(G_{\Sigma_2})(S) & \mathbb{O}^{4\times 2} & \mathbb{O}^{4\times 2} \\ \mathbb{O}^{4\times 2} & A_{bc}(G_{\Sigma_2})(S) & \mathbb{O}^{4\times 2} \\ \mathbb{O}^{4\times 2} & \mathbb{O}^{4\times 2} & A_{ca}(G_{\Sigma_2})(S) \end{bmatrix}, \tag{3-6}$$

with $S = [s_a \ s_b \ s_c]^T \in \{0, 1\}^3$ and $B_{\Sigma_2} = [b_{p4} \ b_{p7} \ b_{p5} \ b_{p8} \ b_{p6} \ b_{p9}]^T$. Then, focus on the dual graph in Figure 3-5b. We have the reference matrix

$$A(G_r^*) = \begin{bmatrix} 0 & 1 \\ 1 & 0 \\ -1 & 0 \\ 0 & 1 \end{bmatrix},$$

and the four disconnection-reconnection matrices

$$M_1(G^*_{\Sigma_2})(s_j^*) = \begin{bmatrix} 0 & 0 & 0 & 0 \\ 0 & 0 & 0 & s_j^* \\ 0 & 0 & 0 & 0 \\ 0 & 0 & 0 & -s_j^* \end{bmatrix}, \qquad M_2(G^*_{\Sigma_2})(s_k^*) = \begin{bmatrix} 0 & 0 & 0 & 0 \\ 0 & 0 & 0 & 0 \\ 0 & 0 & -s_k^* & 0 \\ 0 & 0 & s_k^* & 0 \end{bmatrix},$$

$$M_3(G^*_{\Sigma_2})(s_k^*) = \begin{bmatrix} -(1 - s_k^*) & 0 & 0 & 0 \\ 0 & 0 & 0 & 0 \\ (1 - s_k^*) & 0 & 0 & 0 \\ 0 & 0 & 0 & 0 \end{bmatrix}, \quad M_4(G^*_{\Sigma_2})(s_j^*) = \begin{bmatrix} 0 & (1 - s_j^*) & 0 & 0 \\ 0 & -(1 - s_j^*) & 0 & 0 \\ 0 & 0 & 0 & 0 \\ 0 & 0 & 0 & 0 \end{bmatrix},$$

with $s_j^*, s_k^* \in \{0, 1\}$. Subsequently, computing (2-30), substituting $s_j^* = 1 - s_j$, $s_k^* = 1 - s_k$ and simplifying the result, yields

$$A_{jk}(G^*_{\Sigma_2})(S_{jk}) = \begin{bmatrix} -s_j(s_k - 1) & s_k - 1 \\ -s_k(s_j - 1) & 1 - s_j \\ s_k(s_j s_k - 1) & -s_k \\ s_j(s_k - 1) & s_j \end{bmatrix}, \tag{3-7}$$

which defines $A_{ab}(G^*_{\Sigma_2})(S_{ab})$, $A_{bc}(G^*_{\Sigma_2})(S_{bc})$ and $A_{ca}(G^*_{\Sigma_2})(S_{ca})$. Hence, the PIM denoting the KVL for Σ_2 is

$$A(G^*_{\Sigma_2})(S) = \begin{bmatrix} A_{ab}(G^*_{\Sigma_2})(S) & \mathbb{O}^{4\times 2} & \mathbb{O}^{4\times 2} \\ \mathbb{O}^{4\times 2} & A_{bc}(G^*_{\Sigma_2})(S) & \mathbb{O}^{4\times 2} \\ \mathbb{O}^{4\times 2} & \mathbb{O}^{4\times 2} & A_{ca}(G^*_{\Sigma_2})(S) \end{bmatrix}, \tag{3-8}$$

[2]Computing the PIM yields large expressions in terms of the switch states. The result presented here has been simplified. For example, the following relations have been identified and substituted $s(s - 1) := 0 \ \forall s \in \{0, 1\}$ and $s_k - (s_j - 1)(1 - s_k) - 1 = s_j(s_k - 1) \ \forall (s_j, s_k) \in \{0, 1\}^2$.

with $B^*_{\Sigma_2} = [b^*_{p4}\ b^*_{p7}\ b^*_{p5}\ b^*_{p8}\ b^*_{p6}\ b^*_{p9}]^T$.

Subsystem Σ_3: the graph in Figure 3-6a gives the incidence matrix

$$A(G_{\Sigma_3}) = \left[\begin{array}{ccccccccc|ccccccc} 1 & 0 & -1 & 1 & 0 & 0 & 0 & 0 & 0 & & & & & & \\ -1 & 1 & 0 & 0 & 1 & 0 & 0 & 0 & 0 & & & & & & \\ 0 & -1 & 1 & 0 & 0 & 1 & 0 & 0 & 0 & & & \mathbb{O}^{6\times 6} & & & \\ 0 & 0 & 0 & -1 & 0 & 0 & 1 & 0 & 0 & & & & & & \\ 0 & 0 & 0 & 0 & -1 & 0 & 0 & 1 & 0 & & & & & & \\ 0 & 0 & 0 & 0 & 0 & -1 & 0 & 0 & 1 & & & & & & \\ \hline & & & & & & -1 & 0 & 0 & 1 & 0 & 0 & 1 & 0 & -1 \\ & & & & & & 0 & -1 & 0 & 0 & 1 & 0 & -1 & 1 & 0 \\ & & & \mathbb{O}^{4\times 6} & & & 0 & 0 & -1 & 0 & 0 & 1 & 0 & -1 & 1 \\ & & & & & & 0 & 0 & 0 & -1 & -1 & -1 & 0 & 0 & 0 \end{array}\right],$$

with the corresponding vector $B_{\Sigma_3} = [b_{p10}\ b_{p11}\ b_{p12}\ b_2\ b_3\ b_4\ b_5\ b_6\ b_7\ b_8\ b_9\ b_{10}\ b_{11}\ b_{12}\ b_{13}]^T$. Moreover, the incidence matrix corresponding to the dual graph in Figure 3-6b is

$$A(G^*_{\Sigma_3}) = \left[\begin{array}{ccccccccc|ccccccc} 0 & 0 & 1 & 1 & 0 & -1 & 1 & 0 & -1 & 0 & 0 & 0 & 0 & 0 & -1 \\ -1 & -1 & -1 & 0 & 0 & 0 & 0 & 0 & 0 & 0 & 0 & 0 & 0 & 0 & 0 \\ 1 & 0 & 0 & -1 & 1 & 0 & -1 & 1 & 0 & 0 & 0 & 0 & -1 & 0 & 0 \\ 0 & 1 & 0 & 0 & -1 & 1 & 0 & -1 & 1 & 0 & 0 & 0 & 0 & -1 & 0 \\ \hline & & & & & & & & & 1 & -1 & 0 & -1 & 0 & 0 \\ & & & & \mathbb{O}^{3\times 9} & & & & & 0 & 1 & -1 & 0 & -1 & 0 \\ & & & & & & & & & -1 & 0 & 1 & 0 & 0 & -1 \end{array}\right],$$

with $B^*_{\Sigma_3} = [b^*_{p10}\ b^*_{p11}\ b^*_{p12}\ b^*_2\ b^*_3\ b^*_4\ b^*_5\ b^*_6\ b^*_7\ b^*_8\ b^*_9\ b^*_{10}\ b^*_{11}\ b^*_{12}\ b^*_{13}]^T$.

The subsystems are not stand alone systems and have a port that connects them to one another at the points where they are separated. The interconnection of Σ_1 and Σ_2 is given by the relations

$$\begin{aligned} b_\ell &= -b_{\ell+3}, \\ b^*_\ell &= b^*_{\ell+3}, \end{aligned} \tag{3-9}$$

with $\ell = 1, 2, 3$. The first equation denotes the interconnection of the currents and the second the interconnection between the voltages. Likewise, the interconnection of Σ_2 and Σ_3 is given by

$$\begin{aligned} b_{p\ell+6} &= -b_{p\ell+9}, \\ b^*_{p\ell+6} &= b^*_{p\ell+9}. \end{aligned} \tag{3-10}$$

3-2-2 Formulating the Dirac structure

Following the theory from Section 2-2 and Section 2-3, the Dirac structure is methodically obtained by rearranging the incidence matrices and rewriting the interconnection constraints in (3-9) and (3-10) to form the matrices E and F. This results into a Dirac structure conform Proposition 1. However, doing this requires us to identify the currents and voltages as efforts and flows at this stage. The currents and voltages for the storage elements are defined by (2-4) (see Appendix A), but this raises the question: *how to identify the remaining voltages*

and currents as efforts and flows? The answer to this question is not as simple as it may seen and is intimately related to the notion of causality within the PH framework. Therefore, before continuing, it is convenient to discuss the notion of causality and the efforts and flows in more detail.

Breedveld discusses causality in the PH framework in [20] and in [3, Ch.1.4, Ch.1.7]. He concludes that, although it is physically speaking impossible to speak of causality among conjugate variables, i.e., the one causes the other, from a control and computational viewpoint such a definition is required, because we actuate only one of the variables and solve accordingly. Indeed, the notion of causality underlines the general constitutive relation for the storage elements in (2-4) (in this case integrative causality is also physically more correct, see [3, Ch.1.7.2] for more details). The flow is input, effort is output viewpoint is also present in the general constitutive relation for the resistive elements $e_{\mathcal{R}} = \hat{D} f_{\mathcal{R}}$ [12, 3], which implies that the flow is again an input and the effort and an output. This causal definition has three consequences. One, the framework formally distinguishes between voltage-driven resistors, *conductors*, and current-driven resistors, *resistors*. Although such separation seems trivial for linear resistors, it is not so for nonlinear resistors and conductors, where $\hat{D} : \mathcal{F}_{\mathcal{R}} \to \mathcal{E}_{\mathcal{R}}$ may not be *bijective*[3], see [15, Ch.1.2]. Two, the mappings in the ISO structures with respect to their domains and co-domains are: $J : \mathcal{E} \to \mathcal{F}$, $g : \mathcal{F} \to \mathcal{F}$ and $g^T : \mathcal{E} \to \mathcal{E}$ ($Z : \mathcal{F} \to \mathcal{E}$ in the case of direct feedthrough). Three, $f_{\mathcal{P}} = u$ and $e_{\mathcal{P}} = y$. The latter observation also follows form the second.

Based on the above observations, the obvious answer to the question would be to assign the voltages and currents as efforts and flows, such that after computing the ISO model from the Dirac structure, the assignment matches with the mappings of the ISO structure. However, there is a problem with this answer. The objective is to use the kernel representation of the Dirac structure and the Hamiltonian to arrive at the ISO. It makes no sense to use the resulting ISO form to find the E and F matrix *a posteriori*. We need to identity the generalised efforts and flows *a priori* with the information available, which is the network topology and the Kirchhoff laws. Fortunately, through observation of the structure of the Kirchhoff laws and the resulting ISO forms, it is possible to determine which elements are voltage-driven and which are current-driven based on their position in the network.

Realising that the equations in the ISO structure are nothing else but the Kirchhoff laws, i.e., the sums of currents and voltages within the network, we arrive at the following observations: equations belonging to loops or equivalently dual nodes (sums of voltages) always form a state equation if one of the elements is an inductor. This implies that an inductor dominates over a capacitor in terms of the state equation when they are both in a loop. This in turn implies that all elements in a loop with an inductor are voltage-driven (voltage is input). Likewise, loops with a capacitor contain current-driven elements (current is input). In the same sense, a voltage source is a source for an inductor and a current source is a source for a capacitor and consequently, a source in a loop with an inductor must be a voltage source and a source in a loop with only a capacitor must be a current source. Thus, by analysing the topology of the network, the elements and sources can be categorised as voltage- or current-driven and thereby as flows (inputs) and efforts (outputs).

This leaves the assignment of the interconnection variables as efforts and flows. In a subsys-

[3]This automatically implies that, transforming the ISO representation from (2-7) to (2-8) and *vice versa*, may not be possible.

tem with storage elements these can be determined by replacing the connection to another subsystem by a voltage-driven or current-driven impedance or a source. However, for a subsystem without functional elements the correct type of causality is determined by the other subsystems. For instance, the ports in Σ_2 to Σ_1 and to Σ_3 are entirely determined by Σ_1 and Σ_3 and cannot be determined only based on Σ_2. From this we infer that it might be a tedious solution for more complex systems with more subsystems. Although, for the present scenario, the three-phase inverter, this solution would be applicable and manageable. Moreover, the correct assignment of the currents and voltages as efforts and flows only makes sense if one would compute the ISO of an individual subsystem, because, in the end, these ports are *latent variables* that disappear after computing the total mathematical model (shown with Theorem 1). The only real reason for the identification of the interconnection variables is thus to determine what type of interconnection constraint (canonical or gyrative) the interconnection relations between the subsystems are. Hence, the issue of the identification of the correct causal relations feels rather pointless.

Willems debates such issues in [14], where he concludes and arguments that: the interconnection of subsystems must not be analysed or described as input-output processes, but as ports sharing variables. Witness the following quote from Willems [14]:

> "Properties and representations of systems refer to the behaviour."

Indeed, whatever the choice for the assignment of the efforts and flows of the interconnection ports and the consequent interconnection type, does not change the behaviour of the system. In terms of Theorem 1 only the structure of the matrix M changes. This argument does not count for the other elements, for instance the sources, because they also need to respect the ISO structure. We assimilate the viewpoint from Willems regarding the interconnection of the subsystems, which leads us to the following proposition for the modelling of interconnected systems:

Proposition 2. *The separation of a system into two subsystems results in an interconnection port in both subsystems, described by a voltage and a current, who are respectively assigned as effort and flow, and are related to the port variables of the associated subsystem by the canonical interconnection* (2-9)*.*

In light of this, the voltages and currents of the three-phase inverter are identified as follows. For Σ_1, with the exception of b_1, all the branches (currents) are flows. Conversely, with the exception of b_1^*, all the dual branches (voltages) are efforts. For Σ_2 all the branches are flows and all the dual branches are efforts. For Σ_3, the branches $b_2, \ldots, b_7$ are efforts and the rest are flows. Notice that the resistors are voltage-driven due to the inductors. Likewise, the dual branches, $b_2^*, \ldots, b_7^*$ are flows and the rest are efforts. Subsequently, grouping the efforts and flows together in an effort and flow vector for each subsystem leads to the total flow and effort vectors

$$f = \begin{bmatrix} f_{\Sigma_1}^T & f_{\Sigma_2}^T & f_{\Sigma_3}^T \end{bmatrix}^T, \tag{3-11}$$

$$e = \begin{bmatrix} e_{\Sigma_1}^T & e_{\Sigma_2}^T & e_{\Sigma_3}^T \end{bmatrix}^T, \tag{3-12}$$

where

$$f_{\Sigma_1} = \begin{bmatrix} u_{dc} & f_1 & f_2 & f_3 \end{bmatrix}^T,$$
$$e_{\Sigma_1} = \begin{bmatrix} y_{dc} & e_1 & e_2 & e_3 \end{bmatrix}^T,$$
$$f_{\Sigma_2} = \begin{bmatrix} f_4 & f_7 & f_5 & f_8 & f_6 & f_9 \end{bmatrix}^T,$$
$$e_{\Sigma_2} = \begin{bmatrix} e_4 & e_7 & e_5 & e_8 & e_6 & e_9 \end{bmatrix}^T,$$

$$f_{\Sigma_3} = \begin{bmatrix} f_{10} & f_{11} & f_{12} & f_{Ra} & f_{Rb} & f_{Rc} & -\dot{\phi}_a & -\dot{\phi}_b & -\dot{\phi}_c & -\dot{q}_a & -\dot{q}_b & -\dot{q}_c & u_{ab} & u_{bc} & u_{ca} \end{bmatrix}^T,$$
$$e_{\Sigma_3} = \begin{bmatrix} e_{10} & e_{11} & e_{12} & e_{Ra} & e_{Rb} & e_{Rc} & \frac{\partial H}{\partial \phi_a} & \frac{\partial H}{\partial \phi_b} & \frac{\partial H}{\partial \phi_c} & \frac{\partial H}{\partial q_a} & \frac{\partial H}{\partial q_b} & \frac{\partial H}{\partial q_c} & y_{ab} & y_{bc} & y_{ca} \end{bmatrix}^T,$$

ϕ is the flux-linkage across the inductor, q the charge in the capacitor, y_{dc} the current on the DC side, u_{dc} the voltage on the DC side, y_{ab}, y_{bc}, y_{ca} the line-to-line voltages and u_{ab}, u_{bc}, u_{ca} the line-to-line currents of the Δ-connected load. The efforts and flows corresponding to ports are denotes with an index number, where the index corresponds to the index in the branch variable ($f_j = b_{pj}$, $e_j = b^*_{pj}$). Furthermore, the Hamiltonian $H(q, \phi)$ for the inverter is given by (3-2). For simplicity, we write the state vector $x = (x_1\ x_2)^T$, where $x_1 = (q_a\ q_b\ q_c)$ and $x_2 = (\phi_a\ \phi_b\ \phi_c)$.

Subsequently, grouping the columns of the (parametrised) incidence matrices corresponding to flows and to efforts, yields a Dirac structure in accordance with Proposition 1, where the matrices $F \in \mathbb{R}^{36\times 25}$ and $E \in \mathbb{R}^{36\times 25}$ are composed of $F_{\Sigma_1}, E_{\Sigma_1}, \ldots, F_{\Sigma_3}, E_{\Sigma_3}$ and F_I, E_I. The matrices $F_{\Sigma_1}, E_{\Sigma_1}, \ldots, F_{\Sigma_3}, E_{\Sigma_3}$ are in turn given as

$$F_{\Sigma_1} = \begin{bmatrix} A_f(G_{\Sigma_1}) \\ A_f(G^*_{\Sigma_1}) \end{bmatrix}, \qquad F_{\Sigma_2} = \begin{bmatrix} A_f(G_{\Sigma_2})(S) \\ \mathbb{O} \end{bmatrix}, \qquad F_{\Sigma_3} = \begin{bmatrix} A_f(G_{\Sigma_3}) \\ A_f(G^*_{\Sigma_3}) \end{bmatrix}, \tag{3-13}$$

$$E_{\Sigma_1} = \begin{bmatrix} A_e(G_{\Sigma_1}) \\ A_e(G^*_{\Sigma_1}) \end{bmatrix}, \qquad E_{\Sigma_2} = \begin{bmatrix} \mathbb{O} \\ A_e(G^*_{\Sigma_2})(S) \end{bmatrix}, \qquad E_{\Sigma_3} = \begin{bmatrix} A_e(G_{\Sigma_3}) \\ A_e(G^*_{\Sigma_3}) \end{bmatrix}, \tag{3-14}$$

where $S = [s_a\ s_b\ s_c]^T \in \{0,1\}^3$. Observe that there are no non-admissible switch configurations. This means that

$$\mathcal{A}(\Sigma) = \{0,1\}^6.$$

In conclusion, the Dirac structure of the system is now represented in the kernel representation of (2-32). This Dirac structure admits an implicit PH system denoted as[4]

$$\left(-\dot{x}, \frac{\partial H}{\partial x}(x), f_R, e_R, u_{dc}, y_{dc}, u_{AC}, y_{AC}\right) \in \mathcal{D}(S),\ S \in \mathcal{A}(\Sigma),$$

where $f_R = [f_{Ra}\ f_{Rb}\ f_{Rc}]^T$, $e_R = [e_{Ra}\ e_{Rb}\ e_{Rc}]^T$, $u_{AC} = [u_{ab}\ u_{bc}\ u_{ca}]^T$ and $y_{AC} = [y_{ab}\ y_{bc}\ y_{ca}]^T$.

3-2-3 Deriving the differential-algebraic model

This section shows how the mathematical model of the inverter follows form solving the characteristic equation of the Dirac structure. For the inverter this leads to a set of DAEs,

[4]For convenience and clarity, the inputs and outputs are separated for the DC and AC side.

of the form in (2-5). The DAM is the result of modelling the system without assuming a balanced load, because this couples the voltages in the inductors in the phase legs. First, we rewrite the parametrisation of Σ_2 into a more convenient and comprehensible form. Then, we show that computing the model corresponding to $\mathcal{D}_1 \circ \mathcal{D}_2$ (the composition of subsystems Σ_1 and Σ_2) is the mathematical model of a basic inverter given by (3-1). Finally, we give the DAM model of three-phase inverter from Figure 3-1.

The simplified parametrisation of Σ_2

Before deriving the models of the basic three-phase inverter and the inverter in Figure 3-1, it is convenient to rewrite the parametrisation of Σ_2. The matrices $E_{\Sigma_2}(S)$ and $F_{\Sigma_2}(S)$ (which are equal to (3-6) and (3-8), respectively) are first simplified by computing the equations for every switch configuration, $(s_a, s_b, s_c) \in \{0,1\}^3$. Computing the characteristic equation with the matrices (3-5) and (3-7) with the flow vector $[f_\ell \ f_{\ell+3}]^T$ and effort vector $[e_\ell \ e_{\ell+3}]^T$ provides the following results.
For $(s_j, s_k) = (0,0)$:

$$\begin{aligned} f_\ell &= 0, \\ e_{\ell+3} &= 0. \end{aligned}$$

For $(s_j, s_k) = (1,0)$:

$$\begin{aligned} f_\ell &= -f_{\ell+3}, \\ e_{\ell+3} &= e_{\ell+3}. \end{aligned}$$

For $(s_j, s_k) = (0,1)$:

$$\begin{aligned} f_\ell &= f_{\ell+3}, \\ e_{\ell+3} &= -e_{\ell+3}. \end{aligned}$$

For $(s_j, s_k) = (1,1)$:

$$\begin{aligned} f_\ell &= 0, \\ e_{\ell+3} &= 0. \end{aligned}$$

Rewriting the result into a simplified parametrised form leads to the matrices

$$\begin{aligned} F_{\Sigma_2}(S) &= \begin{bmatrix} & (s_a - s_b) & 0 & 0 \\ \mathbb{I}^{3\times 3} & 0 & (s_b - s_c) & 0 \\ & 0 & 0 & (s_c - s_a) \\ & & \mathbb{O}^{3\times 6} & \end{bmatrix}, \\ E_{\Sigma_2}(S) &= \begin{bmatrix} & & \mathbb{O}^{3\times 6} & \\ (s_a - s_b) & 0 & 0 & \\ 0 & (s_b - s_c) & 0 & -\mathbb{I}^{3\times 3} \\ 0 & 0 & (s_c - s_a) & \end{bmatrix}, \end{aligned} \tag{3-15}$$

where $S = [s_a \ s_b \ s_c]^T$ and the corresponding effort and flow vector f_{Σ_2} and e_{Σ_2} are defined in (3-11) and (3-12).

The basic three-phase inverter model

Consider the models of Σ_1 and Σ_2. Denoting f_7, f_8, f_9 as inputs and e_7, e_8, e_9 as outputs and composing Σ_1 and Σ_2 with Theorem 1 yields

$$\begin{aligned} y_{dc} &= -f_7(s_a - s_b) - f_8(s_b - s_c) - f_9(s_c - s_a), \\ e_7 &= u_{dc}(s_a - s_b), \\ e_8 &= u_{dc}(s_b - s_c), \\ e_9 &= u_{dc}(s_c - s_a). \end{aligned} \tag{3-16}$$

The equations in (3-16) represent the model of a general three-phase inverter with a DC source and with a unspecified Δ-connected output. Observe that y_{dc} is defined in the opposite direction of the current in Figure 2-7a, which causes the minus sign difference when comparing the output equation of (3-16) and the one in (3-1). Furthermore, the DC current is expressed as a function of the line-to-line current as opposed to the phase currents in (3-1).

The DAM of the three-phase inverter

Computing the composed system matrices of $\mathcal{D}_1 \circ \mathcal{D}_2 \circ \mathcal{D}_3$ and solving the characteristic equation for $\dot{x}, y$ and $e_{\mathcal{R}}$ leads to the DAM[5]:

$$\begin{aligned} \begin{bmatrix} \mathbb{I}^{3\times3} & & \mathbb{O}^{3\times3} & \\ & 1 & -1 & 0 \\ \mathbb{O}^{3\times3} & 0 & 1 & -1 \\ & -1 & 0 & 1 \end{bmatrix} \dot{x} &= \begin{bmatrix} & \mathbb{O}^{3\times3} & & \mathbb{I}^{3\times3} \\ 1 & -1 & 0 & \\ 0 & 1 & -1 & \mathbb{O}^{3\times3} \\ -1 & 0 & 1 & \end{bmatrix} \frac{\partial H}{\partial x}(x) + \\ &\quad \begin{bmatrix} & \mathbb{O}^{3\times3} & \\ 1 & -1 & 0 \\ 0 & 1 & -1 \\ -1 & 0 & 1 \end{bmatrix} f_R - \begin{bmatrix} \mathbb{O}^{3\times1} \\ s_a - s_b \\ s_b - s_c \\ s_c - s_a \end{bmatrix} u_{dc} + \\ &\quad \begin{bmatrix} 1 & 0 & -1 \\ -1 & 1 & 0 \\ 0 & -1 & 1 \\ & \mathbb{O}^{3\times3} & \end{bmatrix} u_{AC}, \\ &\text{s.t.} \quad \dot{q}_a + \dot{q}_b + \dot{q}_c = 0, \\ e_R &= \begin{bmatrix} \mathbb{O}^{3\times3} & \mathbb{I}^{3\times3} \end{bmatrix} \frac{\partial H}{\partial x}(x), \\ y_{dc} &= \begin{bmatrix} \mathbb{O}^{1\times3} & -s_a & -s_b & -s_c \end{bmatrix} \frac{\partial H}{\partial x}(x), \\ y_{AC} &= \underbrace{\begin{bmatrix} 1 & -1 & 0 & \\ 0 & 1 & -1 & \mathbb{O}^{3\times3} \\ -1 & 0 & 1 & \end{bmatrix}}_{g_{AC}^T} \frac{\partial H}{\partial x}(x), \end{aligned} \tag{3-17}$$

[5]The detailed derivation is included in Appendix C-1.

with $s_a, s_b, s_c \in \{0, 1\}$, the Hamiltonian given by (3-2) and the resistive relation[6]

$$e_R = \begin{bmatrix} -\frac{1}{R_a} & 0 & 0 \\ 0 & -\frac{1}{R_b} & 0 \\ 0 & 0 & -\frac{1}{R_c} \end{bmatrix} f_R.$$

Concluding, a DAM is obtained when starting form the interconnection of the efforts and flows (or similarly, voltages and currents), because the voltages in the phases a, b, c always depend on the voltages in the loops ab, bc, ca and are therefore not independent. To obtain explicit equations some additional insight and rewriting of the equations is needed. The derivation of the explicit equations is treated in the next section. Furthermore, we showed that following this PH modelling procedure yields a model of a three-phase inverter in a structured and systematic way, which is valid for any load, unbalanced or balanced, linear or nonlinear.

3-2-4 Deriving the input-state-output model

This section shows how the coupling of the voltages can be removed and the DAM model transformed into an ISO model of the structure in (2-7) by assuming a balanced system ($L_a = L_b = L_c = L$), $C_a = C_b = C_c = C$ and $R_a = R_b = R_c = R$). The assumption of a balanced system is widely applied in the modelling of three-phase systems and in practise most systems can be regarded as balanced [2], [21, Ch.3].

Focus on the equations in (3-17) that relate to $\dot{x}_2$. If we consider the potentials in the inverter circuit (see Figure 3-2) a certain structure in these equations becomes apparent:

$$\underbrace{\frac{\partial H}{\partial q_a}(x) + f_{Ra} - \dot{\phi}_a}_{\lambda_{2a}-\lambda_6} - \underbrace{\left(\frac{\partial H}{\partial q_c}(x) + f_{Rc} - \dot{\phi}_c\right)}_{\lambda_{2c}-\lambda_6} + \underbrace{(s_c - s_a)u_{dc}}_{\lambda_{2c}-\lambda_{2a}} = 0, \tag{3-18}$$

$$\underbrace{\frac{\partial H}{\partial q_b}(x) + f_{Rb} - \dot{\phi}_b}_{\lambda_{2b}-\lambda_6} - \underbrace{\left(\frac{\partial H}{\partial q_a}(x) + f_{Ra} - \dot{\phi}_a\right)}_{\lambda_{2a}-\lambda_6} + \underbrace{(s_a - s_b)u_{dc}}_{\lambda_{2a}-\lambda_{2b}} = 0, \tag{3-19}$$

$$\underbrace{\frac{\partial H}{\partial q_c}(x) + f_{Rc} - \dot{\phi}_c}_{\lambda_{2c}-\lambda_6} - \underbrace{\left(\frac{\partial H}{\partial q_b}(x) + f_{Rb} - \dot{\phi}_b\right)}_{\lambda_{2b}-\lambda_6} + \underbrace{(s_b - s_c)u_{dc}}_{\lambda_{2b}-\lambda_{2c}} = 0. \tag{3-20}$$

In a balanced system the input (line-to-line voltage) term in the above equations can be divided into two phase voltages, each expressed with respect to potential λ_6, as

$$\underbrace{(s_j - s_k)u_{dc}}_{\lambda_{2j}-\lambda_{2k}} = \underbrace{u_{dc}\left(\frac{2}{3}s_j - \frac{1}{3}s_k - \frac{1}{3}s_\ell\right)}_{\lambda_{2j}-\lambda_6} - \underbrace{u_{dc}\left(\frac{2}{3}s_k - \frac{1}{3}s_j - \frac{1}{3}s_\ell\right)}_{\lambda_{2k}-\lambda_6}. \tag{3-21}$$

where $jk \in \{ab, bc, ca\}$, $\ell \in \{a, b, c\}$ and $j \neq k \neq \ell$. In other words, λ_6 has become the *datum*

[6] The minus sign is because $\langle e_\mathcal{R} | f_\mathcal{R} \rangle$ denotes incoming power into the Dirac structure.

node of the system. Substituting (3-21) into (3-18)-(3-20) yields

$$\underbrace{\frac{\partial H}{\partial q_a}(x) + f_{Ra} - \dot{\phi}_a}_{\lambda_{2a}-\lambda_6} - \underbrace{\left(\frac{\partial H}{\partial q_c}(x) + f_{Rc} - \dot{\phi}_c\right)}_{\lambda_{2c}-\lambda_6} + \underbrace{u_{dc}\left(\frac{2}{3}s_c - \frac{1}{3}s_a - \frac{1}{3}s_b\right)}_{\lambda_{2c}-\lambda_6} - \underbrace{u_{dc}\left(\frac{2}{3}s_a - \frac{1}{3}s_c - \frac{1}{3}s_b\right)}_{\lambda_{2a}-\lambda_6} = 0,$$
$$\underbrace{\frac{\partial H}{\partial q_b}(x) + f_{Rb} - \dot{\phi}_b}_{\lambda_{2b}-\lambda_6} - \underbrace{\left(\frac{\partial H}{\partial q_a}(x) + f_{Ra} - \dot{\phi}_a\right)}_{\lambda_{2a}-\lambda_6} + \underbrace{u_{dc}\left(\frac{2}{3}s_a - \frac{1}{3}s_b - \frac{1}{3}s_c\right)}_{\lambda_{2a}-\lambda_6} - \underbrace{u_{dc}\left(\frac{2}{3}s_b - \frac{1}{3}s_a - \frac{1}{3}s_c\right)}_{\lambda_{2b}-\lambda_6} = 0,$$
$$\underbrace{\frac{\partial H}{\partial q_c}(x) + f_{Rc} - \dot{\phi}_c}_{\lambda_{2c}-\lambda_6} - \underbrace{\left(\frac{\partial H}{\partial q_b}(x) + f_{Rb} - \dot{\phi}_b\right)}_{\lambda_{2b}-\lambda_6} + \underbrace{u_{dc}\left(\frac{2}{3}s_b - \frac{1}{3}s_c - \frac{1}{3}s_a\right)}_{\lambda_{2b}-\lambda_6} - \underbrace{u_{dc}\left(\frac{2}{3}s_c - \frac{1}{3}s_b - \frac{1}{3}s_a\right)}_{\lambda_{2c}\lambda_6} = 0.$$

Denote the potential differences with respect to λ_6 as voltages with the subscript o ($\lambda_\ell - \lambda_6 = v_{\ell o}$). Then, the above equations in terms of phase voltages reads as

$$\begin{aligned} v_{ao} - v_{co} + v_{co} - v_{ao} &= 0, \\ v_{bo} - v_{ao} + v_{ao} - v_{bo} &= 0, \\ v_{co} - v_{bo} + v_{bo} - v_{co} &= 0. \end{aligned}$$

From this we infer that the following formulae must hold

$$\begin{aligned} \frac{\partial H}{\partial q_a}(x) + f_{Ra} - \dot{\phi}_a - u_{dc}\left(\frac{2}{3}s_a - \frac{1}{3}s_b - \frac{1}{3}s_c\right) &= 0, \\ \frac{\partial H}{\partial q_b}(x) + f_{Rb} - \dot{\phi}_b - u_{dc}\left(\frac{2}{3}s_b - \frac{1}{3}s_a - \frac{1}{3}s_c\right) &= 0, \\ \frac{\partial H}{\partial q_c}(x) + f_{Rc} - \dot{\phi}_c - u_{dc}\left(\frac{2}{3}s_c - \frac{1}{3}s_a - \frac{1}{3}s_b\right) &= 0. \end{aligned}$$

Thus, the differential equations for x_2 can be explicitly written as

$$\dot{x}_1 = \begin{bmatrix} 1 & 0 & 0 \\ 0 & 1 & 0 \\ 0 & 0 & 1 \end{bmatrix} \frac{\partial H}{\partial x_1}(x) + \underbrace{\begin{bmatrix} 1 & 0 & 0 \\ 0 & 1 & 0 \\ 0 & 0 & 1 \end{bmatrix}}_{g_R} f_R - \underbrace{\begin{bmatrix} \frac{2}{3}s_a - \frac{1}{3}s_b - \frac{1}{3}s_c \\ \frac{2}{3}s_b - \frac{1}{3}s_a - \frac{1}{3}s_c \\ \frac{2}{3}s_c - \frac{1}{3}s_a - \frac{1}{3}s_b \end{bmatrix}}_{g_{dc}(S)} u_{dc}.$$

The expression of the DC current in (3-17) does not seem to be equal to $g_{dc}^T(S)\frac{\partial H}{\partial x_1}(x)$. However, the output matrix in (3-17) can be replaced by the transpose of the input matrix $g_{dc}(S)$, because the mappings are equivalent.

Proof.

$$\begin{aligned}
y_{dc} =& -\begin{bmatrix} \frac{2}{3}s_a - \frac{1}{3}s_b - \frac{1}{3}s_c \\ \frac{2}{3}s_b - \frac{1}{3}s_a - \frac{1}{3}s_c \\ \frac{2}{3}s_c - \frac{1}{3}s_a - \frac{1}{3}s_b \end{bmatrix}^T \frac{\partial H}{\partial x_1}(x), \\
=& -\left(s_a - \frac{1}{3}s_a - \frac{1}{3}s_b - \frac{1}{3}s_c\right)\frac{\partial H}{\partial \phi_a}(x) - \left(s_b - \frac{1}{3}s_a - \frac{1}{3}s_b - \frac{1}{3}s_c\right)\frac{\partial H}{\partial \phi_b}(x) - \\
& \left(s_c - \frac{1}{3}s_a - \frac{1}{3}s_b - \frac{1}{3}s_c\right)\frac{\partial H}{\partial \phi_c}(x), \\
=& -s_a\frac{\partial H}{\partial \phi_a}(x) - s_b\frac{\partial H}{\partial \phi_b}(x) - s_c\frac{\partial H}{\partial \phi_c}(x) + \frac{1}{3}\left(\frac{\partial H}{\partial \phi_a}(x) + \frac{\partial H}{\partial \phi_b}(x) + \frac{\partial H}{\partial \phi_c}(x)\right)s_a + \\
& \frac{1}{3}\left(\frac{\partial H}{\partial \phi_a}(x) + \frac{\partial H}{\partial \phi_b}(x) + \frac{\partial H}{\partial \phi_c}(x)\right)s_b + \frac{1}{3}\left(\frac{\partial H}{\partial \phi_a}(x) + \frac{\partial H}{\partial \phi_b}(x) + \frac{\partial H}{\partial \phi_c}(x)\right)s_c.
\end{aligned}$$

In a balanced system the term $\frac{\partial H}{\partial \phi_a}(x)+\frac{\partial H}{\partial \phi_b}(x)+\frac{\partial H}{\partial \phi_c}(x)$ is per definition zero and the expression reduces to

$$y_{dc} = -s_a\frac{\partial H}{\partial \phi_a}(x) - s_b\frac{\partial H}{\partial \phi_b}(x) - s_c\frac{\partial H}{\partial \phi_c}(x).$$

Thereby recovering the DC output equation in (3-17). □

Combining the results leads to the ISO-PH model for a three-phase inverter with a balanced load

$$\begin{aligned}
\dot{x} &= \begin{bmatrix} \mathbb{O}^{3\times3} & -\mathbb{I}^{3\times3} \\ \mathbb{I}^{3\times3} & \mathbb{O}^{3\times3} \end{bmatrix}\frac{\partial H}{\partial x}(x) + \begin{bmatrix} \mathbb{O}^{3\times3} \\ g_R \end{bmatrix} f_R - \begin{bmatrix} \mathbb{O}^{3\times1} \\ g_{dc}(S) \end{bmatrix} u_{dc} + g_{AC}u_{AC}, \\
e_R &= \begin{bmatrix} \mathbb{O}^{3\times3} & g_R^T \end{bmatrix}\frac{\partial H}{\partial x}(x), \\
y_{dc} &= -\begin{bmatrix} \mathbb{O}^{1\times3} & g_{dc}^T(S) \end{bmatrix}\frac{\partial H}{\partial x}(x), \\
y_{AC} &= g_{AC}^T\frac{\partial H}{\partial x}(x),
\end{aligned} \tag{3-22}$$

with the Hamiltonian in (3-2) and the resistance relation

$$e_R = -\frac{1}{R}\cdot\mathbb{I}^{3\times3}f_R.$$

In conclusion, the resulting model in (3-22) is the same model as the one in (3-3), but with the AC-side input and output given for a Δ-connection[7] and the resistive structure is expressed as an additional input-output port. There is a sign difference between the models in (3-3) and (3-22), due to the power flow convention for Dirac structures. This difference is omitted in the procedure to derive the PH system in [10, 11], because Mu et al. equate $v_L = \dot{\phi}_L$, while in this derivation $f_{\mathcal{S}} = -v_L = -\dot{\phi}_L$, because we define the power flow into the Dirac structure as positive. The same holds for the resistive relation.

[7]Obviously, for a Y-connected load, such as in [10, 11], the input-output matrix, g_{AC}, reduces to the input-output mapping in (3-3), where the inputs are the phase currents and the outputs the phase voltages.

3-3 Modelling the inverter with nonlinear element method

This section presents the derivation of the PH model with NEM, where the switches are viewed as nonlinear elements. First, the separation of the system into subsystems and their mathematical representations are discussed (Section 3-3-1). Subsequently, the Dirac structure is formulated (Section 3-3-2). Finally, the DAM and the ISO model are derived by solving the characteristic equation (Section 3-3-3).

3-3-1 Separating the system into planar subsystems

The advantage of this technique over the previous one is that the graphs of the systems only need to satisfy Assumption 1-3. Hence, the system is divided into the same three planar subsystems, see Figures 3-2. As a result, the graphs of subsystems Σ_1 and Σ_3 are the same, see Figure 3-3 and Figure 3-6. The graph of Σ_2 in Figure 3-5 changes to the graph in Figure 3-7, where the switching elements are now functional branches. The branches b_{sj} and b_{sk} represent the upper switches S_1, S_2, S_3, and the branches $\hat{b}_{sj}$ and $\hat{b}_{sk}$ represent the lower switches S_4, S_5, S_6. In terms of the switch state, the conduction of the branches $b_{sj}, b_{sk}, \hat{b}_{sj}, \hat{b}_{sk}$ corresponds to $s_j, s_k, 1-s_j, 1-s_k$, respectively.

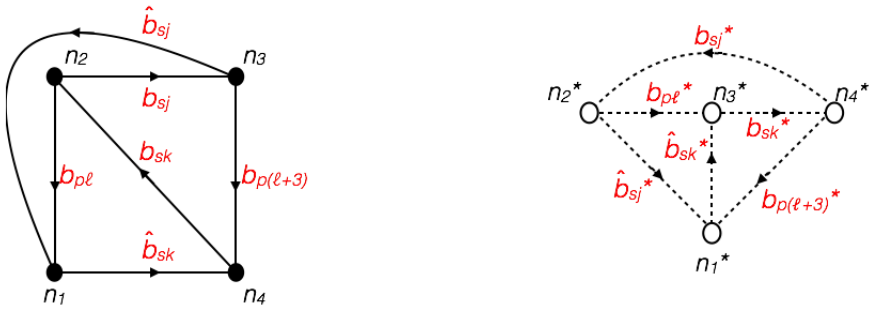

(a) Graph of Σ_2. **(b)** Dual graph of Σ_2.

Figure 3-7: The simplified graph and dual graph of Σ_2 with the switches as nonlinear elements.

Because the graphs and dual graphs for Σ_1 and Σ_3 are the same their incidence matrices are too. The incidence matrix for Σ_2 does change, because of the addition of functional branches. The incidence matrix corresponding to the graph and dual graph in Figure 3-7 are given by

$$A_{jk}(G_{\Sigma_2}) = \begin{bmatrix} -1 & 0 & 0 & 1 & -1 & 0 \\ 1 & 1 & -1 & 0 & 0 & 0 \\ 0 & -1 & 0 & 0 & 1 & 1 \\ 0 & 0 & 1 & -1 & 0 & -1 \end{bmatrix},$$

$$A_{jk}(G^*_{\Sigma_2}) = \begin{bmatrix} 0 & 0 & 0 & 1 & -1 & -1 \\ 1 & -1 & 0 & 0 & 1 & 0 \\ -1 & 0 & 1 & -1 & 0 & 0 \\ 0 & 1 & -1 & 0 & 0 & 1 \end{bmatrix}.$$

with $B_{\Sigma_2} = [b_{p\ell} \quad b_{sj} \quad b_{sk} \quad \hat{b}_{sk} \quad \hat{b}_{sj} \quad b_{p(\ell+3)}]^T$ and $B^*_{\Sigma_2} = [b^*_{p\ell} \quad b^*_{sj} \quad b^*_{sk} \quad \hat{b}^*_{sk} \quad \hat{b}^*_{sj} \quad b^*_{p(\ell+3)}]^T$, where $jk = ab, bc, ca$ and $\ell = 4, 5, 6$. These matrices describe the interconnection of a DC to line-to-line terminal loop. By slightly rearranging the matrices and combining them together the total incidence matrices describing Σ_2 can be expressed as

$$A(G_{\Sigma_2}) = \begin{bmatrix} -1 & 0 & 0 & 0 & 0 & 0 & -1 & 1 & 0 & 0 & 0 & 0 \\ 1 & 0 & 0 & 1 & -1 & 0 & 0 & 0 & 0 & 0 & 0 & 0 \\ 0 & 0 & 0 & -1 & 0 & 0 & 1 & 0 & 0 & 1 & 0 & 0 \\ 0 & 0 & 0 & 0 & 1 & 0 & 0 & -1 & 0 & -1 & 0 & 0 \\ 0 & -1 & 0 & 0 & 0 & 0 & 0 & -1 & 1 & 0 & 0 & 0 \\ 0 & 1 & 0 & 0 & 1 & -1 & 0 & 0 & 0 & 0 & 0 & 0 \\ 0 & 0 & 0 & 0 & -1 & 0 & 0 & 1 & 0 & 0 & 1 & 0 \\ 0 & 0 & 0 & 0 & 0 & 1 & 0 & 0 & -1 & 0 & -1 & 0 \\ 0 & 0 & -1 & 0 & 0 & 0 & 1 & 0 & -1 & 0 & 0 & 0 \\ 0 & 0 & 1 & -1 & 0 & 1 & 0 & 0 & 0 & 0 & 0 & 0 \\ 0 & 0 & 0 & 0 & 0 & -1 & 0 & 0 & 1 & 0 & 0 & 1 \\ 0 & 0 & 0 & 1 & 0 & 0 & -1 & 0 & 0 & 0 & 0 & -1 \end{bmatrix}, \tag{3-23}$$

with $B_{\Sigma_2} = [b_{p4} \; b_{p5} \; b_{p6} \; b_{sa} \; b_{sb} \; b_{sc} \; \hat{b}_{sa} \; \hat{b}_{sb} \; \hat{b}_{sc} \; b_{p7} \; b_{p8} \; b_{p9}]^T$, and

$$A(G^*_{\Sigma_2}) = \begin{bmatrix} 0 & 0 & 0 & 0 & 0 & 0 & -1 & 1 & 0 & -1 & 0 & 0 \\ 1 & 0 & 0 & -1 & 0 & 0 & 0 & 0 & 0 & 0 & 0 & 0 \\ -1 & 0 & 0 & 0 & 1 & 0 & 0 & -1 & 0 & 0 & 0 & 0 \\ 0 & 0 & 0 & 1 & -1 & 0 & 0 & 0 & 0 & 1 & 0 & 0 \\ 0 & 0 & 0 & 0 & 0 & 0 & 0 & -1 & 1 & 0 & -1 & 0 \\ 0 & 1 & 0 & 0 & -1 & 0 & 0 & 1 & 0 & 0 & 0 & 0 \\ 0 & -1 & 0 & 0 & 0 & 1 & 0 & 0 & -1 & 0 & 0 & 0 \\ 0 & 0 & 0 & 0 & 1 & -1 & 0 & 0 & 0 & 0 & 1 & 0 \\ 0 & 0 & 0 & 0 & 0 & 0 & 1 & 0 & -1 & 0 & 0 & -1 \\ 0 & 0 & 1 & 0 & 0 & -1 & 0 & 0 & 1 & 0 & 0 & 0 \\ 0 & 0 & -1 & 1 & 0 & 0 & -1 & 0 & 0 & 0 & 0 & 0 \\ 0 & 0 & 0 & -1 & 0 & 1 & 0 & 0 & 0 & 0 & 0 & 1 \end{bmatrix}, \tag{3-24}$$

with $B^*_{\Sigma_2} = [b^*_{p4} \; b^*_{p5} \; b^*_{p6} \; b^*_{sa} \; b^*_{sb} \; b^*_{sc} \; \hat{b}^*_{sa} \; \hat{b}^*_{sb} \; \hat{b}^*_{sc} \; b^*_{p7} \; b^*_{p8} \; b^*_{p9}]^T$. To conclude, the interconnection of the subsystems are again given by (3-9) and (3-10).

3-3-2 Formulating the Dirac structure

To formulate the Dirac structure with Proposition 1, the branches and dual branches of the switches must be assigned as efforts and flows (the assignment of the other branches is the same the one Section 3-2-2). The assignment of the currents and voltages of the switches to the efforts and flows boils down to the question: *are the switches, which are nonlinear elements, current- or voltage-driven?* It turns out that for the switches such a viewpoint not correct and their assignment is ambiguous. The choice for their causal relation does not depend on their place in the network topology, like the place of the position of the resistive element makes it either a conductor or resistor. This statement will be shown in the next section. For now we propose to assign the efforts and flows of the switches with the following proposition.

Proposition 3. *When regarding the switches as nonlinear, resistive-type elements, assign their currents as flows and their voltages as efforts.*

Note that a direct consequence of Proposition 3 is that the ISO form can have flows as outputs and efforts as inputs.

By Proposition 2 and Proposition 3 all branches corresponding to $A(G_{\Sigma_2})$ are flows and all dual branches corresponding to $A(G^*_{\Sigma_2})$ are efforts. Hence, with the incidence matrices, the interconnection and the efforts and flows defined, the Dirac structure of the total system can be formulated with Proposition 1. The flow and effort vectors of the total system are given by (3-11) and (3-12), where f_{Σ_1}, e_{Σ_1}, f_{Σ_3} and e_{Σ_3} are the same, but for Σ_2 the flow and effort vectors become[8]

$$f_{\Sigma_2} = \begin{bmatrix} f_4 & f_5 & f_6 & f_{sa} & f_{sb} & f_{sc} & \hat{f}_{sa} & \hat{f}_{sb} & \hat{f}_{sc} & f_7 & f_8 & f_9 \end{bmatrix}^T,$$
$$e_{\Sigma_2} = \begin{bmatrix} e_4 & e_5 & e_6 & e_{sa} & e_{sb} & e_{sc} & \hat{e}_{sa} & \hat{e}_{sb} & \hat{e}_{sc} & e_7 & e_8 & e_9 \end{bmatrix}^T.$$

This results in a kernel representation with the matrices, $F \in \mathbb{R}^{36\times 31}$, $E \in \mathbb{R}^{36\times 31}$ composed of the matrices $F_{\Sigma_1}, E_{\Sigma_1}, \ldots, F_{\Sigma_3}, E_{\Sigma_3}$, which are now

$$F_{\Sigma_1} = \begin{bmatrix} A_f(G_{\Sigma_1}) \\ A_f(G^*_{\Sigma_1}) \end{bmatrix}, \qquad F_{\Sigma_2} = \begin{bmatrix} A_f(G_{\Sigma_2}) \\ \mathbb{O} \end{bmatrix}, \qquad F_{\Sigma_3} = \begin{bmatrix} A_f(G_{\Sigma_3}) \\ A_f(G^*_{\Sigma_3}) \end{bmatrix}, \tag{3-25}$$

$$E_{\Sigma_1} = \begin{bmatrix} A_e(G_{\Sigma_1}) \\ A_e(G^*_{\Sigma_1}) \end{bmatrix}, \qquad E_{\Sigma_2} = \begin{bmatrix} \mathbb{O} \\ A_e(G^*_{\Sigma_2}) \end{bmatrix}, \qquad E_{\Sigma_3} = \begin{bmatrix} A_e(G_{\Sigma_3}) \\ A_e(G^*_{\Sigma_3}) \end{bmatrix}. \tag{3-26}$$

3-3-3 Deriving the differential-algebraic model and input-state-output model

Solving the characteristic equation of the kernel representation yields the mathematical model of the system. In this case, the PH model has additional inputs and outputs, because the switches are modelled as nonlinear elements. Nonetheless, parametrising this model in terms of the switch states, by computing the equations for each switch state, should yield the same model as with the VEM. We shall show this in the two ways: first, by showing that the representations for Σ_2 are equivalent (Σ_2 is the only subsystem that changed). The purpose of this is to provide insight and arguments for Proposition 2 and 3. Second, by parametrising the resulting ISO system and thereby showing that the ISO representations are equivalent.

Analysing the mathematical representation of Σ_2

Consider the general mathematical expression for the DC (f_ℓ, e_ℓ) to AC terminal $(f_{\ell+3}, e_{\ell+3})$ loop in Σ_2, where $\ell = 4, 5, 6$. Rewriting

$$F_{\Sigma_2} f_{\Sigma_2} + E_{\Sigma_2} e_{\Sigma_2} = 0,$$

leads to the mathematical input-output model

$$\begin{aligned} f_\ell &= f_{\ell+3} - f_{sj} + \hat{f}_{sk}, \\ e_{\ell+3} &= -e_\ell + e_{sk} - \hat{e}_{sj}, \end{aligned} \tag{3-27}$$

[8] For convenience, the arguments of the switch state $f_{\mathcal{W}}(s), e_{\mathcal{W}}(s)$ are omitted in the switch variables.

$$\begin{aligned} \hat{f}_{sj} &= f_{sj} - f_{\ell+3}, \\ f_{sk} &= f_{\ell+3} + \hat{f}_{sk}, \\ \hat{e}_{sk} &= e_{sk} - e_{\ell}, \\ e_{sj} &= e_{\ell} + \hat{e}_{sj}, \end{aligned} \tag{3-28}$$

where $jk \in \{ab, bc, ca\}$. It is apparent that this is only one of many input-output representations, e.g. $[f_\ell \; e_\ell]^T$ or $[f_{\ell+3} \; e_{\ell+3}]^T$ qualify just as well as outputs of Σ_2. Therefore, based solely on analyses of Σ_2, the correct ("causal") input-output model cannot be chosen. The correct causality for Σ_2 is dictated by Σ_1 and Σ_3 and although this correct causal definition is easily uncovered in this case, it might not be necessarily the case for any kind of interconnected subsystem (this arguments for Proposition 2). Furthermore, one would expect that, based on the positions within the network, the voltages of the switches are flows (inputs) and the currents efforts (outputs). However, this is clearly not true based from the resulting equations (3-27) and (3-28). In fact, some of the switches have currents as inputs or outputs and some have voltages. Defining which of the switches have currents and which ones voltages is a matter of choice, e.g, $f_{sj}, \hat{f}_{sk}$ could also have been chosen as the inputs. Therefore, the correct effort and flow for the switches are ambiguous and potentially are a matter of choice. (for this reason Proposition 3 is constructed).

Computing (3-28) for every switch configuration and substituting the result in (3-27) yields

$$\begin{aligned}
s_j = 0,\ s_k = 0 \Rightarrow &\begin{cases} f_{sj} = f_{sk} = 0 \Rightarrow & \hat{f}_{sj} = -f_{\ell+3},\ \hat{f}_{sk} = -f_{\ell+3} \Rightarrow \quad f_\ell = 0, \\ \hat{e}_{sj} = \hat{e}_{sk} = 0 \Rightarrow & e_{sk} = e_\ell,\ e_{sj} = e_\ell \Rightarrow \quad e_{\ell+3} = 0. \end{cases} \\
s_j = 1,\ s_k = 1 \Rightarrow &\begin{cases} \hat{f}_{sj} = \hat{f}_{sk} = 0 \Rightarrow & f_{sj} = f_{\ell+3},\ f_{sk} = f_{\ell+3} \Rightarrow \quad f_\ell = 0, \\ e_{sj} = e_{sk} = 0 \Rightarrow & \hat{e}_{sk} = -e_\ell,\ \hat{e}_{sj} = -e_\ell \Rightarrow \quad e_{\ell+3} = 0. \end{cases} \\
s_j = 1,\ s_k = 0 \Rightarrow &\begin{cases} \hat{f}_{sj} = f_{sk} = 0 \Rightarrow & f_{sj} = f_{\ell+3},\ \hat{f}_{sk} = -f_{\ell+3} \Rightarrow \quad f_\ell = -f_{\ell+3}, \\ e_{sj} = \hat{e}_{sk} = 0 \Rightarrow & e_{sk} = e_\ell,\ \hat{e}_{sj} = -e_\ell \Rightarrow \quad e_{\ell+3} = e_\ell. \end{cases} \\
s_j = 0,\ s_k = 1 \Rightarrow &\begin{cases} f_{sj} = \hat{f}_{sk} = 0 \Rightarrow & \hat{f}_{sj} = -f_{\ell+3},\ f_{sk} = f_{\ell+3} \Rightarrow \quad f_\ell = f_{\ell+3}, \\ \hat{e}_{sj} = e_{sk} = 0 \Rightarrow & \hat{e}_{sk} = -e_\ell,\ e_{sj} = e_\ell \Rightarrow \quad e_{\ell+3} = -e_\ell. \end{cases}
\end{aligned}$$

This reduces to the following input-output model, parametrised by the switch states $s_j, s_k \in \{0, 1\}$,

$$\begin{aligned} f_\ell &= -f_{\ell+3}(s_j - s_k), \\ e_{\ell+3} &= e_\ell(s_j - s_k), \end{aligned}$$

with $jk \in \{ab, bc, ca\}$ and $\ell = 4, 5, 6$. This model coincides with the parametrised kernel representation in (3-15). Therefore, both representations are equivalent.

Parametrising the resulting differential-algebraic model

The DAM model of the system with the switches modelled as input-output ports reads as

$$\begin{bmatrix} \mathbb{I}^{3\times3} & & \mathbb{O}^{3\times3} & \\ & 1 & -1 & 0 \\ \mathbb{O}^{3\times3} & 0 & 1 & -1 \\ & -1 & 0 & 1 \end{bmatrix} \dot{x} = \begin{bmatrix} & \mathbb{O}^{3\times3} & & \mathbb{I}^{3\times3} \\ 1 & -1 & 0 & \\ 0 & 1 & -1 & \mathbb{O}^{3\times3} \\ -1 & 0 & 1 & \end{bmatrix} \frac{\partial H}{\partial x}(x) + \begin{bmatrix} & \mathbb{O}^{3\times3} & \\ 1 & -1 & 0 \\ 0 & 1 & -1 \\ -1 & 0 & 1 \end{bmatrix} f_R -$$

$$\begin{bmatrix} \mathbb{O}^{3\times1} \\ 1 \\ 1 \\ 1 \end{bmatrix} u_{dc} - \begin{bmatrix} \mathbb{O}^{3\times3} \\ 0 & 1 & 0 \\ 0 & 0 & 1 \\ 1 & 0 & 0 \end{bmatrix} \begin{bmatrix} e_{s_a} \\ e_{s_b} \\ e_{s_c} \end{bmatrix} + \begin{bmatrix} \mathbb{O}^{3\times3} \\ \mathbb{I}^{3\times3} \end{bmatrix} \begin{bmatrix} \hat{f}_{e_a} \\ \hat{e}_{s_b} \\ \hat{e}_{s_c} \end{bmatrix} + g_{AC} u_{AC},$$

$$\text{s.t.} \quad \dot{q}_a + \dot{q}_b + \dot{q}_c = 0,$$

$$e_R = \begin{bmatrix} \mathbb{O}^{3\times3} & \mathbb{I}^{3\times3} \end{bmatrix} \frac{\partial H}{\partial x}(x),$$

$$y_{dc} = f_{10} - f_{sa} + \hat{f}_{sb} + f_{11} - f_{sb} + \hat{f}_{sc} + f_{12} - f_{sc} + \hat{f}_{sa},$$

$$\hat{f}_{sa} = f_{sa} - f_{10},$$

$$f_{sb} = f_{10} + \hat{f}_{sb},$$

$$\hat{f}_{sb} = f_{sb} - f_{11},$$

$$f_{sc} = f_{11} + \hat{f}_{sc},$$

$$\hat{f}_{sc} = f_{sc} - f_{12},$$

$$f_{sa} = f_{12} + \hat{f}_{sa},$$

$$\text{s.t.} \quad \begin{bmatrix} -f_{10} + f_{11} \\ f_{10} - f_{11} \\ f_{11} - f_{12} \end{bmatrix} = \frac{\partial H}{\partial x}(x),$$

$$\hat{e}_{sb} = e_{sb} - u_{dc},$$

$$e_{sa} = u_{dc} + \hat{e}_{sa},$$

$$\hat{e}_{sc} = e_{sc} - u_{dc},$$

$$e_{sb} = u_{dc} + \hat{e}_{sb},$$

$$\hat{e}_{sa} = e_{sa} - u_{dc},$$

$$e_{sc} = u_{dc} + \hat{e}_{sc},$$

$$y_{AC} = g_{AC}^T \frac{\partial H}{\partial x}(x),$$

with $s_a, s_b, s_c \in \{0, 1\}$, the Hamiltonian given by (3-2) and the resistive relation

$$e_R = \begin{bmatrix} -\frac{1}{R_a} & 0 & 0 \\ 0 & -\frac{1}{R_b} & 0 \\ 0 & 0 & -\frac{1}{R_c} \end{bmatrix} f_R.$$

Computing the DC output and input matrix for each switch configuration in the same manner as we parametrised the input-output model of Σ_2 leads to the DAM model, parametrised by the switch state, in (3-17). The details of the derivation are given in Appendix C-2. Since the parametrised DAMs are the same, assuming a balanced systems leads to the ISO model of the three-phase converter described by (3-22). Thus, both the NEM and the VEM lead to the same model.

Observe that it is not possible to write the non-parametrised DAM in such a way that the latent interconnection variables, f_{10}, f_{11}, f_{12} are removed. Moreover, because the structure in the non-parametrised DAM does not seem to be PH at all. This result is unexpected and seems wrong for a number of reasons. For instance, Theorem 1 proves that composing

Dirac structures always removes the latent variables whose proof is considered watertight, and it seems odd we can start with a PH system and end with one, but have a intermediate result that is not a PH system. On the other hand ,there are some arguments that make this result seem logical. For one, the E and F matrices consist of the incidence matrices that correspond to the graph and dual graph. We separated the system into subsystems for the exact reason that a dual graph did not exits of the total system. The non-existence of a dual graph advocates that we should not be able to find a E and a F matrix of the complete system, because having these would imply we can deduce $A(G^*)$ and be able to draw the dual graph of the system. Clearly, this conflicts with the original premisses of the non-existence of the dual graph. Subsequently, one would counter argument that it should therefore also not be possible to remove all latent variables in the DAM obtained with the VEM. However, there is an important difference. Indeed, the VEM requires us to split the system into planar subsystem, but the non-planarity is entirely contained within the virtual graph. The reference graph is planar the graphs for each switch configuration are also planar. Therefore, $E(S)$ and $F(S)$ always correspond to a planar system. This is clearly not the case in the NEM, where the switches are elements and the Dirac structure non-planar. Unfortunately, which of the two viewpoint are right remains unclear and an exact and satisfying answer still eludes the author.

Concluding, both methods yield the same mathematical models, but the VEM provides a more structured approach for finding the parametrised mathematical model. However, as seen in the previous section, the VEM can yield inconvenient and complex parametrisations, which must be simplified in order to make sense and be comprehensible. Two advantages of the NEM are that it does not change if the switches are no longer ideal, provided that only the constitutive relation changes, and that gets the parametrisation that is expected. On the other hand, the DAM obtained with the NEM seems to point to some deficiency in the model procedure or in the model itself. Furthermore, the assignment of the generalised efforts and flows beforehand can become a tedious, complicated and unintuitive problem with regard to the switching elements and interconnection ports. These problems are avoided by introducing Proposition 2 and Proposition 3, which, in essence is the non-generalised effort and flow definitions for electrical systems[9]. The identification of voltages and currents as efforts and flows in electrical systems are worth to be given more thought.

[9]In the non-generalised port-Hamiltonian framework, the efforts and flows for electrical systems are defined as voltages and currents, respectively, see [20, 22].

Chapter 4

Modelling the three-phase rectifier

This chapter features the modelling of the three-phase rectifier using the two methods presented in Chapter 2. In short, the procedure for both methods comes down to: (i) determine the subsystems and corresponding subgraphs, (ii) express the Dirac structure of the system in a kernel representation with the (parametrised) incidence matrices, (iii) solve the characteristic equation of the kernel representation to find the differential-algebraic model (DAM) and (iv) derive the input-state-output (ISO) model from the DAM by assuming a balanced system. The structure of this chapter is as follows. First, Section 4-1 presents the reference model of the rectifier from literature, which is used for validation and comparison. Then, Section 4-2 shows the derivation of the models by using the VEM. Subsequently, Section 4-3 deals with the modelling of the power converter with the NEM. Last, Section 4-4 is dedicated to modelling a rectifier with the inverter model from the previous chapter.

4-1 The reference model of the three-phase rectifier

Figure 4-1 presents the three-phase rectifier from Tang et al. [9]. The DC side load is represented as a resistance R_L. The network of the three-phase rectifier is assumed to be balanced ($L_a = L_b = L_c = L$, $R_a = R_b = R_c = R$). The Hamiltonian corresponding to the rectifier in Figure 4-1 is

$$H(\phi, q) = \sum_{k=a,b,c} \left(\frac{1}{2} \frac{\phi_k}{L} \right) + \frac{1}{2} \frac{q}{C}, \tag{4-1}$$

where $\phi = (\phi_a \ \phi_b \ \phi_c)^T$ denotes the flux-linkage of the inductors, and q denotes the charge in the capacitor. The corresponding ISO model is[1]

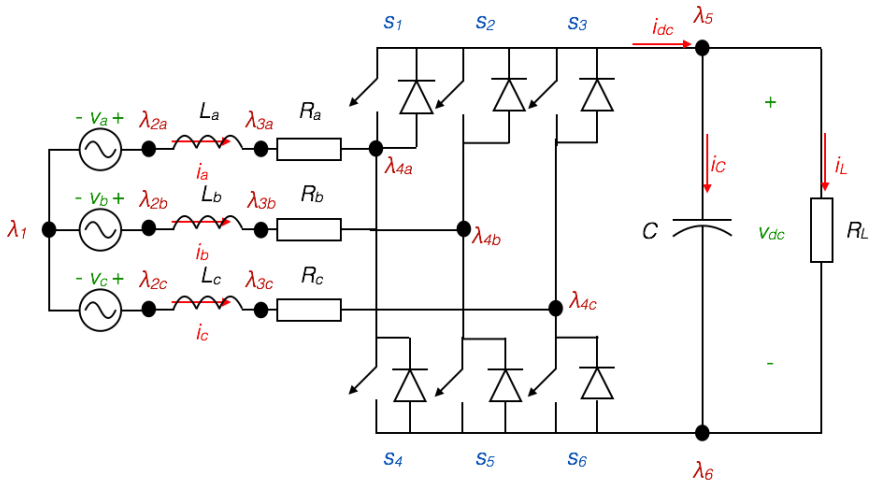

Figure 4-1: Three-phase voltage soure rectifier with resistive load.

$$\begin{aligned}
\begin{bmatrix} \dot{\phi} \\ \dot{q} \end{bmatrix} &= \begin{bmatrix} -R & 0 & 0 & -\hat{s}_a \\ 0 & -R & 0 & -\hat{s}_b \\ 0 & 0 & -R & -\hat{s}_c \\ \hat{s}_a & \hat{s}_b & \hat{s}_c & -\frac{1}{R_L} \end{bmatrix} \begin{bmatrix} \frac{\partial H}{\partial \phi} \\ \frac{\partial H}{\partial q} \end{bmatrix} + \begin{bmatrix} 1 & 0 & 0 \\ 0 & 1 & 0 \\ 0 & 0 & 1 \\ 0 & 0 & 0 \end{bmatrix} \begin{bmatrix} u_a \\ u_b \\ u_c \end{bmatrix}, \\
\begin{bmatrix} y_a \\ y_b \\ y_c \end{bmatrix} &= \begin{bmatrix} 1 & 0 & 0 & 0 \\ 0 & 1 & 0 & 0 \\ 0 & 0 & 1 & 0 \end{bmatrix} \begin{bmatrix} \frac{\partial H}{\partial \phi} \\ \frac{\partial H}{\partial q} \end{bmatrix},
\end{aligned} \tag{4-2}$$

where $u_j = v_j$, $y_j = i_j$ and $\hat{s}_j = s_j - \frac{1}{3} \sum_{k=a,b,c} s_k$, $j \in \{a, b, c\}$.

4-2 Modelling the rectifier with the virtual element method

This section presents the modelling of the three-phase rectifier with the VEM. First, in Section 4-2-1 we discuss the separation of the network into planar subsystems. Second, in Section 4-2-2 the Dirac structure of the system is formulated. Then, in Section 4-2-3 the DAM is derived by solving the characteristic equation. Finally, Section 4-2-4 shows how the DAM is transformed into an ISO model by assuming a balanced system.

4-2-1 Separating the system into planar subsystems

Clearly, the graph of the network in Figure 4-1 is not planar. Hence, the system is separated into three planar subsystems by separating the AC input side, the switching structure and the DC output side, see Figure 4-2. Observe the similarity between the division of the rectifier and the inverter. Indeed, both Σ_2's have the same structure, but with the input and output swapped.

[1] Additional details can be found in Appendix B-3.

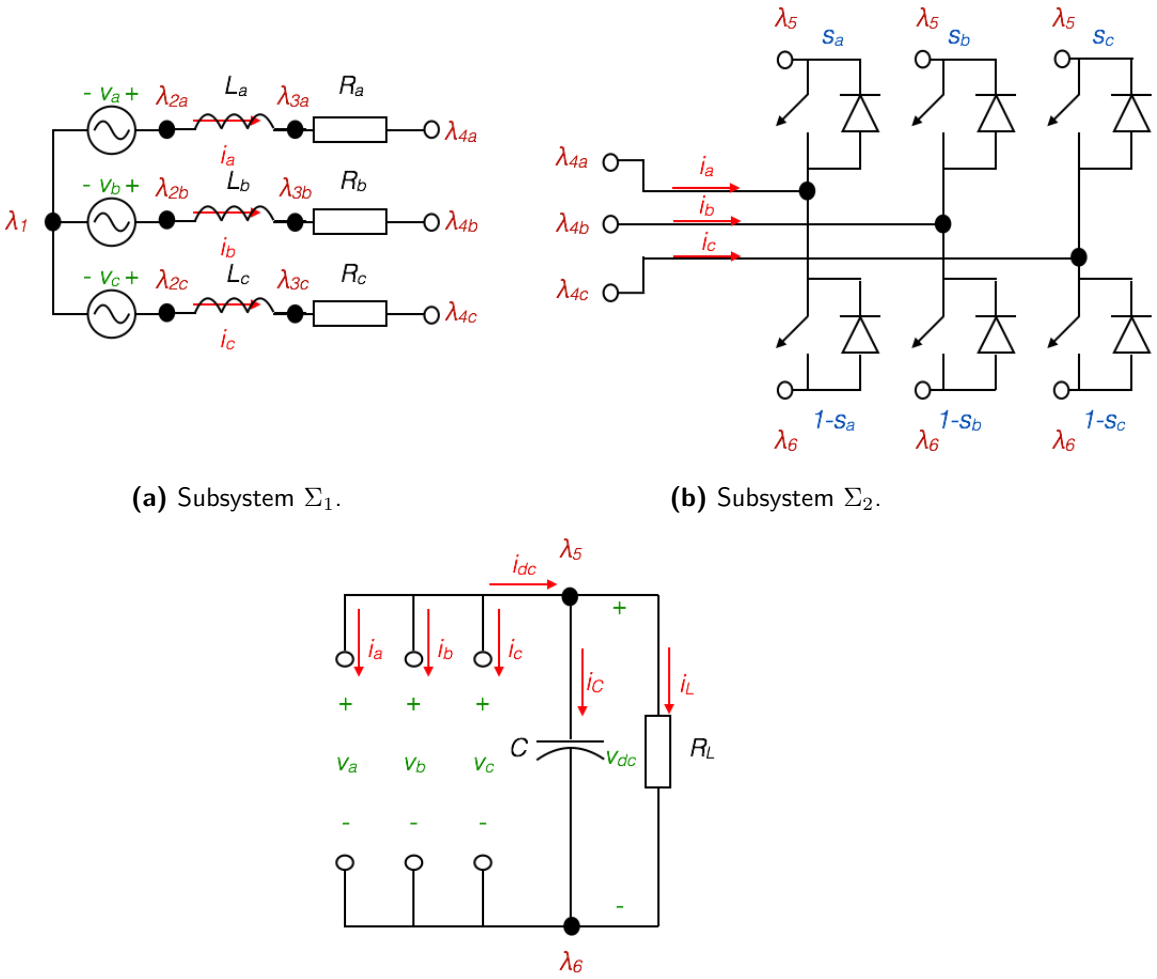

(a) Subsystem Σ_1.

(b) Subsystem Σ_2.

(c) Subsystem Σ_3.

Figure 4-2: The three-phase rectifier split into three subsystems, Σ_1, Σ_2 and Σ_3.

The graphs representing the subsystems are given in Figure 4-3 for Σ_1, Figure 4-4 for Σ_2 and Figure 4-5 for Σ_3. Again, we can identify three identical graphs in Σ_2. This allows us to represent Σ_2 by a single graph for each line-to-line-AC to DC loop, see Section 3-2-1. The branches denoting the terminals interconnecting the subsystems are given the additional subscript p. For the sake of simplicity the structure of the graphs of Σ_2 for the rectifier and inverter are kept the same and only the port branches swap positions in the vectors. This corresponds to a reversed direction of the power flow. To satisfy Assumption 5, the switch states $s_1, \ldots, s_6$ are coupled through (3-4), which implies that the switch states corresponding to the branches b_{s1}, b_{s2}, b_{s3}, b_{s4} are s_j, s_k, $1-s_j$ and $1-s_k$, respectively, where $jk \in \{ab, bc, ca\}$.

Capturing the interconnection of the branches in the incidence matrices with the CCL yields

$$A(G_{\Sigma_1}) = \begin{bmatrix} -1 & -1 & -1 & 0 & 0 & 0 & & & & & & \\ 1 & 0 & 0 & 1 & 0 & 0 & & & & & & \\ 0 & 1 & 0 & 0 & 1 & 0 & & & & & \mathbb{O}^{4\times 6} & \\ 0 & 0 & 1 & 0 & 0 & 1 & & & & & & \\ & & & -1 & 0 & 0 & 1 & 0 & 0 & & & \\ & \mathbb{O}^{3\times 3} & & 0 & -1 & 0 & 0 & 1 & 0 & & \mathbb{O}^{3\times 3} & \\ & & & 0 & 0 & -1 & 0 & 0 & 1 & & & \\ & & & & & & -1 & 0 & 0 & 1 & 0 & -1 \\ & \mathbb{O}^{3\times 6} & & & & & 0 & -1 & 0 & -1 & 1 & 0 \\ & & & & & & 0 & 0 & -1 & 0 & -1 & 1 \end{bmatrix},$$

for the graph of Σ_1. Likewise, the dual graph of Σ_1 yields the incidence matrix

$$A(G^*_{\Sigma_1}) = \begin{bmatrix} -1 & 0 & 1 & 1 & 0 & -1 & 1 & -1 & 0 & 0 & 0 & -1 \\ 0 & 1 & -1 & 0 & -1 & 1 & 0 & -1 & 1 & 0 & -1 & 0 \\ 1 & -1 & 0 & -1 & 1 & 0 & -1 & 1 & 0 & -1 & 0 & 0 \\ 0 & 0 & 0 & 0 & 0 & 0 & 0 & 0 & 0 & 1 & 1 & 1 \end{bmatrix},$$

and the corresponding vectors for these matrices are, respectively,

$$B_{\Sigma_1} = \begin{bmatrix} b_1 & b_2 & b_3 & b_4 & b_5 & b_6 & b_7 & b_8 & b_9 & b_{p1} & b_{p2} & b_{p3} \end{bmatrix}^T,$$
$$B^*_{\Sigma_1} = \begin{bmatrix} b^*_1 & b^*_2 & b^*_3 & b^*_4 & b^*_5 & b^*_6 & b^*_7 & b^*_8 & b^*_9 & b^*_{p1} & b^*_{p2} & b^*_{p3} \end{bmatrix}^T.$$

The PIMs are the same, because the structure of the graphs of Σ_2 for the inverter and the rectifier are the same. Thus, (3-5) is the PIM of the graph in Figure 3-5a and (3-7) is the PIM of the dual graph of in Figure 3-5b. Consequently, the PIMs for the KCL and KVL are given by (3-6) and (3-8), respectively, with the vectors

$$B_{\Sigma_2} = \begin{bmatrix} b_{p7} & b_{p4} & b_{p8} & b_{p5} & b_{p9} & b_{p6} \end{bmatrix}^T,$$
$$B^*_{\Sigma_2} = \begin{bmatrix} b^*_{p7} & b^*_{p4} & b^*_{p8} & b^*_{p5} & b^*_{p9} & b^*_{p6} \end{bmatrix}^T.$$

Expressing the last subsystem. The incidence matrix for the graph of Σ_3 is

$$A(G_{\Sigma_3}) = \begin{bmatrix} 1 & 1 & 1 & 1 & 1 \\ -1 & -1 & -1 & -1 & -1 \end{bmatrix},$$

with the vector $B_{\Sigma_3} = [b_{p10} \quad b_{p11} \quad b_{p12} \quad b_{10} \quad b_{11} \quad b_{12}]^T$. The incidence matrix for the dual graph of Σ_3 is

$$A(G^*_{\Sigma_3}) = \begin{bmatrix} 1 & 0 & 0 & 0 & -1 \\ -1 & 1 & 0 & 0 & 0 \\ 0 & -1 & 1 & 0 & 0 \\ 0 & 0 & -1 & 1 & 0 \\ 0 & 0 & 0 & -1 & 1 \end{bmatrix},$$

with $B^*_{\Sigma_3} = [b^*_{p10} \quad b^*_{p11} \quad b^*_{p12} \quad b^*_{10} \quad b^*_{11} \quad b_{12}]^T$. Lastly, the interconnection of the subsystem is achieved by relating the voltages and currents of the interconnection ports. The interconnection between the Σ_1 and Σ_2 is given by (3-9) and the interconnection between Σ_2 and Σ_3 by (3-10).

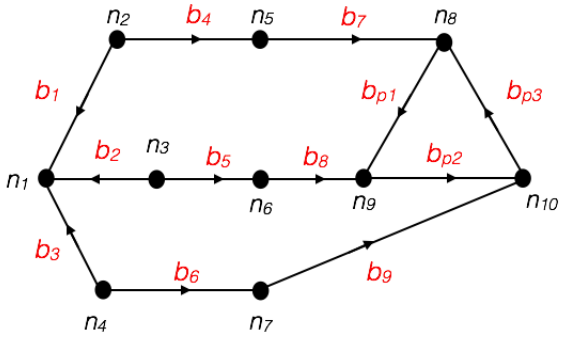

(a) Graph of Σ_1.

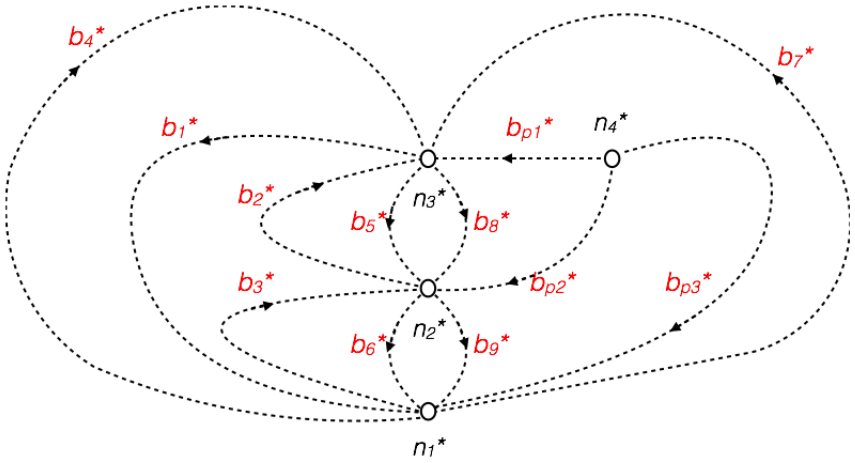

(b) Dual graph of Σ_1.

Figure 4-3: The graph and dual graph of Σ_1.

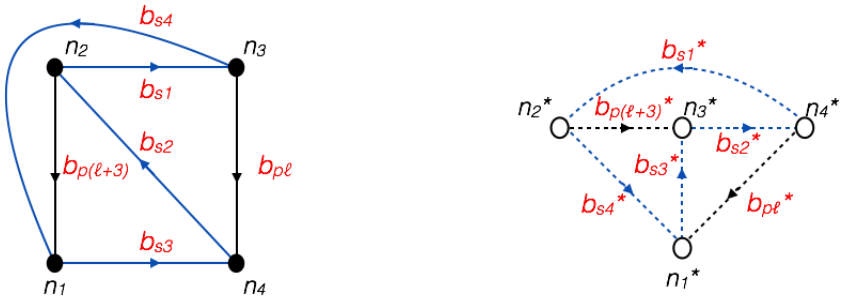

(a) Graph of Σ_2.

(b) Dual graph of Σ_2.

Figure 4-4: The simplified graph and dual graph of Σ_2.

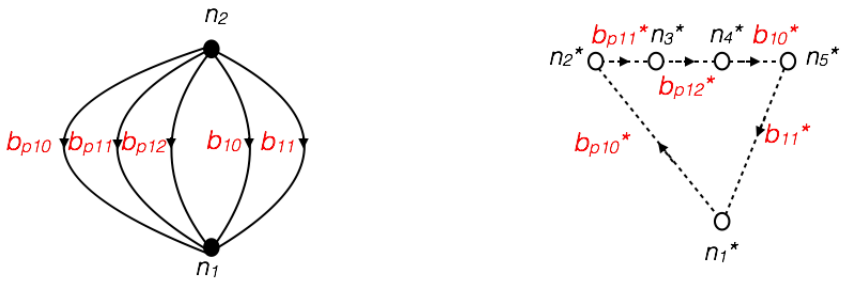

(a) Graph of Σ_3. **(b)** Dual graph Σ_3.

Figure 4-5: The graph and dual graph of Σ_3.

4-2-2 Formulating the Dirac structure

Proposition 2 defines that the branches of the port variables are flows and the dual branches of the port variables are efforts. The voltages in the inductors and the current in the capacitor are flows due to the definition of efforts and flows for storage elements (2-4). The other voltages and currents are identified by analysing the network in Figure 4-1. The AC voltage sources are inputs and hence also flows. The resistors R_a, R_b, R_c are in series with the inductors, which means that their voltages are flows (voltage-driven). R_L's current is a flow (current-driven). Thus, for Σ_1 the branches $b_1, \ldots, b_9$ and dual branches $b^*_{p1}, b^*_{p2}, b^*_{p3}$ are efforts, while the dual branches $b^*_1, \ldots, b_9$ and the branches b_{p1}, b_{p2}, b_{p3} are flows. For Σ_2 and Σ_3 all branches are flows and all dual branches are efforts. Subsequently, compiling the flows and efforts into one flow and one effort vector and substituting $f_{\mathcal{S}}, e_{\mathcal{S}}$ by $-\dot{x}, \frac{\partial H}{\partial x}$, $f_{\mathcal{P}}, e_{\mathcal{P}}$ by u, y yields the vectors

$$f = \begin{bmatrix} f_{\Sigma_1}^T & f_{\Sigma_2}^T & f_{\Sigma_3}^T \end{bmatrix}^T, \tag{4-3}$$

$$e = \begin{bmatrix} e_{\Sigma_1}^T & e_{\Sigma_2}^T & e_{\Sigma_3}^T \end{bmatrix}^T, \tag{4-4}$$

where

$$f_{\Sigma_1} = \begin{bmatrix} u_a & u_b & u_c & -\dot{\phi}_a & -\dot{\phi}_b & -\dot{\phi}_c & f_{Ra} & f_{Rb} & f_{Rc} & f_1 & f_2 & f_3 \end{bmatrix}^T,$$

$$e_{\Sigma_1} = \begin{bmatrix} y_a & y_b & y_c & \frac{\partial H}{\partial \phi_a} & \frac{\partial H}{\partial \phi_b} & \frac{\partial H}{\partial \phi_c} & e_{Ra} & e_{Rb} & e_{Rc} & e_1 & e_2 & e_3 \end{bmatrix}^T,$$

$$f_{\Sigma_2} = \begin{bmatrix} f_7 & f_4 & f_8 & f_5 & f_9 & f_6 \end{bmatrix}^T,$$

$$e_{\Sigma_2} = \begin{bmatrix} e_7 & e_4 & e_8 & e_5 & e_9 & e_6 \end{bmatrix}^T,$$

$$f_{\Sigma_3} = \begin{bmatrix} f_{10} & f_{11} & f_{12} & -\dot{q} & f_R \end{bmatrix}^T,$$

$$e_{\Sigma_3} = \begin{bmatrix} e_{10} & e_{11} & e_{12} & \frac{\partial H}{\partial q} & e_R \end{bmatrix}^T.$$

The efforts and flows denoting an interconnection between two subsystems are indexed, where the index e_j, f_j corresponds with the index of the port branch b_{pj}, b^*_{pj}. The corresponding $F \in \mathbb{R}^{33\times 23}$, $E \in \mathbb{R}^{33\times 23}$ matrices are composed of the matrices $F_{\Sigma_1}, E_{\Sigma_1}, \ldots, F_{\Sigma_3}, E_{\Sigma_3}$ defined in (3-13) and (3-14) and F_I and E_I, which are the canonical interconnection rewritten in

a matrix form. Notice that there are no non-admissible switch configurations due to the dependency of the switch states, which means that $\mathcal{A}(\Sigma) = \{0,1\}^3$. As a result, the Dirac structure defines an implicit PH system as

$$\left(\begin{bmatrix} -\dot{\phi} \\ -\dot{q} \end{bmatrix}, \begin{bmatrix} \frac{\partial H}{\partial \phi} \\ \frac{\partial H}{\partial q} \end{bmatrix}, f_R, e_R, f_{R_L}, e_{R_L}, u, y \right) \in \mathcal{D}(S),\ S \in \mathcal{A}(\Sigma),$$

where $y = [y_a\ y_b\ y_c]^T$, $u = [u_a\ u_b\ u_c]^T$, $\phi = [\phi_a\ \phi_b\ \phi_c]^T$, $f_R = [f_{Ra}\ f_{Rb}\ f_{Rc}]^T$ and $e_R = [e_{Ra}\ e_{Rb}\ e_{Rc}]^T$.

4-2-3 Deriving the differential-algebraic model

Solving the characteristic equation of the kernel representation yields a differential-algebraic-model (DAM), because the voltages (and therefore the flux-linkages) in every inductor are dependent. In this section we show the derivation of the DAM model by solving the characteristic equation for $\dot{\phi}$, $\dot{q}$, y, e_R and e_{R_L}. First, simplifying the parametrisation of Σ_2 by computing the characteristic equation for each switch configuration, which yields the more convenient model

$$\begin{aligned} f_{\ell+3} &= -f_\ell(s_j - s_k), \\ e_\ell &= e_{\ell+3}(s_j - s_k), \end{aligned} \tag{4-5}$$

where $\ell = 4,5,6$ and $jk \in \{ab, bc, ca\}$. The model in (4-5) is the reversed equivalent of (3-15). Then, computing the composed kernel representation for $\dot{x}, y, e_R$ and e_{R_L} yields the DAM[2]

$$\begin{aligned} \begin{bmatrix} 1 & -1 & 0 & 0 \\ 0 & 1 & -1 & 0 \\ -1 & 0 & 1 & 0 \\ 0 & 0 & 0 & 1 \end{bmatrix} \dot{x} &= \begin{bmatrix} 0 & 0 & 0 & (s_a - s_b) \\ 0 & 0 & 0 & (s_b - s_c) \\ 0 & 0 & 0 & (s_c - s_a) \\ -s_a & -s_b & -s_c & 0 \end{bmatrix} \frac{\partial H}{\partial x} + \\ &\quad \begin{bmatrix} 1 & -1 & 0 & 0 \\ 0 & 1 & -1 & 0 \\ -1 & 0 & 1 & 0 \\ 0 & 0 & 0 & 1 \end{bmatrix} \begin{bmatrix} f_R \\ f_{R_L} \end{bmatrix} + \begin{bmatrix} -1 & 1 & 0 & 0 \\ 0 & -1 & 1 & 0 \\ 1 & 0 & -1 & 0 \\ 0 & 0 & 0 & 0 \end{bmatrix} u, \\ \begin{bmatrix} e_R \\ e_{R_L} \end{bmatrix} &= \begin{bmatrix} \mathbb{I}^{4\times 4} \end{bmatrix} \frac{\partial H}{\partial x}, \\ y &= \begin{bmatrix} -\mathbb{I}^{3\times 3}\ \mathbb{O}^{3\times 1} \end{bmatrix} \frac{\partial H}{\partial x}, \\ &\text{s.t. } y_a + y_b + y_c = 0, \end{aligned} \tag{4-6}$$

where $x = [\phi_a\ \phi_b\ \phi_c\ q]^T$, the Hamiltonian in (4-1) and the resistive relation given by

$$\begin{bmatrix} e_R \\ e_{R_L} \end{bmatrix} = \begin{bmatrix} -\frac{1}{R_a} & 0 & 0 & 0 \\ 0 & -\frac{1}{R_b} & 0 & 0 \\ 0 & 0 & -\frac{1}{R_c} & 0 \\ 0 & 0 & 0 & -R_L \end{bmatrix} \begin{bmatrix} f_R \\ f_{R_L} \end{bmatrix}.$$

[2]For the complete derivation see Appendix C-3.

4-2-4 Deriving the input-state-output model

The DAM in (4-6) can be subsequently transformed into a set of explicit differential equations (the ISO structure) by assuming that the system is balanced ($L_a = L_b = L_c = L$, $R_a = R_b = R_c = R$). Subsequently, the line-to-line voltages in (4-6) can be expressed in terms of the phase voltages with respect to the common potential[3] λ_1. This yields the independent differential equations

$$\begin{aligned}
\dot{\phi}_a &= e_{Ra} + \left(\frac{2}{3}s_a - \frac{1}{3}s_b - \frac{1}{3}s_c\right)\frac{\partial H}{\partial q} - u_a,\\
\dot{\phi}_b &= e_{Rb} + \left(\frac{2}{3}s_b - \frac{1}{3}s_a - \frac{1}{3}s_c\right)\frac{\partial H}{\partial q} - u_b,\\
\dot{\phi}_c &= e_{Rc} + \left(\frac{2}{3}s_c - \frac{1}{3}s_a - \frac{1}{3}s_b\right)\frac{\partial H}{\partial q} - u_c.
\end{aligned}$$

Likewise, the current through the capacitor can be rewritten in terms of the phase currents by assuming a balanced load. This is easiest to see in the following way. Consider the following equations of $\mathcal{D}_2 \circ \mathcal{D}_3$

$$\dot{q} = f_{R_L} - f_1(s_a - s_b) - f_2(s_b - s_c) - f_3(s_c - s_a), \tag{4-7}$$

and the following equations of $\mathcal{D}_1$

$$\begin{aligned}
f_1 - f_3 &= \frac{\partial H}{\partial \phi_a},\\
f_2 - f_1 &= \frac{\partial H}{\partial \phi_b},\\
f_3 - f_2 &= \frac{\partial H}{\partial \phi_c}.
\end{aligned} \tag{4-8}$$

First, rewrite (4-7) to

$$\begin{aligned}
\dot{q} =& f_{R_L} - \left(f_1\left(\frac{2}{3}s_a - \frac{1}{3}s_b - \frac{1}{3}s_c\right) - f_1\left(\frac{2}{3}s_b - \frac{1}{3}s_a - \frac{1}{3}s_c\right) + f_2\left(\frac{2}{3}s_b - \frac{1}{3}s_a - \frac{1}{3}s_c\right) - \right.\\
& \left. f_2\left(\frac{2}{3}s_c - \frac{1}{3}s_a - \frac{1}{3}s_b\right) + f_3\left(\frac{2}{3}s_c - \frac{1}{3}s_a - \frac{1}{3}s_b\right) - f_3\left(\frac{2}{3}s_a - \frac{1}{3}s_b - \frac{1}{3}s_c\right)\right),\\
=& f_{R_L} - \left((f_1 - f_3)\left(\frac{2}{3}s_a - \frac{1}{3}s_b - \frac{1}{3}s_c\right) + (f_2 - f_1)\left(\frac{2}{3}s_b - \frac{1}{3}s_a - \frac{1}{3}s_c\right) + \right.\\
& \left.(f_3 - f_2)\left(\frac{2}{3}s_c - \frac{1}{3}s_a - \frac{1}{3}s_b\right)\right).
\end{aligned}$$

Then, substituting (4-8) gives the expression for $\dot{q}$ in terms of the phase currents

$$\dot{q} = f_{R_L} - \left(\frac{2}{3}s_a - \frac{1}{3}s_b - \frac{1}{3}s_c\right)\frac{\partial H}{\partial \phi_a} - \left(\frac{2}{3}s_b - \frac{1}{3}s_a - \frac{1}{3}s_c\right)\frac{\partial H}{\partial \phi_b} - \left(\frac{2}{3}s_c - \frac{1}{3}s_a - \frac{1}{3}s_b\right)\frac{\partial H}{\partial \phi_c}.$$

[3] This procedure is the same as the one applied to the inverter, see Section 3-2-4.

The resulting ISO model for the balanced system is

$$\begin{aligned} \dot{x} &= \begin{bmatrix} 0 & 0 & 0 & \hat{s}_a \\ 0 & 0 & 0 & \hat{s}_b \\ 0 & 0 & 0 & \hat{s}_c \\ -\hat{s}_a & -\hat{s}_b & -\hat{s}_c & 0 \end{bmatrix} \frac{\partial H}{\partial x} + \begin{bmatrix} \mathbb{I}^{4\times4} \end{bmatrix} \begin{bmatrix} f_R \\ f_{R_L} \end{bmatrix} + \begin{bmatrix} -\mathbb{I}^{3\times3} \\ \mathbb{O}^{1\times3} \end{bmatrix} u, \\ \begin{bmatrix} e_R \\ e_{R_L} \end{bmatrix} &= \begin{bmatrix} \mathbb{I}^{4\times4} \end{bmatrix} \frac{\partial H}{\partial x}, \\ y &= \begin{bmatrix} -\mathbb{I}^{3\times3} & \mathbb{O}^{3\times1} \end{bmatrix} \frac{\partial H}{\partial x}, \end{aligned} \tag{4-9}$$

where $\hat{s}_j = s_j - \frac{1}{3} \sum_{k=a,b,c} s_k$, $j \in \{a, b, c\}$, the Hamiltonian is given in (4-1) and the resistive relation is

$$\begin{bmatrix} e_R \\ e_{R_L} \end{bmatrix} = \begin{bmatrix} -\frac{1}{R_a} & 0 & 0 & 0 \\ 0 & -\frac{1}{R_b} & 0 & 0 \\ 0 & 0 & -\frac{1}{R_c} & 0 \\ 0 & 0 & 0 & -R_L \end{bmatrix} \begin{bmatrix} f_R \\ f_{R_L} \end{bmatrix}.$$

The model in (4-9) is the same as the reference model in (4-2), but again with some sign differences, because the direction of the power flow from the perspective of the Dirac structure is not taken into account [9].

4-3 Modelling the rectifier with the nonlinear element method

This section features the modelling of the three-phase rectifier with the NEM. First, Section 4-3-1 presents the separation of the system into the planar subsystems. Subsequently, Section 4-3-2 deals with the formulation of the Dirac structure. Finally, Section 4-3-3 presents the derivation of the DAM and ISO model.

4-3-1 Separating the system into planar subsystems

Just as in Section 4-2-1 the system is divided into the three planar subsystems in Figure 4-2. With the exception of Σ_2 the graphs (and dual graphs) corresponding to the subsystems are the same, see Figure 4-3 and Figure 4-5. The graph and dual graph of Σ_2 are depicted in Figure 4-6, where the branches b_{sj}, b_{sk} represent the upper switches S_1, S_2, S_3 and the branches $\hat{b}_{sj}, \hat{b}_{sk}$ represent the lower switches S_4, S_5, S_6.

The structure of the graphs is the same as the structure shown in Figure 4-4, but the port branches have swapped position. Consequently, the incidence matrices describing the graphs in Figure 4-6 are given by (3-23) and (3-24) and the corresponding vectors are given by

$$\begin{aligned} B_{\Sigma_2} &= \begin{bmatrix} b_{p7} & b_{p8} & b_{p9} & b_{sa} & b_{sb} & b_{sc} & \hat{b}_{sa} & \hat{b}_{sb} & \hat{b}_{sc} & b_{p4} & b_{p5} & b_{p6} \end{bmatrix}^T, \\ B^*_{\Sigma_2} &= \begin{bmatrix} b^*_{p7} & b^*_{p8} & b^*_{p9} & b^*_{sa} & b^*_{sb} & b^*_{sc} & \hat{b}^*_{sa} & \hat{b}^*_{sb} & \hat{b}^*_{sc} & b^*_{p4} & b^*_{p5} & b^*_{p6} \end{bmatrix}^T. \end{aligned}$$

Furthermore, the interconnections between the subsystems is given by (3-9) and (3-10).

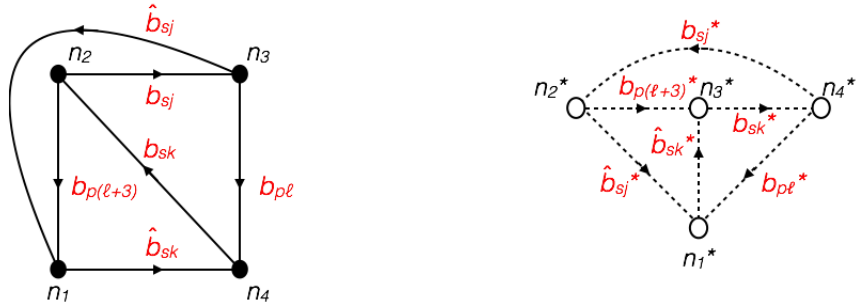

(a) Graph of Σ_2. **(b)** Dual graph of Σ_2.

Figure 4-6: The simplified graph and dual graph of Σ_2 with the switches as nonlinear elements.

4-3-2 Formulating the Dirac structure

The additional variables introduced by viewing the switches as functional elements are assigned with Proposition 3, i.e., the branches belonging to the switching elements are flows and the dual branches belonging to switching elements are efforts. The assignment of the other branches and dual branches, as efforts and flows, is the same as the one in Section 4-2-2. As such, the flow and effort vector of the whole system are given by (4-3) and (4-4), respectively, but the flow and effort vector for Σ_2 are replaced by

$$f_{\Sigma_2} = \begin{bmatrix} f_7 & f_8 & f_9 & f_{sa} & f_{sb} & f_{sc} & \hat{f}_{sa} & \hat{f}_{sb} & \hat{f}_{sc} & f_4 & f_5 & f_6 \end{bmatrix}^T,$$
$$e_{\Sigma_2} = \begin{bmatrix} e_7 & e_8 & e_9 & e_{sa} & e_{sb} & e_{sc} & \hat{e}_{sa} & \hat{e}_{sb} & \hat{e}_{sc} & e_4 & e_5 & e_6 \end{bmatrix}^T.$$

Thus, the Dirac structure of the three-phase rectifier with the switches modelled as nonlinear elements is given by (2-32) with a $F \in \mathbb{R}^{33\times 29}, E \in \mathbb{R}^{33\times 29}$ composed of the matrices $F_{\Sigma_1}, E_{\Sigma_1}, \ldots, F_{\Sigma_3}, E_{\Sigma_3}$. These latter matrices are given by (3-25) and (3-26), and they are in turn composed of the incidence matrices defined in the previous section.

4-3-3 Deriving the differential-algebraic model and input-state-output model

Rewriting the characteristic equation of the kernel representation leads to a DAM model

$$\begin{bmatrix} 1 & -1 & 0 \\ 0 & 1 & -1 \\ -1 & 0 & 1 \end{bmatrix} \dot{\phi} = -\begin{bmatrix} 1 \\ 1 \\ 1 \end{bmatrix} \frac{\partial H}{\partial q} + \begin{bmatrix} 0 & 1 & 0 \\ 0 & 0 & 1 \\ 1 & 0 & 0 \end{bmatrix} \begin{bmatrix} e_{sa} \\ e_{sb} \\ e_{sc} \end{bmatrix} - \mathbb{I}^{3\times 3} \begin{bmatrix} \hat{e}_{sa} \\ \hat{e}_{sb} \\ \hat{e}_{sc} \end{bmatrix} + \begin{bmatrix} 1 & -1 & 0 \\ 0 & 1 & -1 \\ -1 & 0 & 1 \end{bmatrix} f_R - \begin{bmatrix} 1 & -1 & 0 \\ 0 & 1 & -1 \\ -1 & 0 & 1 \end{bmatrix} u,$$
$$\dot{q} = f_{R_L} + f_1 + f_{sa} - \hat{f}_{sb} + f_2 + f_{sb} - \hat{f}_{sc} + f_3 + f_{sc} - \hat{f}_{sa},$$

$$
\begin{aligned}
\hat{e}_{sb} =& e_{sb} - \frac{\partial H}{\partial q},\\
e_{sa} =& \frac{\partial H}{\partial q} + \hat{e}_{sa},\\
\hat{e}_{sc} =& e_{sc} - \frac{\partial H}{\partial q},\\
e_{sb} =& \frac{\partial H}{\partial q} + \hat{e}_{sb},\\
\hat{e}_{sa} =& e_{sa} - \frac{\partial H}{\partial q},\\
e_{sc} =& \frac{\partial H}{\partial q} + \hat{e}_{sc},\\
\hat{f}_{sa} =& f_{sa} + f_1,\\
f_{sb} =& -f_1 + \hat{f}_{sb},\\
\hat{f}_{sb} =& f_{sb} + f_2,\\
f_{sc} =& -f_2 + \hat{f}_{sc},\\
\hat{f}_{sc} =& f_{sc} + f_3,\\
f_{sa} =& -f_3 + \hat{f}_{sa},\\
&\text{s.t.} \quad \begin{bmatrix} f_1 - f_3 \\ f_2 - f_1 \\ f_3 - f_2 \end{bmatrix} = \frac{\partial H}{\partial x},\\
\begin{bmatrix} e_R \\ e_{R_L} \end{bmatrix} =& \mathbb{I}^{4\times 4} \frac{\partial H}{\partial x},\\
y =& \begin{bmatrix} -\mathbb{I}^{3\times 3} & \mathbb{O}^{3\times 1} \end{bmatrix} \frac{\partial H}{\partial x},\\
&\text{s.t. } y_a + y_b + y_c = 0,
\end{aligned}
$$

with the Hamiltonian in (4-1) and the resistive relation

$$
\begin{bmatrix} e_R \\ e_{R_L} \end{bmatrix} = \begin{bmatrix} -\frac{1}{R_a} & 0 & 0 & 0 \\ 0 & -\frac{1}{R_b} & 0 & 0 \\ 0 & 0 & -\frac{1}{R_c} & 0 \\ 0 & 0 & 0 & -R_L \end{bmatrix} \begin{bmatrix} f_R \\ f_{R_L} \end{bmatrix}.
$$

Computing the model for each switch state and parametrising the result accordingly yields the DAM parametrised by the switch state in (4-6). See Appendix C-4 for further details of the parametrisation. Consequently, the DAM model reduces to the ISO model in (4-9) after assuming a balanced load, see Section 4-2-4 for the derivation. This means that both the methods yield the same model. Furthermore, we again encounter the problem that not all the latent variables are removed during the interconnection. Recall the final discussion in Section 3-3-3.

4-4 Modelling a rectifier with the inverter model

The essential difference between a rectifier and an inverter is the primary direction of the power flow. Thus, in the inverter's case we view the power flowing from the DC-side to the AC-side and in the rectifier's case from the AC-side to the DC-side. These viewpoints have lead us to implicitly define a direction for the relations of the currents and voltages in Σ_2. For the inverter we express the DC-side current as a function of the current on the AC-side and the AC-side voltage as a function of the voltage on the DC-side, see (3-15). Likewise, for the rectifier the AC-side current is expressed as a function of the DC-side current and the DC-side voltage as a function of the AC-side voltage, see (4-5). However, the relations in (3-15) and (4-5) are not invertible. This raises the question: *is a model of a power converter modelled as an inverter also suitable as a rectifier and* vice versa*?* Logically, this should be the case, because the inverter model has inputs and outputs for both the DC- and AC-side. In this section we show that this is the true by using the inverter's ISO model to derive a model of a rectifier.

Consider the network in Figure 4-7, whose ISO model reads as

$$\begin{aligned} \dot{q}_L &= f_{R_L} - u_L, \\ e_{R_L} &= \frac{\partial H_L}{\partial q_L}, \\ y_L &= -\frac{\partial H_L}{\partial q_L}, \end{aligned} \tag{4-10}$$

where the Hamiltonian is $H_L = \frac{1}{2C_L} q_L^2$ and the resistive relation is

$$e_{R_L} = -\frac{1}{R_L} f_{R_L}.$$

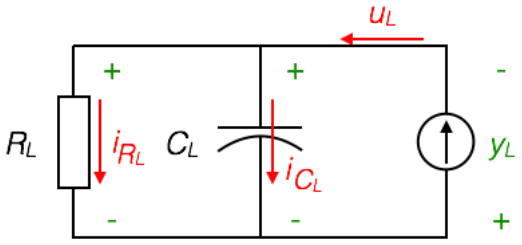

Figure 4-7: The network of the DC-load.

Subsequently, composing the ISO model of the inverter in (3-22) with the model in (4-10)

with the gyrative interconnection (2-10), $y_L = -u_{dc}$, $u_L = y_{dc}$, yields the combined model

$$\begin{bmatrix} \dot{x} \\ \dot{q}_L \end{bmatrix} = \begin{bmatrix} \mathbb{O}^{3\times3} & -\mathbb{I}^{3\times3} & \mathbb{O}^{3\times1} \\ \mathbb{I}^{3\times3} & \mathbb{O}^{3\times3} & -g_{dc}(S) \\ \mathbb{O}^{1\times3} & g_{dc}^T(S) & 0 \end{bmatrix} \begin{bmatrix} \frac{\partial H'}{\partial x} \\ \frac{\partial H'}{\partial q_L} \end{bmatrix} + \begin{bmatrix} \mathbb{O}^{4\times4} \\ \mathbb{I}^{4\times4} \end{bmatrix} \begin{bmatrix} f_R \\ f_{R_L} \end{bmatrix} + \begin{bmatrix} g_{AC} \\ \mathbb{O}^{4\times3} \end{bmatrix} u_{AC},$$

$$\begin{bmatrix} e_R \\ e_{R_L} \end{bmatrix} = \begin{bmatrix} \mathbb{O}^{4\times4} & \mathbb{I}^{4\times4} \end{bmatrix} \begin{bmatrix} \frac{\partial H'}{\partial x} \\ \frac{\partial H'}{\partial q_L} \end{bmatrix},$$

$$y_{AC} = \begin{bmatrix} g_{AC}^T & \mathbb{O}^{3\times4} \end{bmatrix} \begin{bmatrix} \frac{\partial H'}{\partial x} \\ \frac{\partial H'}{\partial q_L} \end{bmatrix},$$

where $S = [s_a \ s_b \ s_c]^T$, $H' = H + H_L$ and the resistive relation is

$$\begin{bmatrix} e_R \\ e_{R_L} \end{bmatrix} = \begin{bmatrix} -R \cdot \mathbb{I}^{3\times3} & \mathbb{O}^{3\times1} \\ \mathbb{O}^{1\times3} & -\frac{1}{R_L} \end{bmatrix} \begin{bmatrix} f_R \\ f_{R_L} \end{bmatrix}.$$

This shows that the ISO model of the inverter also functions as a rectifier. Thus, modelling Σ_2 with a predefined direction does not yield a model that is only valid for this predefined direction. The model of the inverter in (3-17) and (3-22) can work as both a rectifier and an inverter. The inputs to this rectifier are currents and the outputs are voltages due to the topology of the inverter in Figure 3-1. Likewise, modelling the rectifier in Figure 4-1 without the DC load yields a PH model that also functions as a three-phase inverter with the DC current as input and a DC voltage as output.

Chapter 5

Conclusions and recommendations

5-1 Conclusions

The port-Hamiltonian modelling of power converters has been an ongoing research for the past couple of years. However, the focus of most of the research has been on the modelling of DC/DC converters, such as the Buck, Boost and Ćuk-converters and little attention is given to the modelling of three-phase power converters, such as the three-phase rectifier and three-phase inverter. The research that is available on port-Hamiltonian models of the three-phase converters do not treat the modelling part from a port-Hamiltonian viewpoint, but rewrite conventional models by substituting port-Hamiltonian variables. Therefore, the modelling of a three-phase rectifier and three-phase inverter in the generalised port-Hamiltonian framework is investigated in this thesis. Modelling the power converters from a port-Hamiltonian viewpoint starts with expressing their Dirac structures together with their Hamiltonians and deriving their mathematical models from these mathematical expressions. The research has lead to the following conclusions:

- Modelling a system from a fundamental port-Hamiltonian viewpoint requires a mathematical expression of the Dirac structure and the Hamiltonian. The Dirac structure of a switching electrical system is methodically represented in a matrix kernel representation by using the network graph and dual network graph of the system. Following the literature on the subject, the switching elements are either represented as virtual elements in the graph (virtual element method), who connect and disconnect nodes, or as nonlinear elements (nonlinear element method), whose efforts and flows depend on the switch state. The mathematical models are then derived by solving the characteristic equation of the kernel representation for the time-derivatives of the state and the outputs. This leads to a differential-algebraic model for the three-phase inverter and rectifier, because the voltages in the phases are coupled. For the three-phase power converters the explicit input-state-output models from literature are recovered by assuming a balanced network.

- It has been shown that the network graphs of the three-phase DC/AC and AC/DC converters are not planar, which means that a dual graph does not exist. To overcome this issue the systems are divided into planar subsystems, such that each subsystem can be represented in a matrix kernel representation together with their interconnections. Thereby we exploit a fundamental feature of port-Hamiltonian system theory, which is that the interconnection of multiple port-Hamiltonian systems is relatively straightforward.

- A key issue to derive the models from the mathematical expression of the Dirac structure is the identification or assignment of the voltages and currents in the network as efforts and flows *a priori*, i.e., without referring to the final mathematical model. It has been reasoned that, because the assignment of voltages and currents of the storage elements are predefined, they define the assignment of the resistive and source elements. From this we infer a way to analyse the network topology to determine the assignment of the voltages and currents *a priori*. However, the assignment of currents and voltages of the interconnection ports turned out to be a problem, because the casual relation is difficult to identify. Moreover, it seems pointless to do so, since these variables disappear after interconnection. Hence, we can assign them *ad libitum*. Additionally, we showed that for switches modelled as nonlinear elements this causality is ambiguous. For both these situations the currents are taken as flows and the voltages as efforts.

- The two modelling methods, the nonlinear element method (NEM) and the virtual element method (VEM), are both capable of yielding the correct mathematical models of the three-phase converters. In terms of the efficiency, effectiveness and practicality the VEM method yields a parametrised model in a more efficient way. However, the parametrisation of the model in terms of the switch state can become incomprehensible. Apart from this, the VEM requires the graphs to satisfy more requirements, which might prove restrictive for the modelling of larger systems. The NEM is less efficient for finding the parametrisation, but poses less constraints on the graph, its parametrisation is easier to interpret and naturally allows for the modelling of non-ideal switches. However, there remains the question, why the modelling with the NEM delivers a non-parametrised DAM that seems to be non-port-Hamiltonian.

- Although modelling switching electrical systems with the NEM or VEM is not necessarily the fastest or the most efficient in obtaining the correct mathematical models. The modelling procedures have the advantage that they are not influenced by the size or complexity of the system and are by nature modular. Replacing certain parts of the network, like the load or the input source, is easily achieved in this framework. Furthermore, systems from other domains should be straightforward to incorporate, because we use the generalised effort and flow definitions. For instance, the inverter model can be coupled to a port-Hamiltonian model of an squirl-cage motor and its mechanical load.

5-2 Recommendations

As mentioned, the goal of this thesis is to model two three-phase power converters from a port-Hamiltonian perspective, with which it complements the research from literature that consider the modelling of various DC/DC-converters. However, it does not exhausts or completes the

topic. There are many further developments to explore in further studies. Based on this research we formulate the following recommendations:

- To cope with the non-planarity of the three-phase converters the system is separated into planar subsystems. Such an approach might not be the most optimal solution for larger and more complex switching networks, where the number of subsystems becomes large and the interconnections potentially complex. Although it seems feasible that a planar subsystem can always be found, the dimensions of the representation grow quickly with each separation. Furthermore, there is no guarantee that there always exist graphs that satisfy Assumption 1-5 for the VEM. Ideally one would like to extent the modelling theories – especially the theory from [5, 6, 7] – to cope with non-planar graphs. We suggested that using elements from tensor theory might provide a foundation to deal with these situations.

- In this thesis we encountered the issue of identifying the voltages and currents of individual elements as efforts and flows – which in the generalised port-Hamiltonian framework are regarded as a type of inputs and outputs – without having to refer to the final mathematical model. We propose to identify the efforts and flows of the resistive elements and sources based on the network topology (the efforts and flows of the storage elements fixed [3, 12, 20] and form the foundation to do this). However, identifying the efforts and flows for the interconnection ports and switches remains unclear. To overcome this problem, the currents are fixed as flows and the voltages as efforts based on arguments from [14]. However, both these proposals are heuristic and it is worth giving the identification of generalised efforts and flows in networks (systems) some additional thought.

- The switches are assumed ideal in most literature concerning power converters, including this thesis, but in practise the switches are semiconductors and are not ideal. Researching the incorporation of such elements into the port-Hamiltonian modelling theory would be an interesting topic for future studies and an important development to analyse and produce more detailed models of power converters. We already mentioned that including non-ideal models of switches is possible with the NEM. Moreover, the port-Hamiltonian theory might provide a solid foundation for researching controllers that take the non-ideal behaviour of the switches into account.

- The focus of the research has been the modelling of two multi-phase power converters: the three-phase rectifier and three-phase inverter. Although these are two fundamental power converters in multi-phase networks, they are not the only ones. Hence, further research could consider the modelling of matrix converters, cyclo-converters and multi-level inverters. We suspect that it is possible to model these systems with the theory provided in this thesis.

Appendix A

Additional information on efforts, flows and states

This appendix features some additional port-Hamiltonian theory regarding the relation between states (x), efforts (e) and flows (f), and their physical interpretation. The information within this appendix is entirely taken from [12, Ch.B].

In the PH framework the dynamics of systems are determined by the combination of the storage and resistive elements of which the storage elements define the states of the system. The total energy storage of the system is defined by a state-space $\mathcal{X}$, together with a *Hamiltonian* $H : \mathcal{X} \to \mathbb{R}$ denoting the total energy [12, Ch.2.3]. The state-space $\mathcal{X}$ is in general a smooth manifold in Euclidean space. The states of the system ($x \in \mathcal{X}$) can be seen as "accumulation variables", which are related to the efforts and flows of the storage elements through

$$\dot{x} = f_{\mathcal{S}}, \tag{A-1}$$

$$e_{\mathcal{S}} = \frac{\partial H}{\partial x}(x). \tag{A-2}$$

Figure A-1 gives a schematic representation of this relationship and Table A-1 lists the physical interpretation of the states, efforts and flows for the different physical domains.

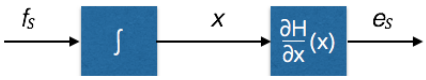

Figure A-1: Schematic representation of the relation between flows, states and efforts.

The Hamiltonian H of a storage element is formally given by

$$H(x) = \int \Phi(x) \mathrm{d}x, \tag{A-3}$$

Table A-1: Classification of the states, efforts and flows for several (sub)domains.

(Sub)domain	Flow $f \in \mathcal{F}$	Effort $e \in \mathcal{E}$	storage state $x \in \mathcal{X}$
Electric	Current	Voltage	Charge
Magnetic	Voltage	Current	Flux linkage
Potential translation	Velocity	Force	Displacement
Kinetic translation	Force	Velocity	Momentum
Potential rotation	Angular velocity	Torque	Angular displacement
Kinetic rotation	Torque	Angular velocity	Angular momentum
Potential hydraulic	Volume flow	Pressure	Volume
Kinetic hydraulic	Pressure	Volume flow	flow tube momentum
Chemical	Molar flow	Chemical potential	Number of moles
Thermal	Entropy flow	Temperature	Entropy

where $\Phi(x)$ represents the constitutive relation of the storage element. In other words, the Hamiltonian represents the area underneath the curve in the (e, x)-plane. For example, for a linear inductor $\Phi(x) = \frac{\phi}{L}$, where ϕ is the flux-linkage and L the inductance. The total Hamiltonian of a system Σ with m storage elements is simply the sum of all the Hamiltonians

$$H_\Sigma = \sum_{k=1}^{m} H_k(x). \tag{A-4}$$

Finally, the resistive elements are modelled by the constitutive relations between the effort and flows of the form $\mathcal{R}(e_\mathcal{R}, f_\mathcal{R}) = 0$. For instance, the constitutive relation for an linear electric (Ohmic) resistor is given as $e_\mathcal{R} = -Rf_\mathcal{R}$, where R is the resistance.

Appendix B

Mathematical models of the power converters in literature

This appendix contains the mathematical reference models of power converters from literature. Section B-1 contains the derivation of the basic switching function representation of an inverter from Holmes et al. [17, Ch.1.3], which is used for additional validation. This appendix also contains the transformation of the models in [9, 10, 11] to a form suitable for this thesis. The models are not directly suitable, because they are averaged and given in *dq0-coordinates*. The desired, hybrid representation of these models follows easily from the models in the papers. Section B-2 contains the transformation of the inverter model and Section B-3 deals with the rectifier model.

B-1 The switching function representation of a three-phase inverter

Consider the inverter in Figure B-1 [17, Ch.1.2]. Let $s_1, \ldots, s_6$ denote the switch states of the switches $S_1, \ldots, S_6$ in Figure B-1, where $s = 0$ when the switch is open and $s = 1$ when the switch is closed. Inspection of the network reveals that

$$\begin{aligned} v_{ao} &= v_{dc} s_1, \quad v_{ao} = v_{ao}(1 - s_4), \\ v_{bo} &= v_{dc} s_2, \quad v_{ao} = v_{ao}(1 - s_5), \\ v_{co} &= v_{dc} s_3, \quad v_{ao} = v_{ao}(1 - s_6). \end{aligned} \tag{B-1}$$

Considering the constraints imposed by the circuit, i.e., short-cutting the voltage source is not allowed, leads to the observation that the bottom and top switch can never be closed at the same time. Furthermore, for continuity considerations in each phase leg [17, Ch.1.3]

$$\begin{aligned} s_1 + s_4 &= 1, \\ s_2 + s_5 &= 1, \\ s_3 + s_6 &= 1. \end{aligned} \tag{B-2}$$

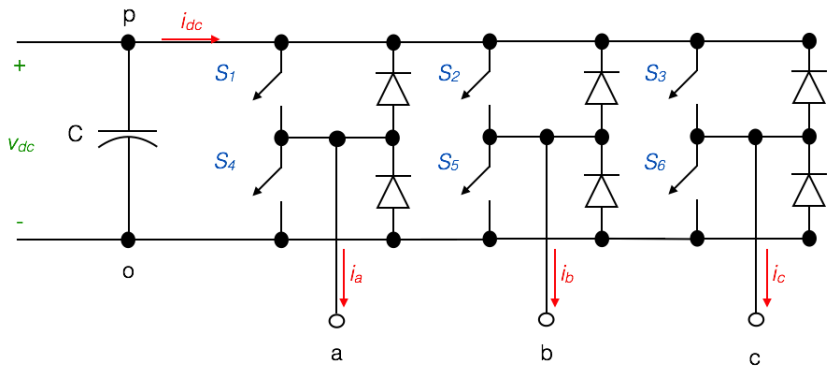

Figure B-1: A basic three-phase voltage source inverter circuit.

The above equations imply that (B-1) can be rewritten into a simplified form. Introducing the new variables $s_a = s_1 = s_4$, $s_b = s_2 = s_5$ and $s_c = s_3 = s_6$ yields the simplified equations

$$\begin{aligned} v_{ao} &= v_{dc} s_a, \\ v_{bo} &= v_{dc} s_b, \\ v_{co} &= v_{dc} s_c, \end{aligned} \tag{B-3}$$

where $s_a, s_b, s_c \in \{0, 1\}$. Hence, the switch states of the two switches of each leg are now expressed by a single switch state for the whole leg. Subsequently, the line-to-line voltages are given by

$$\begin{aligned} v_{ab} &= v_{ao} - v_{bo} = v_{dc}(s_a - s_b), \\ v_{bc} &= v_{bo} - v_{co} = v_{dc}(s_b - s_c), \\ v_{ca} &= v_{co} - v_{ao} = v_{dc}(s_c - s_a). \end{aligned} \tag{B-4}$$

The DC link current can be expressed in terms of the phase currents as

$$i_{dc} = i_a s_a + i_b s_b + i_c s_c, \tag{B-5}$$

or in terms of the line-to-line currents (B-5) as

$$i_{dc} = i_{ab}(s_a - s_b) + i_{bc}(s_b - s_c) + i_{ca}(s_c - s_a). \tag{B-6}$$

In case of a Y-connected load the voltages can be expressed with respect to the neutral point in the load denoted by subscript n. If the loads are balanced, i.e., the impedances are the same in each phase of the load. Their phase voltages are [17, Ch.1.3]

$$\begin{aligned} v_{an} &= v_{dc}\left(\frac{2}{3}s_a - \frac{1}{3}s_b - \frac{1}{3}s_c\right), \\ v_{bn} &= v_{dc}\left(\frac{2}{3}s_b - \frac{1}{3}s_a - \frac{1}{3}s_c\right), \\ v_{cn} &= v_{dc}\left(\frac{2}{3}s_c - \frac{1}{3}s_a - \frac{1}{3}s_b\right). \end{aligned} \tag{B-7}$$

The DC current for a Y-connected load is described by (B-5).

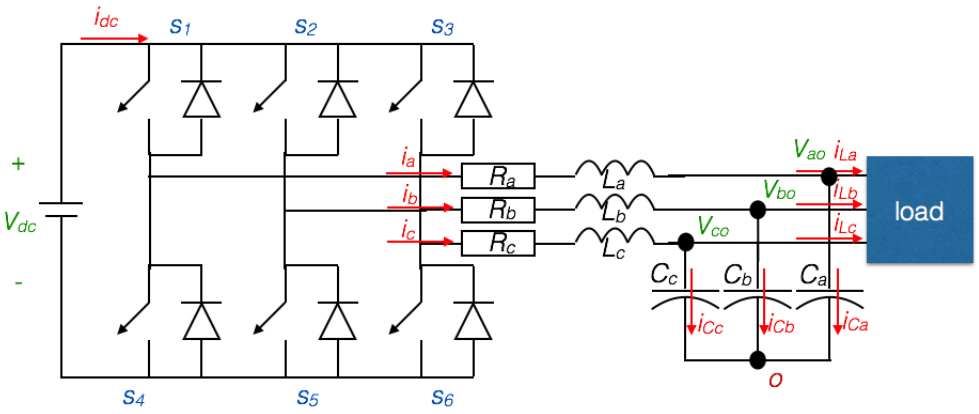

Figure B-2: The three-phase inverter topology.

B-2 The reference model of the three-phase inverter

Consider the three-phase inverter from Mu et al. [10, 11] in Figure B-2, where the subscript L denotes the load. Assume a balanced system such that the inductances $L_1 = L_2 = L_3 = L$, the capacitances $C_1 = C_2 = C_3 = C$ and the resistances $R_1 = R_2 = R_3 = R$. The corresponding mathematical model reads as [10]

$$\begin{aligned}
L\frac{di_a}{dt} &= -Ri_a + \left(s_a - \frac{1}{3}\sum_{k=a,b,c} s_k\right) v_{dc} - v_{ao},\\
L\frac{di_b}{dt} &= -Ri_b + \left(s_b - \frac{1}{3}\sum_{k=a,b,c} s_k\right) v_{dc} - v_{bo},\\
L\frac{di_c}{dt} &= -Ri_c + \left(s_c - \frac{1}{3}\sum_{k=a,b,c} s_k\right) v_{dc} - v_{co},\\
C\frac{dv_{ao}}{dt} &= i_a - i_{La},\ C\frac{dv_{bo}}{dt} = i_b - i_{Lb},\ C\frac{dv_{bo}}{dt} = i_b - i_{Lb}.
\end{aligned} \tag{B-8}$$

Observe that the expression in the parenthesis coincide with the one in (B-7). The Hamiltonian of the system, which denotes the total energy, is given by

$$H(q,\phi) = \sum_{j=a,b,c,} \left(\frac{1}{2}\frac{\phi_j^2}{L} + \frac{1}{2}\frac{q_j^2}{C}\right), \tag{B-9}$$

where $\phi = (\phi_a\ \phi_b\ \phi_c)^T$ is the flux linkage across the inductors and $q = (q_a\ q_b\ q_c)^T$ the charge in the capacitors. The Hamiltonian and the constitutive relations for an inductor and a capacitor [22],

$$\phi_L = L\frac{dq_L}{dt}, \tag{B-10}$$

$$q_C = C\frac{d\phi_C}{dt}, \tag{B-11}$$

allow us to rewrite (B-8) in terms of ϕ, q and the Hamiltonian. Ergo, the currents flowing through the inductors, i_a, i_b and i_c, in terms of the Hamiltonian are expressed as

$$i_j = \frac{\phi_j}{L} = \frac{\partial H}{\partial \phi_j}(q, \phi),\ j = a, b, c.$$

Furthermore, the voltages across the capacitors v_{ao}, v_{bo} and v_{co} in terms of the Hamiltonian are

$$v_{jo} = \frac{q_j}{C} = \frac{\partial H}{\partial q_j}(q, \phi).$$

Hence, the mathematical model of the three-phase inverter of Figure B-2 in PH terms reads as[1]

$$\begin{aligned}
\begin{bmatrix} \dot{q} \\ \dot{\phi} \end{bmatrix} &= \begin{bmatrix} 0 & 0 & 0 & 1 & 0 & 0 \\ 0 & 0 & 0 & 0 & 1 & 0 \\ 0 & 0 & 0 & 0 & 0 & 1 \\ -1 & 0 & 0 & -R & 0 & 0 \\ 0 & -1 & 0 & 0 & -R & 0 \\ 0 & 0 & -1 & 0 & 0 & -R \end{bmatrix} \begin{bmatrix} \frac{\partial H}{\partial q}(q, \phi) \\ \frac{\partial H}{\partial \phi}(q, \phi) \end{bmatrix} + \begin{bmatrix} \mathbb{O}^{3\times 1} \\ \hat{s}_a \\ \hat{s}_b \\ \hat{s}_c \end{bmatrix} v_{dc} \\
&\quad + \begin{bmatrix} -\mathbb{I}^{3\times 3} \\ \mathbb{O}^{3\times 3} \end{bmatrix} \begin{bmatrix} i_{La} \\ i_{Lb} \\ i_{Lc} \end{bmatrix}, \\
i_{dc} &= \begin{bmatrix} \mathbb{O}^{1\times 3} & \hat{s}_a & \hat{s}_b & \hat{s}_c \end{bmatrix} \begin{bmatrix} \frac{\partial H}{\partial q}(q, \phi) \\ \frac{\partial H}{\partial \phi}(q, \phi) \end{bmatrix}, \\
\begin{bmatrix} v_{ao} \\ v_{bo} \\ v_{co} \end{bmatrix} &= \begin{bmatrix} -\mathbb{I}^{3\times 3} & \mathbb{O}^{3\times 3} \end{bmatrix} \begin{bmatrix} \frac{\partial H}{\partial q}(q, \phi) \\ \frac{\partial H}{\partial \phi}(q, \phi) \end{bmatrix},
\end{aligned} \tag{B-12}$$

where $\hat{s}_j = s_j - \frac{1}{3} \sum_{k=a,b,c} s_k$, $j \in \{a, b, c\}$. In the original work [10, 11] the output equations are omitted. They are added here for completeness.

B-3 The reference model of the three-phase rectifier

Consider the three-phase rectifier from Tang et al. [9] in Figure B-3 with $R_a = R_b = R_c = R$, $L_a = L_b = L_c = L$ and that the voltage sources producing a sinusoidal output voltage each phase shifted by 120° with respect to one another. The mathematical model corresponding to this network is [9]

[1] The output equation is originally not given in [10, 11] and added in this thesis for completeness.

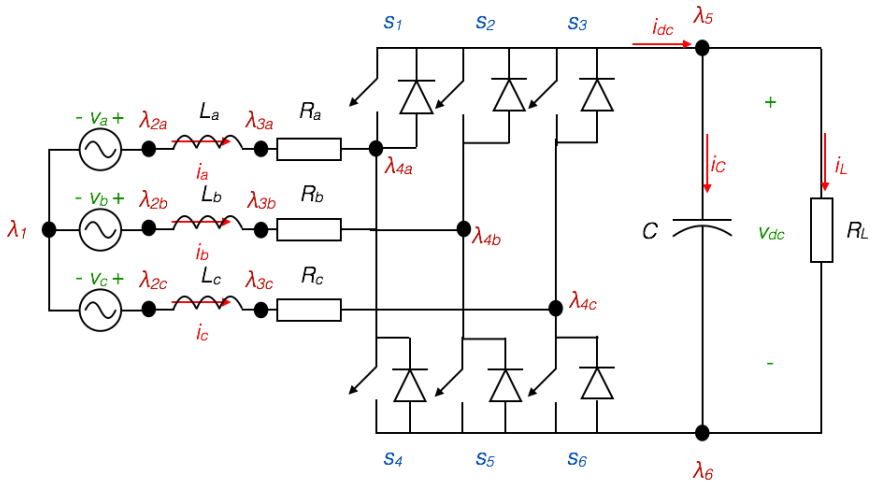

Figure B-3: Three-phase rectifier topology.

$$
\begin{aligned}
L\frac{di_a}{dt} &= v_a - Ri_a - s_a v_{dc} + \frac{v_{dc}}{3}\sum_{j=a,b,c} s_j,\\
L\frac{di_b}{dt} &= v_b - Ri_b - s_b v_{dc} + \frac{v_{dc}}{3}\sum_{j=a,b,c} s_j,\\
L\frac{di_c}{dt} &= v_c - Ri_c - s_c v_{dc} + \frac{v_{dc}}{3}\sum_{j=a,b,c} s_j,\\
C\frac{dv_{dc}}{dt} &= s_a i_a + s_b i_b + s_c i_c - \frac{v_{dc}}{R_L}.
\end{aligned}
\tag{B-13}
$$

Subsequently introducing the Hamiltonian of this system

$$
H(\phi, q) = \sum_{j=a,b,c}\left(\frac{1}{2}\frac{\phi_k}{L}\right) + \frac{1}{2}\frac{q}{C}, \tag{B-14}
$$

where $\phi = (\phi_a\ \phi_b\ \phi_c)^T$, and expressing the constitutive relations for the inductor and capacitor given by (B-10) and (B-11) in terms of the Hamiltonian, leads to the ISO-PH model[2]

$$
\begin{aligned}
\begin{bmatrix}\dot{\phi}\\ \dot{q}\end{bmatrix} &= \begin{bmatrix} -R & 0 & 0 & -\hat{s}_a\\ 0 & -R & 0 & -\hat{s}_b\\ 0 & 0 & -R & -\hat{s}_c\\ \hat{s}_a & \hat{s}_b & \hat{s}_c & -\frac{1}{R_L}\end{bmatrix}\begin{bmatrix}\frac{\partial H}{\partial \phi}\\ \frac{\partial H}{\partial q}\end{bmatrix} + \begin{bmatrix}1 & 0 & 0\\ 0 & 1 & 0\\ 0 & 0 & 1\\ 0 & 0 & 0\end{bmatrix}\begin{bmatrix}u_a\\ u_b\\ u_c\end{bmatrix},\\
\begin{bmatrix}y_a\\ y_b\\ y_c\end{bmatrix} &= \begin{bmatrix}1 & 0 & 0 & 0\\ 0 & 1 & 0 & 0\\ 0 & 0 & 1 & 0\end{bmatrix}\begin{bmatrix}\frac{\partial H}{\partial \phi}\\ \frac{\partial H}{\partial q}\end{bmatrix},
\end{aligned}
\tag{B-15}
$$

where $u_j = v_j$, $y_j = i_j$ and $\hat{s}_j = s_j - \frac{1}{3}\sum_{k=a,b,c} s_k$, $j \in \{a, b, c\}$.

[2]In contrast to the PH model of the inverter given in [10, 11], [9] does give the output of the system. However, this output does not follow directly from the modelling method. The passive output is determined afterwards.

Appendix C

Additional modelling details and derivations

This appendix contains additional information on the modelling steps for the three-phase inverter and rectifier, which are omitted in Chapters 3 and 4. Section C-1 contains complete derivation of the differential-algebraic model of the inverter. Section C-2 reveals the details of the parametrisation of the differential-algebraic model of the inverter in case of the NEM for Section 3-3-3. Section C-3 contains the complete derivation of the differential-algebraic model of the rectifier. Finally, Section C-4 features the parametrisation of the rectifier DAM model in case of the NEM for Section 4-3-3.

C-1 The derivation of the inverter's differential-algebraic model

Subsystem Σ_1 provides the following equations

$$\begin{aligned} y_{dc} &= -f_1 - f_2 - f_3, \\ u_{dc} &= e_1 = e_2 = e_3. \end{aligned} \tag{C-1}$$

Using the simplified result for the equations of Σ_2 from Section 3-2-3[1]

$$\begin{aligned} f_4 &= -f_7(s_a - s_b), \\ f_5 &= -f_8(s_b - s_c), \\ f_6 &= -f_9(s_c - s_a), \\ e_7 &= e_4(s_a - s_b), \\ e_8 &= e_5(s_b - s_c), \\ e_9 &= e_6(s_c - s_a). \end{aligned} \tag{C-2}$$

[1]The derivation of the differential-algebraic model with the switches as nonlinear elements is the same, but where these equations replaced with (3-27) and (3-28).

Combining the formulae in (C-1) and (C-2) through $f_1 = -f_4, f_2 = -f_5, f_3 = -f_6$ and $e_1 = e_4, e_2 = e_5, e_3 = e_6$ leads to the equations

$$\begin{aligned} y_{dc} &= -f_7(s_a - s_b) - f_8(s_b - s_c) - f_9(s_c - s_a), \\ e_7 &= u_{dc}(s_a - s_b), \\ e_8 &= u_{dc}(s_b - s_c), \\ e_9 &= u_{dc}(s_c - s_a). \end{aligned} \tag{C-3}$$

Next, consider the sets of equations describing Σ_3

$$\begin{aligned} e_{Ra} - e_{10} + f_{12} &= 0, \\ e_{Rb} + e_{10} - f_{11} &= 0, \\ e_{Rc} + e_{11} - f_{12} &= 0, \end{aligned} \tag{C-4}$$

$$\frac{\partial H}{\partial \phi_k}(x) - e_{Rk} = 0, \ k = a, b, c, \tag{C-5}$$

$$\begin{aligned} -\dot{q}_a - \frac{\partial H}{\partial \phi_a}(x) + u_{ab} - u_{ca} &= 0, \\ -\dot{q}_b - \frac{\partial H}{\partial \phi_b}(x) + u_{bc} - u_{ab} &= 0, \\ -\dot{q}_c - \frac{\partial H}{\partial \phi_c}(x) + u_{ca} - u_{bc} &= 0, \end{aligned} \tag{C-6}$$

$$\begin{aligned} \frac{\partial H}{\partial q_a}(x) - \frac{\partial H}{\partial q_b}(x) - y_{ab} &= 0, \\ \frac{\partial H}{\partial q_b}(x) - \frac{\partial H}{\partial q_c}(x) - y_{bc} &= 0, \\ \frac{\partial H}{\partial q_c}(x) - \frac{\partial H}{\partial q_a}(x) - y_{ca} &= 0, \end{aligned} \tag{C-7}$$

$$\dot{q}_a + \dot{q}_b + \dot{q}_c = 0, \tag{C-8}$$

$$\begin{aligned} f_{Ra} - f_{Rc} - \dot{\phi}_a + \dot{\phi}_c + e_{12} - y_{ca} &= 0, \\ f_{Rb} - f_{Ra} - \dot{\phi}_b + \dot{\phi}_a + e_{10} - y_{ab} &= 0, \\ f_{Rc} - f_{Rb} - \dot{\phi}_c + \dot{\phi}_b + e_{11} - y_{bc} &= 0, \end{aligned} \tag{C-9}$$

$$f_{10} + f_{11} + f_{12} = 0. \tag{C-10}$$

Substituting (C-5) into (C-4) and the result into (C-3) with $f_7 = -f_{10}, f_8 = -f_{11}, f_9 = -f_{12}$ yields the expression for the DC current

$$y_{dc} = -s_a \frac{\partial H}{\partial \phi_a}(x) - s_b \frac{\partial H}{\partial \phi_b}(x) - s_c \frac{\partial H}{\partial \phi_c}(x). \tag{C-11}$$

Rewriting the set of (C-6) into a matrix form and similarly for (C-7) provides the equations for $\dot{q}$ and the AC outputs:

$$\begin{aligned}\dot{q} &= \begin{bmatrix}-1 & 0 & 0\\ 0 & -1 & 0\\ 0 & 0 & -1\end{bmatrix}\frac{\partial H}{\partial \phi}(x) + \underbrace{\begin{bmatrix}1 & 0 & -1\\ -1 & 1 & 0\\ 0 & -1 & 1\end{bmatrix}}_{g_{AC}} u_{AC},\\ &\text{s.t.} \quad \dot{q}_a + \dot{q}_b + \dot{q}_c = 0,\\ y_{AC} &= \underbrace{\begin{bmatrix}1 & -1 & 0\\ 0 & 1 & -1\\ -1 & 0 & 1\end{bmatrix}}_{g_{AC}^T}\frac{\partial H}{\partial q}(x).\end{aligned} \tag{C-12}$$

Substituting (C-7) into (C-9) and combining the formulae with the ones in (C-3) through $e_7 = e_{10}, e_8 = e_{11}, e_9 = e_{12}$ results in the equations for $\dot{\phi}$:

$$\begin{bmatrix}1 & -1 & 0\\ 0 & 1 & -1\\ -1 & 0 & 1\end{bmatrix}\dot{x}_2 = \begin{bmatrix}1 & -1 & 0\\ 0 & 1 & -1\\ -1 & 0 & 1\end{bmatrix}\frac{\partial H}{\partial \phi}(x) + \begin{bmatrix}1 & -1 & 0\\ 0 & 1 & -1\\ -1 & 0 & 1\end{bmatrix} f_R - \begin{bmatrix}s_a - s_b\\ s_b - s_c\\ s_c - s_a\end{bmatrix} u_{dc}. \tag{C-13}$$

Observe that the constraint equation (C-10) has disappeared due to the interconnection of the two subsystems. Subsequently, combining (C-5), (C-11), (C-12) and (C-13) leads to the differential-algebraic model in (3-17).

C-2 The parametrisation of the inverter for the nonlinear element method

In order to keep this derivation clear we separate the derivation for the parametrised input matrix and the output equation. First, consider the parametrisation of the output equation for which we use the formulae

$$\begin{aligned}y_{dc} =& f_{10} - f_{sa} + \hat{f}_{sb} + f_{11} - f_{sb} + \hat{f}_{sc} + f_{12} - f_{sc} + \hat{f}_{sa},\\ \hat{f}_{sa} =& f_{sa} - f_{10},\\ f_{sb} =& f_{10} + \hat{f}_{sb},\\ \hat{f}_{sb} =& f_{sb} - f_{11},\\ f_{sc} =& f_{11} + \hat{f}_{sc},\\ \hat{f}_{sc} =& f_{sc} - f_{12},\\ f_{sa} =& f_{12} + \hat{f}_{sa},\\ &\text{s.t.} \quad \begin{bmatrix}-f_{10} + f_{11}\\ f_{10} - f_{11}\\ f_{11} - f_{12}\end{bmatrix} = \frac{\partial H}{\partial x}(x).\end{aligned}$$

In the following we proof that the above formulae lead to the parametrisation of the output equation in (3-17).

Proof. Computing the results for every switch configuration $(s_a\ s_b\ s_c) \in \{0,1\}^3$ yields:

$$(s_a,\ s_b,\ s_c) = (0,0,0) \Rightarrow f_{s_a} = f_{s_b} = f_{s_c} = 0 \Rightarrow \hat{f}_{sa} = -f_{10}, \hat{f}_{sb} = -f_{11}, \hat{f}_{sc} = -f_{12}$$
$$\Rightarrow y = f_{10} - f_{11} + f_{11} - f_{12} + f_{12} = 0.$$

$$(s_a,\ s_b,\ s_c) = (1,0,0) \Rightarrow \hat{f}_{s_a} = f_{s_b} = f_{s_c} = 0 \Rightarrow f_{sa} = f_{12}, \hat{f}_{sb} = -f_{11}, \hat{f}_{sc} = -f_{12}$$
$$\Rightarrow y = f_{10} - f_{12} + f_{11} - f_{11} - f_{12} + f_{12} = -\frac{\partial H}{\partial \phi_a}.$$

$$(s_a,\ s_b,\ s_c) = (0,1,0) \Rightarrow f_{s_a} = \hat{f}_{s_b} = f_{s_c} = 0 \Rightarrow \hat{f}_{sa} = -f_{10}, f_{sb} = f_{10}, \hat{f}_{sc} = -f_{12}$$
$$\Rightarrow y = f_{10} + f_{11} - f_{10} - f_{12} + f_{12} - f_{10} = -\frac{\partial H}{\partial \phi_b}.$$

$$(s_a,\ s_b,\ s_c) = (0,0,1) \Rightarrow f_{s_a} = f_{s_b} = \hat{f}_{s_c} = 0 \Rightarrow \hat{f}_{sa} = -f_{10}, \hat{f}_{sb} = -f_{11}, f_{sc} = f_{11}$$
$$\Rightarrow y = f_{10} - f_{11} + f_{11} + f_{12} - f_{11} - f_{10} = -\frac{\partial H}{\partial \phi_c}.$$

$$(s_a,\ s_b,\ s_c) = (1,1,0) \Rightarrow \hat{f}_{s_a} = \hat{f}_{s_b} = f_{s_c} = 0 \Rightarrow f_{sa} = f_{12}, f_{sb} = f_{10}, \hat{f}_{sc} = -f_{12}$$
$$\Rightarrow y = f_{10} - f_{12} + f_{11} - f_{10} - f_{12} + f_{12} = \frac{\partial H}{\partial \phi_c} = -\frac{\partial H}{\partial \phi_a} - \frac{\partial H}{\partial \phi_b}.$$

$$(s_a,\ s_b,\ s_c) = (1,0,1) \Rightarrow \hat{f}_{s_a} = f_{s_b} = \hat{f}_{s_c} = 0 \Rightarrow f_{sa} = f_{12}, \hat{f}_{sb} = -f_{11}, f_{sc} = f_{11}$$
$$\Rightarrow y = f_{10} - f_{12} - f_{11} + f_{11} + f_{12} - f_{11} = \frac{\partial H}{\partial \phi_b} = -\frac{\partial H}{\partial \phi_a} - \frac{\partial H}{\partial \phi_c}.$$

$$(s_a,\ s_b,\ s_c) = (0,1,1) \Rightarrow f_{s_a} = \hat{f}_{s_b} = \hat{f}_{s_c} = 0 \Rightarrow \hat{f}_{sa} = -f_{10}, f_{sb} = f_{10}, f_{sc} = f_{11}$$
$$\Rightarrow y = f_{10} + f_{11} - f_{10} + f_{12} - f_{11} - f_{10} = \frac{\partial H}{\partial \phi_a} = -\frac{\partial H}{\partial \phi_b} - \frac{\partial H}{\partial \phi_c}.$$

$$(s_a,\ s_b,\ s_c) = (1,1,1) \Rightarrow \hat{f}_{s_a} = \hat{f}_{s_b} = \hat{f}_{s_c} = 0 \Rightarrow f_{sa} = f_{12}, f_{sb} = f_{10}, f_{sc} = f_{11}$$
$$\Rightarrow y = f_{10} - f_{12} + f_{11} - f_{10} + f_{12} - f_{11} = 0.$$

Concluding,

$$y = -s_a \frac{\partial H}{\partial \phi_a} - s_b \frac{\partial H}{\partial \phi_b} - s_c \frac{\partial H}{\partial \phi_c}.$$

□

Now consider the parametrisation of the input matrix for which we use the formulae:

$$\begin{aligned}
&\xi_{ab} - u_{ab} + e_{sb} - \hat{e}_{sa} = 0,\\
&\xi_{bc} - u_{bc} + e_{sc} - \hat{e}_{sb} = 0,\\
&\xi_{ca} - u_{ca} + e_{sa} - \hat{e}_{sc} = 0,\\
&\hat{e}_{sb} = e_{sb} - u_{dc},\\
&e_{sa} = u_{dc} + \hat{e}_{sa},\\
&\hat{e}_{sc} = e_{sc} - u_{dc},\\
&e_{sb} = u_{dc} + \hat{e}_{sb},\\
&\hat{e}_{sa} = e_{sa} - u_{dc},\\
&e_{sc} = u_{dc} + \hat{e}_{sc},
\end{aligned}$$

where $\xi_{jk} = f_{Rk} - f_{Rj} - \dot{\phi}_k + \dot{\phi}_c - y_{jk}$, $jk = ab, bc, ca$. These equations are equivalent with the parametrised equations for $\dot{\phi}$ in (3-17).

Proof. Computing the resulting equations for every switch configuration produces

$$\begin{aligned}(s_a,\ s_b,\ s_c) = (0,0,0) &\Rightarrow \hat{e}_{s_a} = \hat{e}_{s_b} = \hat{e}_{s_c} = 0 \Rightarrow e_{sa} = u_{dc}, e_{sb} = u_{dc}, e_{sc} = u_{dc}\\ &\Rightarrow \xi_{ab} = 0,\\ &\Rightarrow \xi_{bc} = 0,\\ &\Rightarrow \xi_{ca} = 0.\end{aligned}$$

$$\begin{aligned}(s_a,\ s_b,\ s_c) = (1,0,0) &\Rightarrow e_{s_a} = \hat{e}_{s_b} = \hat{e}_{s_c} = 0 \Rightarrow \hat{e}_{sa} = -u_{dc}, e_{sb} = u_{dc}, e_{sc} = u_{dc}\\ &\Rightarrow \xi_{ab} + u_{dc} = 0,\\ &\Rightarrow \xi_{bc} = 0,\\ &\Rightarrow \xi_{ca} - u_d c = 0.\end{aligned}$$

$$\begin{aligned}(s_a,\ s_b,\ s_c) = (0,1,0) &\Rightarrow \hat{e}_{s_a} = e_{s_b} = \hat{e}_{s_c} = 0 \Rightarrow e_{sa} = u_{dc}, \hat{e}_{sb} = -u_{dc}, e_{sc} = u_{dc}\\ &\Rightarrow \xi_{ab} - u_{dc} = 0,\\ &\Rightarrow \xi_{bc} + u_{dc} = 0,\\ &\Rightarrow \xi_{ca} = 0.\end{aligned}$$

$$\begin{aligned}(s_a,\ s_b,\ s_c) = (0,0,1) &\Rightarrow \hat{e}_{s_a} = \hat{e}_{s_b} = e_{s_c} = 0 \Rightarrow e_{sa} = u_{dc}, e_{sb} = u_{dc}, \hat{e}_{sc} = -u_{dc}\\ &\Rightarrow \xi_{ab} = 0,\\ &\Rightarrow \xi_{bc} - u_{dc} = 0,\\ &\Rightarrow \xi_{ca} + u_{dc} = 0.\end{aligned}$$

$$\begin{aligned}(s_a,\ s_b,\ s_c) = (1,1,0) &\Rightarrow e_{s_a} = e_{s_b} = \hat{e}_{s_c} = 0 \Rightarrow \hat{e}_{sa} = -u_{dc}, \hat{e}_{sb} = -u_{dc}, e_{sc} = u_{dc}\\ &\Rightarrow \xi_{ab} = 0,\\ &\Rightarrow \xi_{bc} + u_{dc} = 0,\\ &\Rightarrow \xi_{ca} - u_d c = 0.\end{aligned}$$

$$\begin{aligned}(s_a,\ s_b,\ s_c) = (1,0,1) &\Rightarrow e_{s_a} = \hat{e}_{s_b} = e_{s_c} = 0 \Rightarrow \hat{e}_{sa} = -u_{dc}, e_{sb} = u_{dc}, \hat{e}_{sc} = -u_{dc}\\ &\Rightarrow \xi_{ab} + u_{dc} = 0,\\ &\Rightarrow \xi_{bc} - u_{dc} = 0,\\ &\Rightarrow \xi_{ca} = 0.\end{aligned}$$

$$\begin{aligned}(s_a,\ s_b,\ s_c) = (0,1,1) &\Rightarrow \hat{e}_{s_a} = e_{s_b} = e_{s_c} = 0 \Rightarrow e_{sa} = u_{dc}, \hat{e}_{sb} = -u_{dc}, \hat{e}_{sc} = -u_{dc}\\ &\Rightarrow \xi_{ab} - u_{dc} = 0,\\ &\Rightarrow \xi_{bc} = 0,\\ &\Rightarrow \xi_{ca} + u_{dc} = 0.\end{aligned}$$

$$\begin{aligned}(s_a,\ s_b,\ s_c) = (1,1,1) &\Rightarrow e_{s_a} = e_{s_b} = e_{s_c} = 0 \Rightarrow \hat{e}_{sa} = -u_{dc}, \hat{e}_{sb} = -u_{dc}, \hat{e}_{sc} = -u_{dc}\\ &\Rightarrow \xi_{ab} = 0,\\ &\Rightarrow \xi_{bc} = 0,\\ &\Rightarrow \xi_{ca} = 0.\end{aligned}$$

Concluding

$$\begin{bmatrix} \xi_{ab} \\ \xi_{bc} \\ \xi_{ca} \end{bmatrix} + \begin{bmatrix} s_a - s_b \\ s_b - s_c \\ s_c - s_a \end{bmatrix} u_{dc} = 0.$$

□

C-3 The derivation of the rectifier's differential-algebraic model

For Σ_1 we have the following sets of equations

$$\begin{aligned} y = &- \mathbb{I}^{3\times 3}\frac{\partial H}{\partial \phi}, \\ &\text{s.t.} y_a + y_b + y_c = 0, \end{aligned} \tag{C-14}$$

$$e_R = \mathbb{I}^{3\times 3}\frac{\partial H}{\partial \phi}, \tag{C-15}$$

$$\begin{aligned} f_1 - f_3 &= \frac{\partial H}{\partial \phi_a}, \\ f_2 - f_1 &= \frac{\partial H}{\partial \phi_b}, \\ f_3 - f_2 &= \frac{\partial H}{\partial \phi_c}, \end{aligned} \tag{C-16}$$

$$\begin{aligned} f_{Rb} - \dot{\phi}_b - u_b - f_{Ra} + \dot{\phi}_a + u_a - e_1 = 0, \\ f_{Rc} - \dot{\phi}_c - u_c - f_{Rb} + \dot{\phi}_b + u_b - e_2 = 0, \\ f_{Ra} - \dot{\phi}_a - u_a - f_{Rc} + \dot{\phi}_c + u_c - e_3 = 0, \\ e_1 + e_2 + e_3 = 0. \end{aligned} \tag{C-17}$$

For Σ_2 the simplified, parametrised relations from Section 4-2-3 are

$$\begin{aligned} f_7 &= -f_4(s_a - s_b), \\ f_8 &= -f_5(s_b - s_c), \\ f_9 &= -f_6(s_c - s_a), \\ e_4 &= e_7(s_a - s_b), \\ e_5 &= e_8(s_b - s_c), \\ e_6 &= e_9(s_c - s_a). \end{aligned} \tag{C-18}$$

The equations describing Σ_3 are

$$\begin{aligned} \dot{q} &= f_{R_L} + f_{10} + f_{11} + f_{12}, \\ e_{R_L} &= \frac{\partial H}{\partial q}, \\ e_{10} = e_{11} &= e_{12} = \frac{\partial H}{\partial q}. \end{aligned} \tag{C-19}$$

Combining (C-17) with the voltage equations in (C-18) through $e_1 = e_4, e_2 = e_5, e_3 = e_6$ and subsequently substituting e_{10}, e_{11}, e_{12} into the results through $e_7 = e_{10}, e_8 = e_{11}, e_9 = e_{12}$ leads to

$$\begin{aligned} f_{Rb} - \dot{\phi}_b - u_b - f_{Ra} + \dot{\phi}_a + u_a - (s_a - s_b)\frac{\partial H}{\partial q} = 0, \\ f_{Rc} - \dot{\phi}_c - u_c - f_{Rb} + \dot{\phi}_b + u_b - (s_b - s_c)\frac{\partial H}{\partial q} = 0, \\ f_{Ra} - \dot{\phi}_a - u_a - f_{Rc} + \dot{\phi}_c + u_c - (s_c - s_a)\frac{\partial H}{\partial q} = 0. \end{aligned} \tag{C-20}$$

Furthermore, combining the equation for the current in the capacitor in (C-19) with the equations of the currents in (C-18), through $f_7 = -f_{10}, f_8 = -f_{11}, f_9 = -f_{12}$ leads to

$$\dot{q} = f_{R_L} + f_4(s_a - s_b) + f_5(s_b - s_c) + f_6(s_c - s_a).$$

Subsequently, substituting (C-16) given that $f_1 = -f_4, f_2 = -f_5, f_3 = -f_6$ yields

$$\dot{q} = f_{R_L} - s_a\frac{\partial H}{\partial \phi_a} - s_b\frac{\partial H}{\partial \phi_b} - s_c\frac{\partial H}{\partial \phi_c}. \tag{C-21}$$

Finally, combining (C-14), (C-15), (C-20), (C-21) and the equation for the load resistance in (C-19) leads to the differential-algebraic model in (4-6).

C-4 The parametrisation of the rectifier for the nonlinear element method

The proof of the parametrisation of the rectifier model with the switches as nonlinear elements will be given in two ways. First, the equivalence of the parametrised equations of the graph of Σ_2, (C-18), and the equations corresponding to the graph of Σ_2 with the switches as nonlinear elements, which are

$$\begin{aligned} f_{\ell+3} &= f_\ell - f_{sj} + \hat{f}_{sk}, \\ e_\ell &= -e_{\ell+3} + e_{sk} - \hat{e}_{sj}, \\ \hat{f}_{sj} &= f_{sj} - f_\ell, \\ f_{sk} &= f_\ell + \hat{f}_{sk}, \\ \hat{e}_{sk} &= e_{sk} - e_{\ell+3}, \\ e_{sj} &= e_{\ell+3} + \hat{e}_{sj}. \end{aligned} \tag{C-22}$$

Proof.

$$\begin{aligned} (s_j, s_k) = (0,0) \Rightarrow f_{sj} = f_{sk} = 0 \Rightarrow \hat{f}_{sj} = \hat{f}_{sk} = -f_\ell \\ \Rightarrow f_{\ell+3} = 0. \\ (s_j, s_k) = (0,0) \Rightarrow \hat{e}_{sj} = \hat{e}_{sk} = 0 \Rightarrow e_{sj} = e_{sk} = e_{\ell+3} \\ \Rightarrow e_\ell = 0. \\ (s_j, s_k) = (1,0) \Rightarrow \hat{f}_{sj} = f_{sk} = 0 \Rightarrow f_{sj} = f_\ell, \hat{f}_{sk} = -f_\ell \\ \Rightarrow f_{\ell+3} = -f_\ell. \\ (s_j, s_k) = (1,0) \Rightarrow e_{sj} = \hat{e}_{sk} = 0 \Rightarrow \hat{e}_{sj} = -e_{\ell+3}, e_{sk} = e_{\ell+3} \\ \Rightarrow e_\ell = e_{\ell+3}. \end{aligned}$$

$$
\begin{aligned}
(s_j, s_k) = (0,1) &\Rightarrow f_{sj} = \hat{f}_{sk} = 0 \Rightarrow \hat{f}_{sj} = -f_\ell, f_{sk} = f_\ell \\
&\Rightarrow f_{\ell+3} = f_\ell. \\
(s_j, s_k) = (0,1) &\Rightarrow \hat{e}_{sj} = e_{sk} = 0 \Rightarrow e_{sj} = e_{\ell+3}, \hat{e}_{sk} = -e_{\ell+3} \\
&\Rightarrow e_\ell = -e_{\ell+3}.
\end{aligned}
$$

$$
\begin{aligned}
(s_j, s_k) = (1,1) &\Rightarrow \hat{f}_{sj} = \hat{f}_{sk} = 0 \Rightarrow f_{sj} = f_{sk} = f_\ell \\
&\Rightarrow f_{\ell+3} = 0. \\
(s_j, s_k) = (1,1) &\Rightarrow e_{sj} = e_{sk} = 0 \Rightarrow \hat{e}_{sj} = \hat{e}_{sk} = -e_{\ell+3} \\
&\Rightarrow e_\ell = 0.
\end{aligned}
$$

Concluding, the mathematical representation with the switches as nonlinear elements (C-22) is equivalent to the parametrised representation (C-18) and therefore lead to the same differential-algebraic model in (3-22). □

Second, we proof that parametrising the complete differential-algebraic model in (4-6) leads to the model in (3-22).

Proof. First consider the parametrisation of the equation for $\dot{q}$

$$
\begin{aligned}
(s_a, s_b, s_c) = (0,0,0) &\Rightarrow f_{sa} = f_{sb} = f_{sc} = 0 \Rightarrow \hat{f}_{sa} = f_3, \hat{f}_{sb} = f_1, \hat{f}_{sc} = f_2 \\
&\Rightarrow \dot{q} = f_{R_L} + f_1 - f_1 + f_2 - f_2 + f_3 - f_3 = f_{R_L}.
\end{aligned}
$$

$$
\begin{aligned}
(s_a, s_b, s_c) = (1,0,0) &\Rightarrow \hat{f}_{sa} = f_{sb} = f_{sc} = 0 \Rightarrow f_{sa} = -f_1, \hat{f}_{sb} = f_1, \hat{f}_{sc} = f_2 \\
&\Rightarrow \dot{q} = f_{R_L} + f_1 - f_1 - f_1 + f_2 - f_2 + f_3 = f_{R_L} - \frac{\partial H}{\partial \phi_a}.
\end{aligned}
$$

$$
\begin{aligned}
(s_a, s_b, s_c) = (0,1,0) &\Rightarrow f_{sa} = \hat{f}_{sb} = f_{sc} = 0 \Rightarrow \hat{f}_{sa} = f_3, f_{sb} = -f_2, \hat{f}_{sc} = f_2 \\
&\Rightarrow \dot{q} = f_{R_L} + f_1 + f_2 - f_2 - f_2 + f_3 - f_3 = f_{R_L} - \frac{\partial H}{\partial \phi_b}.
\end{aligned}
$$

$$
\begin{aligned}
(s_a, s_b, s_c) = (0,0,1) &\Rightarrow f_{sa} = f_{sb} = \hat{f}_{sc} = 0 \Rightarrow \hat{f}_{sa} = f_3, \hat{f}_{sb} = f_1, f_{sc} = -f_3 \\
&\Rightarrow \dot{q} = f_{R_L} + f_1 - f_1 + f_2 - f_3 + f_3 - f_3 = f_{R_L} - \frac{\partial H}{\partial \phi_c}.
\end{aligned}
$$

$$
\begin{aligned}
(s_a, s_b, s_c) = (1,1,0) &\Rightarrow \hat{f}_{sa} = \hat{f}_{sb} = f_{sc} = 0 \Rightarrow f_{sa} = -f_1, f_{sb} = -f_2, \hat{f}_{sc} = f_2 \\
&\Rightarrow \dot{q} = f_{R_L} + f_1 - f_1 + f_2 - f_2 - f_2 + f_3 = f_{R_L} + \frac{\partial H}{\partial \phi_c} = f_{R_L} - \frac{\partial H}{\partial \phi_a} - \frac{\partial H}{\partial \phi_b}.
\end{aligned}
$$

$$
\begin{aligned}
(s_a, s_b, s_c) = (1,0,1) &\Rightarrow \hat{f}_{sa} = f_{sb} = \hat{f}_{sc} = 0 \Rightarrow f_{sa} = -f_1, \hat{f}_{sb} = f_1, f_{sc} = -f_3 \\
&\Rightarrow \dot{q} = f_{R_L} + f_1 - f_1 - f_1 + f_2 + f_3 - f_3 = f_{R_L} + \frac{\partial H}{\partial \phi_b} = f_{R_L} - \frac{\partial H}{\partial \phi_c} - \frac{\partial H}{\partial \phi_a}.
\end{aligned}
$$

$$
\begin{aligned}
(s_a, s_b, s_c) = (0,1,1) &\Rightarrow f_{sa} = \hat{f}_{sb} = \hat{f}_{sc} = 0 \Rightarrow \hat{f}_{sa} = f_3, f_{sb} = -f_2, f_{sc} = -f_3 \\
&\Rightarrow \dot{q} = f_{R_L} + f_1 + f_2 - f_2 + f_3 - f_3 - f_3 = f_{R_L} + \frac{\partial H}{\partial \phi_a} = f_{R_L} - \frac{\partial H}{\partial \phi_b} - \frac{\partial H}{\partial \phi_c}.
\end{aligned}
$$

$$
\begin{aligned}
(s_a, s_b, s_c) = (1,1,1) &\Rightarrow \hat{f}_{sa} = \hat{f}_{sb} = \hat{f}_{sc} = 0 \Rightarrow f_{sa} = -f_1, f_{sb} = -f_2, f_{sc} = -f_3 \\
&\Rightarrow \dot{q} = f_{R_L} + f_1 - f_1 + f_2 - f_2 + f_3 - f_3 = f_{R_L}.
\end{aligned}
$$

This indeed leads to the parametrised equation in (C-21). Likewise, consider the parametrisation of the equations $f_{Rk} - \dot{\phi}_k - u_k - f_{Rj} + \dot{\phi}_j + u_j - e_\ell$. For the sake of simplicity denote $\zeta_{jk} = f_{Rk} - \dot{\phi}_k - u_k - f_{Rj} + \dot{\phi}_j + u_j$.

$$\begin{aligned}(s_a, s_b, s_c) = (0,0,0) &\Rightarrow \hat{e}_{sa} = \hat{e}_{sb} = \hat{e}_{sc} = 0 \Rightarrow e_{sa} = e_{sb} = e_{sc} = u_{dc} \\ &\Rightarrow \zeta_{ab} = \zeta_{bc} = \zeta_{ca} = 0.\end{aligned}$$

$$\begin{aligned}(s_a, s_b, s_c) = (1,0,0) &\Rightarrow e_{sa} = \hat{e}_{sb} = \hat{e}_{sc} = 0 \Rightarrow \hat{e}_{sa} = -u_{dc}, e_{sb} = u_{dc}, e_{sc} = u_{dc} \\ &\Rightarrow \zeta_{ab} - u_{dc} = 0, \\ &\Rightarrow \zeta_{bc} = 0, \\ &\Rightarrow \zeta_{ca} + u_{dc} = 0.\end{aligned}$$

$$\begin{aligned}(s_a, s_b, s_c) = (0,1,0) &\Rightarrow \hat{e}_{sa} = e_{sb} = \hat{e}_{sc} = 0 \Rightarrow e_{sa} = u_{dc}, \hat{e}_{sb} = -u_{dc}, e_{sc} = u_{dc} \\ &\Rightarrow \zeta_{ab} + u_{dc} = 0, \\ &\Rightarrow \zeta_{bc} - u_{dc} = 0, \\ &\Rightarrow \zeta_{ca} = 0.\end{aligned}$$

$$\begin{aligned}(s_a, s_b, s_c) = (0,0,1) &\Rightarrow \hat{e}_{sa} = \hat{e}_{sb} = e_{sc} = 0 \Rightarrow e_{sa} = u_{dc}, e_{sb} = u_{dc}, \hat{e}_{sc} = -u_{dc} \\ &\Rightarrow \zeta_{ab} = 0, \\ &\Rightarrow \zeta_{bc} + u_{dc} = 0, \\ &\Rightarrow \zeta_{ca} - u_{dc} = 0.\end{aligned}$$

$$\begin{aligned}(s_a, s_b, s_c) = (1,1,0) &\Rightarrow e_{sa} = e_{sb} = \hat{e}_{sc} = 0 \Rightarrow \hat{e}_{sa} = -u_{dc}, \hat{e}_{sb} = -u_{dc}, e_{sc} = u_{dc} \\ &\Rightarrow \zeta_{ab} = 0, \\ &\Rightarrow \zeta_{bc} - u_{dc} = 0, \\ &\Rightarrow \zeta_{ca} + u_{dc} = 0.\end{aligned}$$

$$\begin{aligned}(s_a, s_b, s_c) = (1,0,1) &\Rightarrow e_{sa} = \hat{e}_{sb} = e_{sc} = 0 \Rightarrow \hat{e}_{sa} = -u_{dc}, e_{sb} = u_{dc}, \hat{e}_{sc} = -u_{dc} \\ &\Rightarrow \zeta_{ab} - u_{dc} = 0, \\ &\Rightarrow \zeta_{bc} + u_{dc} = 0, \\ &\Rightarrow \zeta_{ca} 0 = 0.\end{aligned}$$

$$\begin{aligned}(s_a, s_b, s_c) = (0,1,1) &\Rightarrow \hat{e}_{sa} = e_{sb} = e_{sc} = 0 \Rightarrow e_{sa} = u_{dc}, \hat{e}_{sb} = -u_{dc}, \hat{e}_{sc} = -u_{dc} \\ &\Rightarrow \zeta_{ab} + u_{dc} = 0, \\ &\Rightarrow \zeta_{bc} = 0, \\ &\Rightarrow \zeta_{ca} - u_{dc} = 0.\end{aligned}$$

$$\begin{aligned}(s_a, s_b, s_c) = (1,1,1) &\Rightarrow e_{sa} = e_{sb} = e_{sc} = 0 \Rightarrow \hat{e}_{sa} = \hat{e}_{sb} = \hat{e}_{sc} = -u_{dc} \\ &\Rightarrow \zeta_{ab} = \zeta_{bc} = \zeta_{ca} = 0.\end{aligned}$$

This leads to the parametrised equations in (C-20) and hence the differential-algebraic model in (3-22) is equivalent with the one in (4-6). □

Bibliography

[1] N. Mohan, T.M. Undeland, W.P. Robbins, *Power electronics*. New York: Wiley & Sons, 3rd ed., 2003.

[2] S. Krul, "Port-Hamiltonian modelling of inverters." literature survey, December 2014. Technical University Delft, The Netherlands.

[3] V. Duindam, A. Macchelli, S. Stramigioli, H. Bruyninckx, *Modeling and control of complex physical systems*. Berlin: Springer, 1st ed., 2009.

[4] G. Escobar, A. J. van der Schaft, and R. Ortega, "A hamiltonian viewpoint in the modeling of switching power converters," *Automatica*, vol. 35, no. 3, pp. 445 – 452, 1999.

[5] M. Magos, C. Valentin and B. Maschke, "Non minimal representation of dirac structures for physical systems with switching interconnection," in *International symposium on Mathematical Theory of Networks and Systems*, (Leuven, Belgium), MTNS2004, 2004.

[6] C. Valentin, M. Magos, and B. Maschke, "A port-hamiltonian formulation of physical switching systems with varying constraints," *Automatica*, vol. 43, no. 7, pp. 1125 – 1133, 2007.

[7] C. Valentin, M. Magos, and B. Maschke, "Hybrid port-hamiltonian systems: From parameterized incidence matrices to hybrid automata," *Nonlinear Analysis: Theory, Methods & Applications*, vol. 65, no. 6, pp. 1106 – 1122, 2006.

[8] T. Wildi, *Electrical machines, Drives and Power Systems*. Edinburgh: Pearson, 6th ed., 2014.

[9] Y. Tang, H. Yu, and Z. Zou, "Hamiltonian modeling and energy-shaping control of three-phase ac/dc voltage-source converters," in *Automation and Logistics, 2008. ICAL 2008. IEEE International Conference on*, pp. 591–595, Sept 2008.

[10] X. Mu, J. Wang, H. Xiang, Y. Ma, and D. Yang, "Study on a nonlinear control strategy for three-phase voltage sources pwm dc/ac inverter based on pch model," in *Electrical Machines and Systems (ICEMS), 2011 International Conference on*, pp. 1–4, Aug 2011.

[11] K. Mu, X. Ma, X. Mu, and D. Zhu, "Study on passivity-based control of voltage source pwm dc/ac inverter," in *Electronic and Mechanical Engineering and Information Technology (EMEIT), 2011 International Conference on*, vol. 8, pp. 3963–3967, Aug 2011.

[12] A. van der Schaft and D. Jeltsema, "Port-hamiltonian systems theory: An introductory overview," *Foundations and Trends in Systems and Control*, vol. 1, no. 2-3, pp. 173–378, 2014.

[13] J. Cervera, A. van der Schaft, and A. Baños, "Interconnection of port-hamiltonian systems and composition of dirac structures," *Automatica*, vol. 43, no. 2, pp. 212 – 225, 2007.

[14] J. Willems, "The behavioral approach to open and interconnected systems," *Control Systems, IEEE*, vol. 27, pp. 46–99, Dec 2007.

[15] L.O. Chua, C.A. Desoer, E.S. Kuh, *Linear and nonlinear circuits*. Singapore: McGraw-Hill, 1st ed., 1987.

[16] R. Diestel, *Graph theory*. New York: Springer, 1st ed., 1997.

[17] D.G. Holmes, T.A. Lipo., *Pulse width modulation for power converters*. New York: Wiley-IEEE Press, 1st ed., 2003.

[18] H. Klein Woud, D. Stapersma, *Design of propulsion and electric power generation systems*. London: IMarEST, 1st ed., 2002.

[19] J.F. Schuh, *Mathematical tools for modern physics*. Eindhoven: Philips Technical Library, 1st ed., 1968.

[20] P. C. Breedveld, *Physical systems theory in terms of bond graphs*. PhD thesis, Twente University, 1984.

[21] A. Veltman, *The fish method; Interaction between AC machines and power converters*. PhD thesis, Technical University Delft, Delft, The Netherlands, Jan. 1994.

[22] D. Jeltsema and J. M. A. Scherpen, "Multidomain modeling of nonlinear networks and systems," *Control Systems, IEEE*, vol. 29, pp. 28–59, Aug 2009.

Glossary

List of Acronyms

AC	Alternating Current
CL	Cycle Law
CCL	Co-Cycle Law
DAE	Differential-Algebraic Equation
DAM	Differential-Algebraic Model
DC	Direct Current
ISO	Input-State-Output
KCL	Kirchhoff's Current Law
KVL	Kirchhoff's Voltage Law
NEM	Nonlinear Element Method
PH	Port-Hamiltonian
VEM	Virtual Element Method

List of Symbols

Symbol	**Description**
Greek	
λ	Electrical potential
ϕ	Flux-linkage
Λ	Vector of electrical potentials
Σ	(Sub)system
Φ	Constitutive relation
Roman	
b	Branch
e	Effort
f	Flow
g	Input mapping (matrix)

g^T	Output mapping (matrix)
i	Current
i_L	Loop current
n	Node
q	Charge
s	Switch state
u	Input
v	Voltage
x	State
y	Output

A	Incidence matrix
B	Set of branches
C	Capacitance
C_{cy}	Cycle variables
C_{cocy}	Co-cycle variables
D	Dissipation matrix
$\hat{D}, \tilde{D}$	Dissipative relation
E	Effort interconnection matrix
F	Flow interconnection matrix
G	Graph
G_r	Reference graph
G_v	Virtual graph
H	Hamiltonian
I	Vector of currents
I_L	Vector of loop currents
J	Interconnection matrix
L	Inductance
M	Disconnection-reconnection matrix
N	Set of nodes
N_b	Number of branches
N_n	Number of nodes
N_s	Number of switches
R	Resistance
S	Vector of switch states
V	Vector of voltages
Z	Direct feedthrough matrix

Calligraphic symbols

$\mathcal{A}$	Set of admissible configurations
$\mathcal{D}$	Dirac structure
$\mathcal{E}$	Space of efforts
$\mathcal{F}$	Space of flows
$\mathcal{P}$	Set of (external) ports
$\mathcal{R}$	Set of resistive elements
$\mathcal{S}$	Set of storage elements

$\mathcal{W}$	Set of switching elements
$\mathcal{X}$	State-space

Miscellaneous

$(\cdot)^*$	Dual
$\langle \cdot \vert \cdot \rangle$	Duality product
$\dot{(\cdot)}$	Derivative with respect to time
$(\cdot)^T$	Transpose operator
$\vert\vert \cdot \vert\vert$	Length of a path or cycle
$(\cdot)_{a,b,c}$	Refers to the phases, a, b, c
$(\cdot)_{j,k,\ell}$	Counters and indexes
$(\cdot)_L$	Variable corresponding to a load
$\mathbb{I}$	Identity matrix
$\mathbb{O}$	Matrix of only zeros